

SCIENTIFIC REPORT

**MANAGING SUBSURFACE DRAINAGE WATER
TO OPTIMIZE CROP PRODUCTIVITY, NUTRIENT
USE AND WATER AVAILABILITY IN
CONTEMPORARY AND FUTURE CLIMATE**

PROJECT NO. IA114252:

**QUEBEC-ONTARIO COOPERATION FOR AGRI-
FOOD RESEARCH**

AUGUST 2018

PROJECT CO-LEADS

Merrin L. Macrae, University of Waterloo

Aubert Michaud, Institut de recherche et de développement en agroenvironnement

RESEARCH TEAM

- Merrin L. **Macrae**, University of Waterloo, mmacrae@uwaterloo.ca
- Aubert **Michaud**, Institut de recherche et de développement en agroenvironnement (IRDA), aubert.michaud@irda.qc.ca
- Mohamed Abou **Niang**, Institut de recherche et de développement en agroenvironnement (IRDA), mohamed.niang@irda.qc.ca
- Karlen **Hanke**, graduate student, University of Waterloo, khanke@uwaterloo.ca

COLLABORATORS

Authorized Officers:

- Quebec Institution: Marie Kougioumoutzakis
- Ontario Institution: Thiam Phouthonephackdy

Collaborating Researchers/Partners:

- Blaise Gauvin St-Denis, Marco Braun
OURANOS, Climate scenarios and services group
- Nandita Basu, University of Waterloo
- Craig Merkley, Upper Thames Conservation Authority
- Benoit Laferrière, Club Lavallière
- Wanhong Yang, University of Guelph
- Eveline Mousseau, Club agroenvironnemental Pro-Conseil.
- Karen Maaskant. Upper Thames Conservation Authority
- Kevin McKague, OMAFRA.

ACKNOWLEDGEMENTS

- The Joyal family from GenLouis farm, Yamaska, Québec
- Jacques Dejardins, William Huertas and François Landry, Technicians at IRDA (technical and field support)
- Laurence Taylor (farmer, Londesborough)
- Idhayachandhiran Ilampooranan (graduate student modeller, UWaterloo)
- Vito Lam (field technician, UWaterloo)
- Christopher Wellen (Ryerson University)
- Mohamed Mohamed (Environment and Climate Change Canada)
- Sylvestre Delmotte, Guillaume Jego and René Morissette (Climate scenarios analysis)

Project Executive Summary

This project examined the impacts of controlled drainage on agronomic factors and environmental quality, now and in future, using a combination of field data and modelling exercises. Studies were undertaken at multiple scales, field, small (micro) watershed and larger watersheds, and this was done in both Quebec and Ontario. Future climate scenarios were provided by our partners, Ouranos, that projected changes in precipitation form, magnitude and seasonality, and increased temperatures. Such changes will result in a longer growing season, as well as an intensification of the hydrologic cycle, where periods of drought will be interrupted by more heavy rainfall. This will lead to the potential for considerable moisture stress, where crops may struggle to have enough water to succeed but may also experience periods of flooding. This intensification of the hydrologic cycle will also lead to more peak runoff, which will likely result in degraded water quality. In this project, we explored whether or not controlled drainage (CD) could play a role in mitigating these issues. We found limited feasibility of CD for improving crop success due to the early drawdown of the water table following snowmelt in most seasons. We also found that surface and internal drainage are determinant drivers of the agronomic feasibility and benefits of controlled drainage. With regards to the environmental impacts of CD, we found that the benefits of CD were site-specific. In the Ontario study on a sloping clay loam, we found that CD would exacerbate water quality issues because it would produce more surface runoff as a trade-off through blocking tile drains. In the Quebec study in a flat clay, there was evidence of preferential transport through macropores into tile drains. Controlled drainage had potential to offset these subsurface loads, but only if surface runoff was not generated. Thus, from a land and river stewardship perspective, the effective reduction of P loading to streams calls for mitigation measures on subsurface preferential P transfers together with surface runoff abatement. With regards to the feasibility/efficiency of CD under future climates, the greater spring precipitation that is expected under future climates limits the feasibility of the use of CD, as CD must manage subsurface yields without exacerbating surface runoff. It is likely that the use of CD in spring will be accompanied by increased surface runoff. Although it may be possible to only employ CD in the summer months, when less surface runoff is anticipated, this period is not the primary period for nutrient loss and thus, CD will ultimately have little effect on mitigating nutrient losses during this time. Our project has shown that CD is unlikely to mitigate the water quality risks associated with climate change unless it can be employed earlier in the season than it currently is. However, the use of CD throughout the non-growing season is problematic as it increases surface runoff and exacerbates water quality issues. These findings are based on how CD is currently used (manual closures). If the technology of CD can be advanced to allow “precision management” of tile drains (where tiles are opened or closed based on critical water table stages that vary seasonally), there may be more potential for the use of CD as it may offset moisture stress without enhancing surface runoff.

Résumé

Cette étude a examiné les impacts agronomiques et environnementaux du drainage contrôlé, où des chambres de contrôle sont installés à l'exutoire des collecteurs des systèmes de drainage afin de bloquer l'écoulement des drains lorsque la nappe atteint un seuil critique. Des mesures en continu au champ des hauteurs des nappes d'eau, des débits au drain et des flux associés de sédiments, d'azote et de phosphore au drain ont été mis à profit dans le calage et la validation de modèles hydrologiques afin d'évaluer les effets du drainage contrôlé sur les mouvements de l'eau et des nutriments dans les sols et les cours d'eau. Suivant le calage des modèles sur la base de données historiques, la faisabilité du drainage contrôlé a été examinée en climat futur en introduisant des scénarios climatiques représentatifs de l'horizon 2040-2070. Ces changements dans la forme, l'intensité et la saisonnalité des précipitations, de même que dans l'augmentation de la température ont été développés par l'équipe d'OURANOS, partenaire de réalisation du projet. Les changements projetés du climat vont conduire à une saison de croissance plus longue, de même qu'à une intensification du cycle hydrologique, où des périodes de sécheresse seront interrompues par des épisodes de pluie plus intense, associée à l'augmentation du risque d'inondation. Cette intensification du cycle hydrologique conduira également à une augmentation du taux de ruissellement, exacerbant la pression sur la qualité de l'eau. Dans cette étude, nous avons exploré le potentiel du drainage contrôlé à mitiger ces effets associés aux changements climatiques. Nous avons estimé que la faisabilité du DC était limitée pour réduire le stress hydrique des cultures en raison du rabattement hâtif de la nappe au printemps sous le niveau des drains. Nous avons également estimé que le drainage de surface et interne du sol étaient des facteurs déterminants de la faisabilité agronomique et des bénéfices associés au DC. En ce qui a trait aux effets du DC sur la qualité de l'eau, il est apparu que les bénéfices étaient spécifiques aux sites à l'étude. Dans l'étude Ontarienne réalisée sur un loam argileux en pente, l'activation du DC a exacerbé l'émission du ruissellement de surface et conduit à la détérioration de la qualité de l'eau de surface. Dans l'étude québécoise, une migration préférentielle de phosphore au drain via les macropores du sol a été observée sur des champs argileux au relief plat. Il est estimé que le DC peut réduire ces charges souterraines de phosphore, à la condition qu'il ne conduise pas à un accroissement du ruissellement de surface. Ainsi, dans une perspective de saine gestion des terres, la réduction tangible des charges de phosphore à la rivière passe par l'atténuation des transferts par le ruissellement de surface, de même que par les systèmes de drainage souterrain, où la nature du sol favorise les écoulements préférentiels. En ce qui a trait à la faisabilité du DC en climat futur, malgré le réchauffement hâtif au printemps, la faisabilité de retenir de l'eau par la fermeture des collecteurs demeure limitée en raison de l'augmentation anticipée des précipitations hivernale et printanière en climat futur, qui accroissent les risques de ruissellement de surface. Les modèles prédisent cependant que la faisabilité de limiter le rabattement de la nappe, sans accroître

le ruissellement, est dépendante du type de sol. Bien qu'il soit possible d'utiliser le DC uniquement en saison estivale, alors que le risque de ruissellement de surface est faible, cette période n'est pas propice aux pertes de nutriments par les drains. Le DC n'aura ainsi qu'un effet marginal sur ces charges en été. L'étude a démontré qu'il est peu probable que le DC ait un effet tangible sur la qualité de l'eau en climat futur, s'il n'est pas utilisé plus tôt en saison qu'il ne l'est présentement. Le recours au DC hors de la saison de croissance est cependant problématique, dans la mesure où il peut accroître le ruissellement de surface et détériorer la qualité de l'eau. Ces observations s'appliquent à une fermeture manuelle des drains. Dans une perspective de « gestion de l'eau de précision », où les drains sont ouverts ou fermés suivant des hauteurs variables de contrôle de la nappe selon la saison, le drainage contrôlé offre l'opportunité d'atténuer le stress hydrique des cultures sans accroître le ruissellement de surface.

Table of Contents

List of Abbreviations	14
1 INTRODUCTION	15
2 LITERATURE REVIEW	16
3 Ontario region studies	20
3.1 Medway Creek Watershed Study.....	20
3.1.1 Specific objectives of this portion of the study:.....	20
3.1.2 Description of the Medway Creek Watershed.....	20
3.1.3 Hydrologic and Climate Modelling Procedures.....	21
3.1.4 Model Calibration and Validation Results.....	25
3.1.5 Future and baseline climate simulations.....	26
3.1.6 Model Results: Water balance and flow path changes.....	27
3.1.7 Model Results: Nutrient and sediment loads in the future climate.....	34
3.1.8 Conclusions for Medway Creek Study.....	38
3.2 Londesborough Field Site Study.....	39
3.2.1 Context and Objectives	39
3.2.2 Field Site Description.....	40
3.2.3 Field Data Collection	41
3.2.4 SWAT model description	41
3.2.5 Results: SWAT HRU performance: Surface runoff and tile drainage.....	45
3.2.6 Results: Effects of modified tile depths on runoff and flow paths.....	47
3.2.7 Results: Effects of controlled tile drain management on runoff and phosphorus export .	48
3.2.8 Discussion.....	51
3.2.9 Conclusions	54
4 Quebec region studies	55
4.1 Micro-watershed study: 3rd Petite-Rivière-Pot-au-Beurre.....	55
4.1.1 Site description.....	55
4.1.2 Methods	58
4.1.3 Results	61
4.2 Yamaska field site study	66
4.2.1 Introduction	66
4.2.2 Methodology.....	66
4.2.3 Results	71

4.2.4	Conclusions of the micro-watershed and field scale experiment	86
4.3	David basin study	88
4.3.1	Methods	88
4.3.2	Results	100
4.3.3	Climate change effects under free drainage scenario.....	106
4.3.4	Drainage scenarios effect in future climate	112
5	General conclusions	117
REFERENCES CITED		120
APPENDIX 1. Physico-chemical properties of the soil series from the David river basin		151
(Input to SWAT-MAC modeling procedure).		151

List of Tables

Table 3.1. General Circulation models used in this study after using K-means clustering to reduce the final number of future climate scenarios. Models were obtained from the World Climate Research Programme’s Coupled Intercomparison Project phase 5 (CMIP5).	25
Table 3.2. Performance statistics for each of the calibrated variables in the SWAT model.....	26
Table 3.3. Performance statistic values (NS, PBIAS, and R2) after calibration for surface runoff and tile flow	45
Table 3.4. Average annual water balance with permanent changes in the tile height for the 2012 to 2015 period.	47
Table 3.5. Summarized TP and SRP FWMCs from the field site used to create estimates of TP export from the surface runoff and tile flow paths.	50
Table 4.1. Average annual specific water yields, sediment and nutrient fluxes monitored at PRPB micro-watershed outlet for the September 2009 to October 2011, and the April 2013 to October 2014 period. 62	62
Table 4.2. Cumulative stream discharge, subsurface flow, TSS and nutrient exports monitored at the PRPB micro-watershed outlet for the growing season and recharge periods (averages for the 2010-2014 period).	63
Table 4.3. Cumulative stream discharge, subsurface flow and surface runoff for the Controlled drainage project period (July 2015 to September 2017).....	65
Table 4.4. Soil physical properties of field sites.....	70
Table 4.5. Soil chemical properties of field sites.	70
Table 4.6. Tile water specific yields for the Yamaska field sites, together with PREB micro-watershed water yields separated into surface and subsurface contributions for the corresponding free drainage and controlled drainage periods.	74
Table 4.8. Phosphorus speciation and flow-weighted concentration monitored at tile drainage outlets of the free drainage and controlled drainage site. (Growth period effect = Control-No control/No control). 81	81
Table 4.9. Sediment, phosphorus and mineral nitrogen specific loadings estimated for the free drainage and controlled drainage sites according to controlled drainage (growing season) and free drainage (recharge) periods.	83
Table 4.10. Crop yields of soya (2015 and 2017) and spring wheat (2016) determined manually and from the combine yield monitor for the field zones 1 to 12.....	84
Table 4.11: Monthly precipitation and temperature averages (1981-2010) of the study region (Adapted from Environment Canada, 2018 for Sorel station).	90
Table 4.12. Slope gradients distribution across the David river basin.....	91
Table 4.13: Land use distribution in the watershed.	91
Table 4.14. Sources of data used for the parametrization of the SWAT-MAC model for the David river basin.	96
Table 4.15. : Sources of the climatic scenarios used for the hydrologic modeling of David river.	97
Table 4.16. Observed and projected differences in selected climate indicators between historic and future climatic scenarios, averages for Saint-Hubert, L’Assomption and Nicolet meteorological stations.	97

Table 4.17. Selected parameters for the SWAT-CUP calibration procedure for the David basin.....	99
Table 4.18. Averaged annual hydrologic balance components for the David river basin for the 1985-215 historic period (a) and associated monthly standard deviations (b).....	102
Table 4.19. Averaged annual differences in hydrologic balance components resulting from contrasted drainage scenarios (No Drainage - Free drainage) for the David river basin for the 1985-2015 historic period.	103
Table 4.20. Soil properties of Saint-Jude sandy loam and Sainte-Rosalie clay used as SWAT-MAC model inputs.....	106
Table 4.21. Annual averaged differences in selected water balance components between reference and future climates (Future 2041-2070 – Reference 1981-2010) projected by the five different climate scenarios of the CMIP51.....	109
Table 4.22. Averaged annual hydrologic balance components for the David river basin for the future climate (2041-2070) period (a) and associated monthly standard deviations.....	110
Table 4.23. Annual averaged differences in selected water balance components between reference and future climate (Future 2041-2070 – Reference 1981-2010) projected by the five different climate scenarios of the CMIP51.....	112
Table 4.24. Averaged annual hydrologic balance components for the David river basin for the future climate (2041-2070) period under No drainage scenario (a) and associated monthly standard deviations (b).....	114
Table 4.25. Annual averaged differences in selected water balance components between No Drainage – Free Drainage scenarios in future climate (2041-2070) projected by the five different climate scenarios of the CMIP51.....	114

List of Figures

Figure 3-1 Location of the MCW in Canada. With the distribution of the climate station grid (green) and area inside London city limits (yellow). 21

Figure 3-2. Probability density function of the exponentially fitted distribution of daily precipitation (top panels) and kernel fitted distribution of daily temperature (bottom panels) for the ensemble of two future climate scenarios (red, green) from 2080-2100 compared to the average baseline from 1990-2010 (black). 27

Figure 3-3. Annual and seasonal precipitation, ET, and water yield for the historic (0 forcing; 1990-2010) and future climate periods (RCP4.5 and 8.5 forcing; 2080-2100). Color indicates the climate model, when outside of the interquartile range. * indicates significant difference ($p < 0.05$) from historic model based on two-tailed Student t-test and ^ indicates significant difference ($p < 0.05$) between forcings from unpaired two-sample Student t-tests. 29

Figure 3-4 Annual and seasonal surface runoff, tile flow, and groundwater for the historic (0 forcing; 1990-2010) and future climate periods (RCP4.5 and 8.5 forcing; 2080-2100). Color indicates the climate model, when outside of the interquartile range. * indicates significant difference ($p < 0.05$) from historic model based on two-tailed Student t-test and ^ indicates significant difference ($p < 0.05$) between forcings from unpaired two-sample Student t-tests..... 30

Figure 3-5 Average stream flow changes by season for all scenarios (black line) with each individual scenario grouped by RCP. All were during the period 2080-2100 and values are the difference between the projected and the modelled baseline data from 1990-2010. 31

Figure 3-6. Flow duration curves for the watershed outlet with daily flow in 1990-2010 and for 2080-2100 in each season and future climate scenario 33

Figure 3-7. Boxplots for NO₃- loads and FWMC at the watershed outlet in 2080-2100 grouped seasonally, annually, and by GCM forcing (RCP4.5 and 8.5). With forcing “0” representing the historic period (1990-2100). Color indicates the climate model, when outside of the interquartile range. * indicates significant difference ($p < 0.05$) from historic model based on two-tailed Student t-test and ^ indicates significant difference ($p < 0.05$) between forcings from unpaired two-sample Student t-tests. 35

Figure 3-8. Boxplots for SS loads and FWMC at the watershed outlet in 2080-2100 grouped seasonally, annually, and by GCM forcing (RCP4.5 and 8.5). With forcing “0” representing the historic period (1990-2100). Color indicates the climate model, when outside of the interquartile range. * indicates significant difference ($p < 0.05$) from historic model based on two-tailed Student t-test and ^ indicates significant difference ($p < 0.05$) between forcings from unpaired two-sample Student t-tests. 36

Figure 3-9. Boxplots for TP loads and FWMC at the watershed outlet in 2080-2100 grouped seasonally, annually, and by GCM forcing (RCP4.5 and 8.5). With forcing “0” representing the historic period (1990-2100). Color indicates the climate model, when outside of the interquartile range. * indicates significant difference ($p < 0.05$) from historic model based on two-tailed Student t-test and ^ indicates significant difference ($p < 0.05$) between forcings from unpaired two-sample Student t-tests. 38

Figure 3-10. Location of LON in Canada (left) and other field site details (right; topography, observation station locations, and boundary). Also shows the location of the climate station used to supplement missing data at the field site (Jamestown). 40

Figure 3-11. Shows two typical CD management approaches used in southern Ontario (#1 = RTDGS; #2 = RTDNC). Blue arrows represent the raising or lowering of the drain gate 3 weeks before planting and harvest, while blue lines represents a simplified representation of the water table depth changes. Major

difference is the management during the NGS, which typically occurs from late fall to early spring for most crops.	44
Figure 3-12. Graphical performance of surface runoff (top; SURQ) and tile flow (bottom; TILEQ) after calibration of the LON HRU model. In addition to performance, it shows monthly precipitation (top) and average air temperatures (bottom) over the 2012 to 2015 period. Arrow with ND indicates no data due to sensor failure.	46
Figure 3-13. Monthly changes in the water balance over the 2012 to 2015 period with continuously raised tiles (RTDcont). Bars show the difference between RTDcont and the free tile drainage (FTD) scenario . A positive value denotes an increase in flow and a negative denotes a reduction in flow. Black bars indicate the growing season over the study period and boxes showing the NGS.	48
Figure 3-14. Cumulative tile flow (TILEQ; blue), surface runoff (SURQ; red), and total runoff (black) for RTDGS (solid line) and RTDNC (dotted line) over the 2012 to 2015 period.	49
Figure 3-15. Monthly cumulative loads (lines) and change in loads between RTDGS and RTDNC from 2012 to 2015 for TP and SRP in surface runoff (SURQ; a) and tile flow (TILEQ; b).....	50
Figure 3-16. (a) Changes in the tile flow, surface runoff, and runoff annually in the LON field site transplanted into the MCW during the 1990-2010 period (blue), 2080-2100 period (red), and 2080-2100 period with continuous CD (green). Also, shows tile flow seasonally (b) and surface runoff seasonally (c).53	
Figure 4-1. Location of project experimental sites including 3e Petite-Rivière-Pot-Au-Beurre (PRPB) micro-watershed, Yamaska field sites and David River Basin.	56
Figure 4-2. Soil map (a) and land use map (b) of PRPB micro-watershed (Michaud et al., 2012).....	57
Figure 4-3. PRPB monitoring station including acoustic and barometric probes (a), multi-parameter probe (b) installed within a flotation device.....	58
Figure 4-4. Temporal variability in instantaneous (15 min.) stream flow rate, electrical conductivity and turbidity signals at PRPB monitoring station for a single late fall rainfall event.	59
Figure 4-5. Daily precipitation and specific water yields separated according to the geochemical signal at PRPB micro-watershed outlet for the april 2013 to November 2014 period.....	62
Figure 4-6. Cumulative surface runoff and subsurface flow (a,b), nitrates yields (c) and Total phosphorus yields (d) monitored at PRPB micro-watershed outlet for the 2010-2014 period.	63
Figure 4-7. Temporal variability in the instantaneous (15 min.) electrical conductivity signal at PRPB monitoring station (Green: growing season; Blue: recharge period), shown as a function of stream flow rate and season for the 2016 monitoring period.....	64
Figure 4-8. Daily precipitation and specific surface and subsurface water yields, estimated using geochemical signals at the PRPB micro-watershed outlet for the Controlled drainage project period (July 2015 to September 2017).....	65
Figure 4-9. Aerial photograph, Lidar-derived elevation model and surface flow paths of experimental field sites.	68
Figure 4-10. Location of the 12 observation wells and monitoring stations of the subsurface drain collectors.	68
Figure 4-11. Installation of the observation wells.	69
Figure 4-12. Monitoring stations of the subsurface drain collectors.	69
Figure 4-13 Water table stage variability monitored within individual observation wells for the controlled drainage site (no. 1 to 6) and Free drainage site (no. 7 to 12) for the 2015-2017 period.....	72

Figure 4-14. Precipitation, and averaged water table depth variability for the observation wells from the Controlled drainage site (no. 1 to 6) and the ones from Free drainage site (no. 7 to 12) for the 2015-2017 period.	72
Figure 4-15, Tile drainage water yield and averaged water table depth variability for the observation wells from the Controlled drainage site (no. 1 to 6) and the ones from Free drainage site (no. 7 to 12) for the 2015-2017 period.	73
Figure 4-16. Specific tile drain flow form the Yamaska free drainage site coupled with the hydrometric data from the 3rd Petite-Rivière-Pot-au-Beurre micro-watershed.	76
Figure 4-17. Variability in total phosphorus and nitrates concentrations of tile drainage waters from the free drainage site with respect to instantaneous discharge and date.....	79
Figure 4-18. Variability in total phosphorus and nitrates concentrations of tile drainage waters from controlled drainage sites with respect to instantaneous discharge and date.....	80
Figure 4-19. Sediment, phosphorus and mineral nitrogen loading time series estimated for the free drainage and controlled drainage sites according to controlled drainage and free drainage periods (Note that scales differ among sites).....	82
Figure 4-20. Crop yields of soya (2015 and 2017) and spring wheat (2016) determined manually and from the combine yield monitor for the field zones 1 to 12.....	85
Figure 4-21. Spatial variability in crop yields data captured by the yield monitor for soya in 2015 nd 2017, as well as for spring wheat in 2018.	85
Figure 4-22. Location of the David river basin.....	90
Figure 4-23. Hydrometric network (a), elevation model (b), land use (c) and soil map(d) of David river watershed. The distribution and soil properties of soil map units are described in appendix 1.0.	92
Figure 4-24. Conceptual representation of original SWAT matrix flow algorithms (a) and macropore domain flow algorithms within SWAT-MAC (b) (Adapted from Poon, 2013).....	95
Figure 4-25. Daily minimum, maximum and average stream discharge (m^3sec^{-1}) of David river (323 km^2) for the 1970-2014 period.....	99
Figure 4-26. Average monthly observed and simulated discharges flow of David river basin for the 1985-2015 historic calibration period.	101
Figure 4-27. Average monthly differences in hydrologic balance components resulting from contrasted drainage scenarios (No Drainage - Free drainage) for the David river basin for the 1985-2015 historic period.	105
Figure 4-28. Monthly averages and standard deviation in surface runoff volumes resulting from the modeling of contrasted drainage scenarios (<i>No Drainage - Free drainage</i>) for corn and soybean crops cultivated on Saint-Rosalie clay and Saint-Jude sandy loam soil series for the 1985-2015 historic period.	108
Figure 4-29. Annual averaged differences in water balance components between reference and future climate (Future 2041-2070 – Reference 1981-2010) projected by the five different climate scenarios of the CMIP5.	109
Figure 4-30. Monthly averaged differences in selected water balance components between reference and future climates (Future 2041-2070 – Reference 1981-2010) projected by the five different climate scenarios of the CMIP51.	111
Figure 4-31. Monthly averaged differences in selected water balance components between <i>No drainage</i> and <i>Free drainage</i> scenario in future climates (Future 2041-2070 projected by the five different climate scenarios of the CMIP51.	113

Figure 4-32. Monthly averages and standard deviation in surface runoff volumes resulting from the modeling of contrasted drainage scenarios (No Drainage - Free drainage) for corn and soybean crops cultivated on Saint-Rosalie clay and Saint-Jude sandy loam soil series for the 1985-2015 historic period.
..... 116

List of Abbreviations

AAFC	Agriculture and Agri-food Canada
ArcSWAT	ArcGIS-ArcView extension and interface for SWAT.
CD	Controlled Drainage
CMIP5	Coupled Model Intercomparison Project Phase 5
DDRAIN	Depth to subsurface tile drain (mm)
DEPIMP	Imperveous Layer Depth (mm)
DRAIN_CO	drainage coefficient (mm d-1)
DRP	Dissolved Reactive Phosphorus
ET	Evapotranspiration
FTD	Free Tile Drainage
FWMC	Flow-Weighted Mean Nutrient Concentrations
GCM	General Circulation Model
GDRAIN	tile drain lag time (h)
GHG	Greenhouse Gas
HRU	Hydrological Response Unit
LATKSATF	Lateral Saturated Hydraulic Conductivity (mm h-1)
MCW	Medway Creek Watershed
NO3	Nitrate
NO3 Nitrate	Nitrogen
NS	Nash-Sutcliffe Coefficient
P	Phosphorus
PBIAS	Percent Bias
PET	Potential Evapotranspiration
PRPB	3rd Petite-Rivière-Pot-au-Beurre micro-watershed
RCP	Representative Concentration Pathways
RTDcont	Continuous Raised Tile Drainage (Drainage controlled, year round/continuously)
RTDGS	Controlled Drainage Used During Growing Season Only (planting to harvest)
RTDNC	Controlled Drainage Used Year Round but Tiles Opened before planting and harvest and then closed again
SOL_AWC	Available Water Capacity
SOL_BD	Bulk Density
SOL_K	Saturated hydraulic conductivity
SS	Suspended Sediments
SWAT	Soil Water Assessment Tool
SWAT-CUP	A program designed to integrate various calibration/uncertainty analysis programs for SWAT
TDRAIN	time to drain soil to field capacity (h)
TP	Total Phosphorus
UTRB	Upper Thames Research Basin

1 INTRODUCTION

A dominant portion of the most productive farmland in Ontario and Quebec benefits from artificial drainage. Historically, drainage systems have been installed to clear excess water in spring, and promote early seeding and profitability of crops. The benefits of artificial subsurface drainage on crop productivity are obvious and promote the diversification of crop production. However, drainage waters have been shown to be a significant pathway for nutrients (N and P), where up to 80% of total surface water yields originate from subsurface flow paths. Moreover, climate change studies indicate that water stresses to crop productivity will increase in future climate, together with a longer growing season, related to an earlier snowmelt. The water deficit will be exacerbated by a 1-month earlier loss of the snowpack, higher temperatures, and more infrequent but intense rain storms. These stressors clearly demand technical solutions, namely controlled drainage systems, that has the potential to stabilize soil moisture conditions throughout the growing season and minimize fluctuations in crop yields and economic returns in rural Ontario and Quebec. The potential benefits resulting from greater N and P retention in agroecosystems are thus economic (greater fertilizer use efficiency, higher yields) and environmental (less eutrophication in freshwater systems). Despite the numerous benefits, agricultural producers have been slow to adopt this technology. Hydrologic modeling studies that clearly document water budget, crop response and nutrient fluxes to controlled drainage are lacking.

The main objective of the project was to assess the agronomic and environmental feasibility (limitations) and benefits of controlled drainage, as well as to provide technical guidelines on the application of the method for Quebec and Ontario rural communities. The benefits of controlled drainage systems, where control chambers are installed at existing collection outlets to stop runoff when the water table reaches a critical depth, have been investigated on field sites. Also, through a hydrologic modeling approach, the project team have also simulated the effects of controlled drainage on water budgets and uptake, crop growth, as well as water quality (N and P loads) in the context of climate change within two agricultural watersheds of Ontario (Upper Thames river) and south-western Quebec (Yamaska river).

Following a brief literature review, the following sections of the report first describe the methodology and results from the watershed (Medway creek watershed) and field (Londesborough) studies in Ontario, followed by field (Yamaska), micro-watershed (3e Petite-Rivière-Pot-au-Beurre) and basin studies (David river) in Quebec.

2 LITERATURE REVIEW

This literature review focuses specifically on the hydrology and dynamics of flow nutrients (N and P) in subsurface drainage systems. Since adoption of a new system of controlled drainage depends on the producers' experiences, the feasibility of such a system needs to consider the environmental and agronomic benefits of such a system, which are largely dependent on local climatic conditions. Special attention was paid in this review on the results of studies carried out in Quebec and Ontario.

WATER BALANCE AND DRAINAGE DEPTHS: Since 1997, IRDA has established many long-term hydrometric monitoring sites within watersheds and sub-watersheds. The comprehensive database accumulated by IRDA staff provides in-depth and exhaustive knowledge of the subsurface water transfer, to groundwater and surface recharge, as well as the global water balance for each sub-watershed studied (Michaud et al., 2005; 2009a; 2009b; 2012). Hydrograph separation undertaken on data collected from 18 sub-watersheds permitted the group to distinguish and partition the sources of water reaching the watershed outlet based on the distinct geochemical signals of subsurface drainage, groundwater, surface runoff, and so on. Long term monitoring sites for hydrology and meteorological conditions have also been established in Ontario. Hydrometric data are supported with water quality data collected throughout the watersheds. To date, these data have demonstrated that subsurface flow represent the dominant hydrologic pathway from fields on an annual basis (up to 80%). Work conducted at these sites and others in Ontario (Macrae et al., 2007a,b, Macrae et al., 2010) demonstrates that much of the nutrient loss both at the field scale and watershed scale occurs during storm and thaw events, and the snowmelt period (spring freshet) represents the dominant hydrologic and nutrient flux on an annual basis.

In Quebec, the results of the hydrograph separation analysis revealed that more than 50% of water at the sub-watershed outlet had travelled through subsurface drainage before it re-entered streams and rivers in the Montérégie and Mauricie sub-watersheds. At the basin scale, Macrae et al. (2007a) estimated that 40% of the annual runoff in a headwater catchment was supplied by drainage tiles. In contrast, surface runoff made a major contribution to the water balance and quality in rivers of sub-watersheds in the Estrie, Chaudières-Appalaches and Témiscouata regions. Drainage water level was greater in the Montérégie, since the region is characterized by relatively flat terrain that was almost entirely devoted to agriculture (>95% of the land use in many regions) and was systematically and extensively tile-drained. In the sub-watersheds of Pot-au-Beurre (Sorel), Esturgeon (Saint-Martine) and Ewing (Bedford), approximately 74 to 79% of the water in tributaries was transferred there from terrestrial systems, representing an input of between 193 and 363 mm/year, on average.

Since P concentrations in surface runoff are, on average, 10 times higher than P concentration in subsurface drainage, it is beneficial from a water quality perspective to promote water infiltration

and possibly retain more nutrients in the soil-plant system, allowing for plant uptake or other reactions in the soil matrix, thus protecting surface water quality in freshwater streams and rivers. Considering the agroenvironmental and practical implications of agricultural drainage, there is an extremely important opportunity here to slow down or retain a portion of the subsurface water through the establishment of controlled drainage structures. Controlled drainage structures are not widely used in Ontario. This study, through a combination of modelling and field data collection, permits the examination of whether or not such structures may be feasible in Ontario soils/watersheds both under contemporary and future climate scenarios.

SUBSURFACE FLUXES OF NITROGEN AND PHOSPHORUS: At the same time as water balance measurements were taken, IRDA's network of experimental sub-watersheds were chosen for site-specific research on the mean annual N flux from agricultural fields. Between 6 and 62 kg N/ha-yr were exported to streams and rivers, with the highest N fluxes being mostly in the form of NO₃-N. In sub-watersheds of western Montérégie, which is characterized by intensive annual crop production, the N losses from agricultural land reached 62 kg N/ha-yr, followed by sub-watersheds of Chaudières-Appalaches (43 kg N/ha-yr), an area with high density livestock raising operations. The NO₃-N flux was linked to water that moved through the soil profile and was lost from agroecosystems through subsurface drainage, which is of concern since these values are some of the highest reported for NO₃-N loss in the eastern part of North America. Seasonal partitioning of the NO₃-N fluxes in several sub-watersheds demonstrated that a considerable amount of NO₃-N was lost during the growing season (from May to September). The Esturgeon (Sainte-Martine), Ewing stream (Bedford) and Petit-Pot-au-Beurre (Sorel) lost 31%, 23% and 29%, respectively, of the annual NO₃-N flux during the growing season. Since crops are growing during this period, it seems possible that controlled drainage systems offer an opportunity to retain and utilize NO₃-N (via plant uptake) that is otherwise lost through free-flowing agricultural drainage in these regions. Loss of NO₃-N during the growing season also represents a loss of fertilizer N and lower fertilizer N use efficiency, which is costly for producers and detrimental to water quality in streams and rivers. Clearly, agricultural producers need to know what controlled drainage systems offer with respect to the bottom line. Although little is known about the potential impacts of controlled drainage structures in Ontario systems, tiles represent a significant source of nitrate to surface water bodies (e.g. Mengis et al., 1999; Macrae, 2003). In two field plots on soils with contrasting texture and agricultural drainage systems in eastern Montérégie, Enright and Madramootoo (2004) found that 80% of the annual water volume exported was through subsurface flow in free-flowing agricultural drainage. They estimated that most of the P export from these fields occurred through the agricultural drainage, and further predicted two-fold less P export in drains from a clayey soil than a sandy loam soil, which had the highest soil test P level of the two field plots. In Ontario fields, tiles have been shown to represent the dominant hydrologic pathway from fields (up to 80%), but are a small source of both dissolved and particulate P relative to surface runoff (15-30% of field

scale losses) (Van Esbroeck et al., 2016). This has been shown in both clayey and sandy loam soils. Eastman and collaborators (2010) provided more in-depth study of the same eastern Montérégie sites in Quebec, over several growing seasons, and found that P losses in the drains corresponded to between 33 and 55% of the total P exported each year. Poirier et al. (2012a) studied water quality in surface runoff and subsurface tile drainage outlets of 10 fields in the same region, including contrasting soil texture and crop type as variables in their study. Uniquely, this study was able to couple P export at the field scale with measurements of P concentration at the Ewing sub-watershed outlet, which was instrumented for hydrological measurements by the IRDA research team. This study emphasized the importance of subsurface preferential flow as a major pathway for particulate P transport, as well as the colloidal nature of particulate P and its high bioavailability to cyanobacteria. Realizing that the electrical conductivity signal was distinct between surface runoff water and subsurface water sources, Michaud et al. (2019) estimated that dissolved P discharged through agricultural drainage represented between 43% (in autumn) and 52% (in spring) of the total dissolved P load exported at the field scale.

Most of the dissolved P flux (about 80%) moved through the soil profile through preferentially flow pathways before it reached agricultural tile drainage and was discharged from the agroecosystem. Similar studies using electrical conductivity have yet to be conducted in Ontario, but are necessary to improve scientific understanding of flow paths in soil (matrix vs. preferential flow) and above vs. below the soil surface. A comparison of data collected across Ontario and Quebec will be a significant scientific contribution. Based on the empirical estimation of P losses from agricultural drainage and surface runoff reported by Michaud et al. (2019), Poon (2013) developed and validated an algorithm that partitioned infiltrating water into preferential and matrix flow pathways and predicted their movement through the soil profile to tile drainage, and eventually to the watershed outlet. Model output was calibrated using data from the same sub-watershed studied by Michaud et al. (2019) and Poirier et al. (2012), by integrating the algorithm into the hydrologic model, SWAT-QC, that was previously developed by Michaud and collaborators (2008).

CONTROLLED DRAINAGE TO MITIGATE DIFFUSE POLLUTION IN SURFACE WATERS: Although controlled drainage structures are not widely adopted by agricultural producers in Quebec and Ontario, there is evidence from several experiments indicating the potential of this method to control N loss from agroecosystems. A field plot study under corn production in eastern Ontario by Lalonde et al. (1996) documented the effects of controlled drainage on the water table level, the water volume exported from the field, and the NO₃-N concentration in drainage water. Maintaining the water table at 25 to 50 cm above the tile line (which was installed 1 m below the soil surface) reduced the water flow to the drain by 59 to 95%. There was a 62 to 95% reduction in the NO₃-N concentration of the drainage water, as well. In Soulanges county of Quebec, a subsurface irrigation study that maintained the water table between 70 and 80 cm below the corn crop resulted in a 70% reduction in NO₃-N loss, representing a gain of 6.6 kg N/ha-yr for crop production (Zhou

et al. 2000). This interpretation is supported by a concurrent study at the site by Kaluli et al. (1999), who found no increase in denitrification during the growing season (May to October). Mejia and Madramootoo (1998) also observed a reduction of NO₃-N concentration in agricultural drainage water, of 84% when the water table was set at 50 cm and of 75% when the water table was maintained at 75 cm. In addition, the water volume emitted by the drains was 42% lower in plots where the water table was set at 50 cm, compared to free-flowing agricultural drainage. The authors concluded that controlled drainage provided a number of environmental and economic benefits on farms, notably improved fertilizer use efficiency due to control of N fertilizer loss that typically occurs through drainage in humid temperate climates. However, increased soluble P concentrations were observed under sub-irrigated plots in Montérégie, as compared to free drainage management (Stämpfli and Madramootoo, 2006; Sanchez Valero et al., 2007). The increase was related to elevated P solubility in response to anoxic conditions within the excessively P rich sandy loam.

More recently, the Ontario-based projects in the Canada-wide initiative « Watershed evaluation of beneficial management practices » funded by Agriculture and Agri-Food Canada evaluated the merit of controlled drainage on non-sloping clayey loam soils in the South Nation watershed, near Ottawa. This study demonstrated a clear improvement in crop yields, by 3% in grain corn and 4% in soybean, with controlled drainage. Water quality at the drain outlet was improved with subsurface controlled drainage since nutrient losses were avoided when the water and dissolved nutrients were retained in the agricultural fields. At the watershed outlet, water quality improvements were marked by a 65% reduction in the NO₃-N load and 63% reduction in the P load during the growing season (AAC, 2013).

3 ONTARIO REGION STUDIES

3.1 Medway Creek Watershed Study

3.1.1 Specific objectives of this portion of the study:

In this part of the study, the Soil Water Assessment Tool (SWAT) model was used to evaluate the impacts of climate change on runoff and nutrient loads in the Medway Creek watershed (200 Km²), a subwatershed within the Upper Thames River Watershed in Ontario, Canada, which discharges into Lake St. Clair and eventually Lake Erie. The specific objectives of the study were to determine the effect that future climates will have on the seasonal characteristics of hydrology, suspended sediment, nitrate, and total phosphorus export.

3.1.2 Description of the Medway Creek Watershed

The MCW is a small (205 Km²) watershed located in southwestern Ontario (43°00'52.9"N 81°16'36.6"W; Figure 3.1) and is one of 28 sub-watersheds that contribute to the Upper Thames River Basin (UTRB), which subsequently drains into Lake St. Claire, and eventually into Lake Erie. Land use within the watershed is primarily agricultural (83%), with some natural (11%) and urban (6%) areas. Since most of the land use is agricultural, a significant portion of the MCW has tile drainage (~ 65%) to facilitate field access in spring and improve crop yields. Major crops grown within the watershed consist of corn, pasture, soybean, and winter wheat. There are many livestock operations within the watershed with an average density of 24 animals per hectare. Poultry represent the majority of livestock operations (97%) and P production (31%), and swine operations represent 1% of livestock operations. Populations of dairy and beef cattle are relatively small in the watershed. Approximately 85% of the total soil area within the watershed consists of clay loam (33%), silty loam (32%), or silty clay loams (20%) (Upper Thames River Conservation Authority, 2012). The watershed has a mean slope of 2 degrees, with the northwestern part of the watershed increasingly sloped because the watercourse is located between two moraines causing rolling topography. The southern portion of the watershed is steep as well and mostly consists of urban land use, whereas the central portion is much flatter.

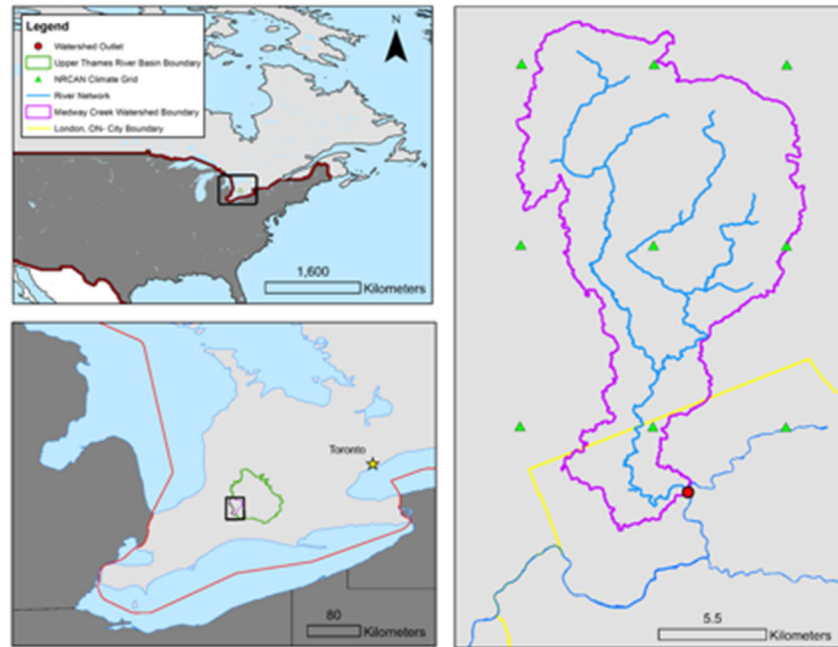


Figure 3-1 Location of the MCW in Canada. With the distribution of the climate station grid (green) and area inside London city limits (yellow).

The climate in this region is classified as humid continental with an average 30-year historic normal monthly precipitation of 84 mm (1012 mm annually, 19% as snowfall) determined using data from the London Airport Environment Canada station. As is typical for the region of southern Ontario, there is a distinct seasonal pattern in annual runoff with maxima in spring associated with snowmelt and convective spring storms, and minima in summer due to high evapotranspiration (ET) rates. Although flow occurs throughout the year, the summer high average temperatures (19.6 °C) can occasionally result in the occurrence of drought-like conditions.

3.1.3 Hydrologic and Climate Modelling Procedures

The Soil-Water-Assessment Tool (SWAT), a semi-distributed physically based watershed model capable of continuous simulation over long periods was used in this study. The model uses a combination of empirical relationships and process-based equations. It operates by dividing the watershed up into sub-basins, which can be further subdivided into hydrological response units (HRUs) which are unique combinations of land use, soils, and slope. Within the model structure, precipitation plays a key role and is a major driver of all other processes that occur. Hydrologic processes simulated by SWAT include surface runoff, infiltration, canopy storage, percolation, evapotranspiration (Hardgreaves method; IPET=2), lateral subsurface flow, and base flow. Soil erosion is determined using the Modified Universal Soil Loss Equation, which is influenced by

rainfall and surface runoff, and estimated using the Soil Conservation Service (SCS) curve number method (ICN=1). Within the soil profile, the SWAT model is able to simulate nutrient transformations and movement using the P and nitrogen (N) cycles. Once the nutrients reach the main channel, an adapted version of QUAL2E is used for nutrient routing. Given that the SWAT model was developed in Texas, percolation through the soil profile is not as representative of what occurs in Canada, where soil textures, moisture conditions and precipitation patterns differ from those in Texas. Therefore, SWAT-MAC was used (modified version of SWAT 2012), as it is adapted to better simulate flow to tile drains by altering the hydrological algorithms influencing percolation through the subsurface.

3.1.3.1 Model Parameterization and Calibration Methods

The DEM (10 m resolution) used was supplied by the Upper Thames River Conservation Authority (UTRCA) and was derived using aerial imagery from the Southwestern Ontario Orthophotography Project (SWOOP) in 2010 (Ministry of Natural Resources and Forestry, 2015). Land use data was obtained from Agriculture and Agri-Food Canada's (AAFC) annual crop inventory in 2014. Soil physical parameters (soil texture, bulk density, soil depths), at a scale of 1:50000 were obtained from the soil map distributed through Land Information Ontario. Soil available water capacity was estimated using a pedotransfer function developed by Saxton and Rawls (2006). Soil albedo was estimated using the ranges mentioned by Dobos (2003). Climate data, including gridded (10 km resolution) daily precipitation and daily maximum and minimum temperatures for 63 years (1950-2013) was generated by Natural Resources Canada (NRCAN) using thin-plate smoothing splines (McKenney et al., 2011; McKenzie et al., 2013) and was provided by Ouranos. Streamflow quantity (daily interval) and quality (monthly sampling interval) of the MCW, collected from 1978-2014 at the watershed outlet, was provided by the UTRCA. Monthly load estimates of sediment and nutrients (TP, NO₃-) were determined using Flux32 and a regression applied to individual daily flows (Method 6) based on the procedure developed by Walker (1996). The mean coefficient of variation was subsequently calculated as a measure of error to assess if the variable would be suitable for modelling.

To delineate subbasins, the automatic watershed delineation option in ArcSWAT with the recommended threshold drainage area and a stream network created by the UTRCA. Land use, soil, and slope were subsequently overlain to create hydrologic response units (HRUs) and a minimum area threshold of 10/15/15 percent respectively was applied to reduce the SWAT model into 19 subbasins with 318 HRUs. For the creation of the HRU management files, crop rotations were identified, but the specific crop type on each HRU on an annual basis was not determined as this was not feasible, and, it was assumed that this would have minimal effect on the overall hydrology at the watershed scale. Given that HRUs were not spatially explicit within the subbasin and eventually cycled back to the original crop, it was assumed that there would be minimal effect

on nutrients over a longer term. Using the AAFC crop inventory data from 2011-2014, a crop rotation map was created through ArcMap overlay and it was determined that the dominant crop rotation was corn-soybean-winter wheat. Representative tillage systems and fertilizer application rates for each crop were developed based on the dominant rotation (UTRCA and Wanhong Yang, personal comm.). Yearly estimates of manure production in the watershed were calculated based on livestock statistics for the MCW, and all manure was divided up amongst the corn HRUs to fulfill N needs. The tile drainage distribution with respect to the HRUs was determined from a dataset obtained from LIO (Ministry of Agriculture, Food and Rural Affairs, 2015). Given that the full extent of tile drainage within Ontario is not known, all cash cropped fields within the MCW were assumed to be tile drained. This is a reasonable assumption given tile drainage trends in Ontario. The tile drainage parameters depth to subsurface tile drain (DDRAIN= 900 mm), time to drain soil to field capacity (TDRAIN= 24 hours), and tile drain lag time (GDRAIN = 12 hours) were set based on what is typically observed in Ontario.

For sensitivity analysis, calibration, and validation of the model, the SWAT- Calibration and Uncertainty Programs (SWAT-CUP) software package was used with the SUFI-2 algorithm for parameter calibration (Abbaspour, 2015). The calibration period was from 2006 to 2010, and the validation period from 2011 to 2013, to capture both wet and dry years, both on a monthly time step with a 3-year warm up period to mitigate the effect of initial conditions. At the watershed outlet, observed flow, SS, NO₃⁻, and TP variables were calibrated sequentially with multiple iterations (3-5) using the SWAT-CUP interface until there was only a marginal increase in the objective function, which was the Nash-Sutcliffe coefficient of model efficiency (NS). To measure the performance of the fitted parameters set and model during the calibration period, NS and the percent bias (PBIAS) were used and evaluated based on criteria developed by Moriasi et al. (2007b).

3.1.3.2 Future Climate Scenarios

To assess the impact that climate change will have on water quality and quantity, a bias corrected Global Circulation Model (GCM) ensemble was developed and coupled with the parameterized SWAT model simulated from 1980-2100, while keeping land use and management constant. A climate ensemble consists of multiple GCMs and GHG emission scenarios that are combined and used in analysis to reduce the uncertainty associated with future climate projections (Fowler et al., 2007; Honti et al., 2014). The bias corrected GCM ensemble consisted of a 10km x 10km gridded daily temperature (max and min) and precipitation dataset provided by Ouranos, a research consortium on regional climatology and adaptation to climate change (Ouranos, 2018).

To develop the climate change scenarios used in this study, all available Coupled Model Intercomparison Project Phase 5 (CMIP5) global climate models with precipitation, minimum temperature, and maximum temperature were obtained (Taylor et al., 2013). For each model, two emission scenarios known as Representative Concentration Pathways (RCP) were used to drive

each of the GCMs. Each RCP is named after the amount of net radiative forcing (W/m^2) expected by 2100 due to projected GHG emissions. In this study, the two RCPS selected were RCP4.5 and RCP8.5, where RCP8.5 is the worst-case scenario in terms of GHG emissions and concentration trajectories. The RCP4.5 emission scenario represents a stabilizing radiative forcing by 2100 due to implementation of GHG emission prices and represents a more optimistic representation of future GHG concentrations.

To reduce the number of scenarios and retain maximum uncertainty coverage in changes of temperature and precipitation in the future, k-means cluster analysis was used (Casajus et al., 2016). In addition, the 22 retained simulations are ordered in such a way that each subset of this selection also seeks to maximize uncertainty coverage. To create the ensemble of catchment-scale future climate scenarios, data was empirically downscaled using the gridded NRCAN (10 km) interpolated station data and the quantile mapping method (Mpelasoka and Chiew, 2009). To reduce SWAT model input/output processing time and still capture the uncertainty associated with climate model outputs, the first 10 scenarios from the final selection were chosen for the final ensemble (Table 3).

Table 3.1. General Circulation models used in this study after using K-means clustering to reduce the final number of future climate scenarios. Models were obtained from the World Climate Research Programme’s Coupled Intercomparison Project phase 5 (CMIP5).

GCM abbreviation	Institute ID	RCP	Description
INM-CM4	INM	4.5 and 8.5	Institute for Numerical Mathematics
GFDL-ESM2M	NOAA GFDL	4.5	NOAA Geophysical Fluid Dynamics Laboratory
MPI-ESM-LR	MPI-M	4.5 and 8.5	Max-Planck-Institut für Meteorologie (Max Planck Institute for Meteorology)
CanESM2	CCCMA	4.5 and 8.5	Canadian Centre for Climate Modelling and Analysis
ACCESS1.3	CSIRO-BOM	4.5 and 8.5	Commonwealth Scientific and Industrial Research Organization (CSIRO) and Bureau of Meteorology (BOM), Australia
BNU-ESM	GCESS	8.5	College of Global Change and Earth System Science, Beijing Normal University

3.1.4 Model Calibration and Validation Results

After sensitivity analysis, the 73 parameters were reduced to those considered the most sensitive to flow at the watershed outlet (23) and sediment and nutrient loads (18). By adjusting these parameters within their realistic maximum and minimum ranges in SWAT-CUP, an acceptable model was achieved. For the calibration and validation periods, the timing of observed peak flows matched the simulated values. Based on the criteria devolved by Moriasi et al. (2007b), all calibrated and validated variables (Table) had a satisfactory performance rating or above, with flow having a very good performance rating with respect to the NS and a good rating based on the PBIAS. During calibration and validation, the overall performance rating for SS was good, while TP and NO₃⁻ were satisfactory with respect to the NS. The model’s PBIAS for sediment and nutrient variables had a very good performance rating in both the calibration and validation period.

Table 3.2. Performance statistics for each of the calibrated variables in the SWAT model.

Variable	Calibration		Validation	
	NS	PBIAS	NS	PBIAS
Stream Flow	0.87	-10.2	0.81	-10.9
Suspended Sediment	0.75	2.2	0.62	-14.8
Nitrate	0.61	-0.2	0.57	3.9
Total Phosphorus	0.62	17.9	0.52	14.8

3.1.5 Future and baseline climate simulations

The models used in the current study project mean annual temperatures to increase by 0.9 to 3 degrees Celsius by 2050, and 1.3 to 7.1 by 2100. The downscaled GCM ensemble in the current study, Figure 3-2) shows greater temperature increases in winter than in summer. These estimates are comparable to previous research that projected mean annual air temperatures in the Lake Erie basin to increase by 2.4 to 7.2 °C by 2080 (McDermid et al., 2015).

The current model projections corroborate the work of Reid et al. (2007) who suggested that Ontario would experience shorter winters, longer growing seasons, and more extreme heat waves in summer as a result of climate change. Indeed, the current study predicts an increase in the probability of extreme temperatures and a decrease in lower temperatures in all seasons (Figure 3-2). Annual projections for the Great Lakes Basin indicate an average annual increase in precipitation of 106 mm for the RCP4.5 and RCP8.5 scenarios by 2080 (McDermid et al., 2015), which is comparable to the average of the ensemble projections in the current study that indicate a 90 mm annual precipitation increase.

The NGS is an important factor contributing to total annual water yields and nutrient export in southern Ontario (Macrae et al., 2007; Van Esbroeck et al., 2017). The ensemble projections indicate that in winter and spring there will be a greater intensification of the climate, and the models unanimously predict increases in the frequency and magnitude of extreme precipitation events (Figure 3-2) and volumes, and, a greater proportion of precipitation will fall as rain, and there will be more snowmelt events (Marianne et al., 2003). Trends during the summer period are more variable and less clear. King et al. (2012) also projected increased summer precipitation variability in the UTRB. Overall, the projected shifts in precipitation and temperature distributions indicate a shift towards longer dry periods between events, further increasing drought risk, with drought

periods interrupted by more extreme rainfall. Such changes are anticipated to have impacts on runoff quantity and quality.

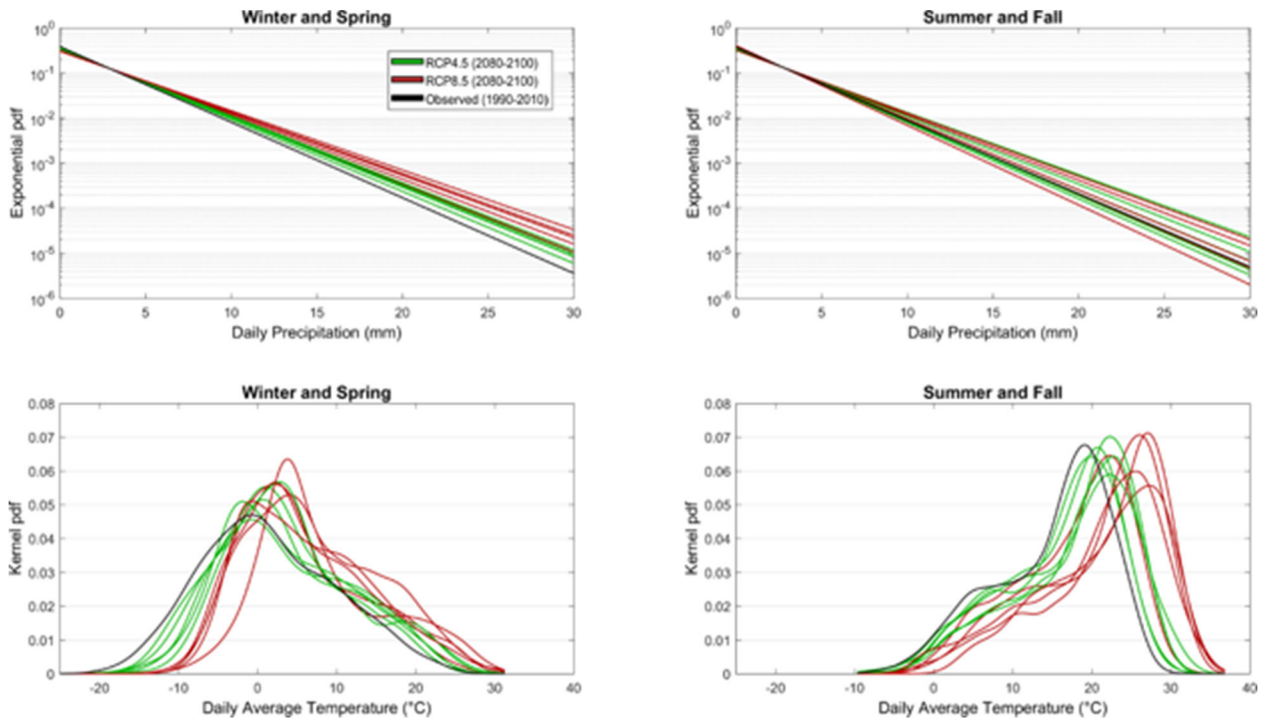


Figure 3-2. Probability density function of the exponentially fitted distribution of daily precipitation (top panels) and kernel fitted distribution of daily temperature (bottom panels) for the ensemble of two future climate scenarios (red, green) from 2080-2100 compared to the average baseline from 1990-2010 (black).

3.1.6 Model Results: Water balance and flow path changes

3.1.6.1 Annual and seasonal changes in flow paths and magnitudes

The future climate ensemble projects that by the 2080-2100 period, the average annual precipitation will increase by 90 mm (range: 4 to 205 mm), and changes will be most pronounced during winter. The SWAT model predicts ET to increase on average by only 50 mm (range: 6 to 88 mm), resulting in an increase in surplus water. Consequently, the model projected that water yield would increase by an average of 38 mm (range: -4 to 114 mm) annually by the 2080-2100 period (Figure 3-3a, f, and k). Seasonally, the SWAT model, using the future climate ensemble, projected that water yield would increase in winter (JFM) and summer (JAS), but decrease in the spring (AMJ) and fall (OND) (Figure 3-3) (with the exception of the RCP4.5 group that projected an increase in spring). In winter, the model projected a large increase in subsurface flow through tiles and a simultaneous decrease in surface runoff for both RCP groups (Figure 3-3), whereas in spring projected changes are much smaller, although water surpluses are large (Precipitation change > ET). In contrast, projected water balance changes in summer and fall months are small

relative to winter and spring, have greater variability, and are generally not significant, with the exception of fall ET and water yield, and summer tile flow (RCP8.5 group; Figure 3-3 and 3-4).

In winter, the model projects increased tile flow because air temperatures in the future climate are warmer, which leads to modification of the soil frost extent and the dominant flow pathways in winter. As the surface air temperature becomes increasingly higher, there will be an increase in the number of days that soil temperatures are above freezing, which was corroborated for other areas in the region (Sinha & Cherkauer, 2010). Within the model, this will result in increased infiltration and subsurface activity causing decreased in surface runoff and reduced soil water storage. This is also supported by Jyrkama & Sykes (2007), who projected increased infiltration and groundwater recharge in a southern Ontario watershed due to decreased ground frost, making soil freezing dynamics an important factor controlling projected pathway losses (Xiuqing & Flerchinger, 2001).

Although there were large water surpluses in spring (precipitation > ET = 16 mm), a significant change in surface runoff was not found during this period. This is likely a result of increased hydrologic activity in winter that lessens the potential for saturation overland flow in spring. Indeed, as temperatures increase in winter, the amount of precipitation as snow and snowpack will decrease, spring melt will occur earlier (Demaria et al., 2016), and the large tile flow increases in winter will decrease the water availability in spring. This is somewhat corroborated by surface runoff increase in spring for the RCP4.5 GFDL-ESM2M scenario (Figure 3-4c), which had the smallest tile flow increase in winter (Figure 3-4l).

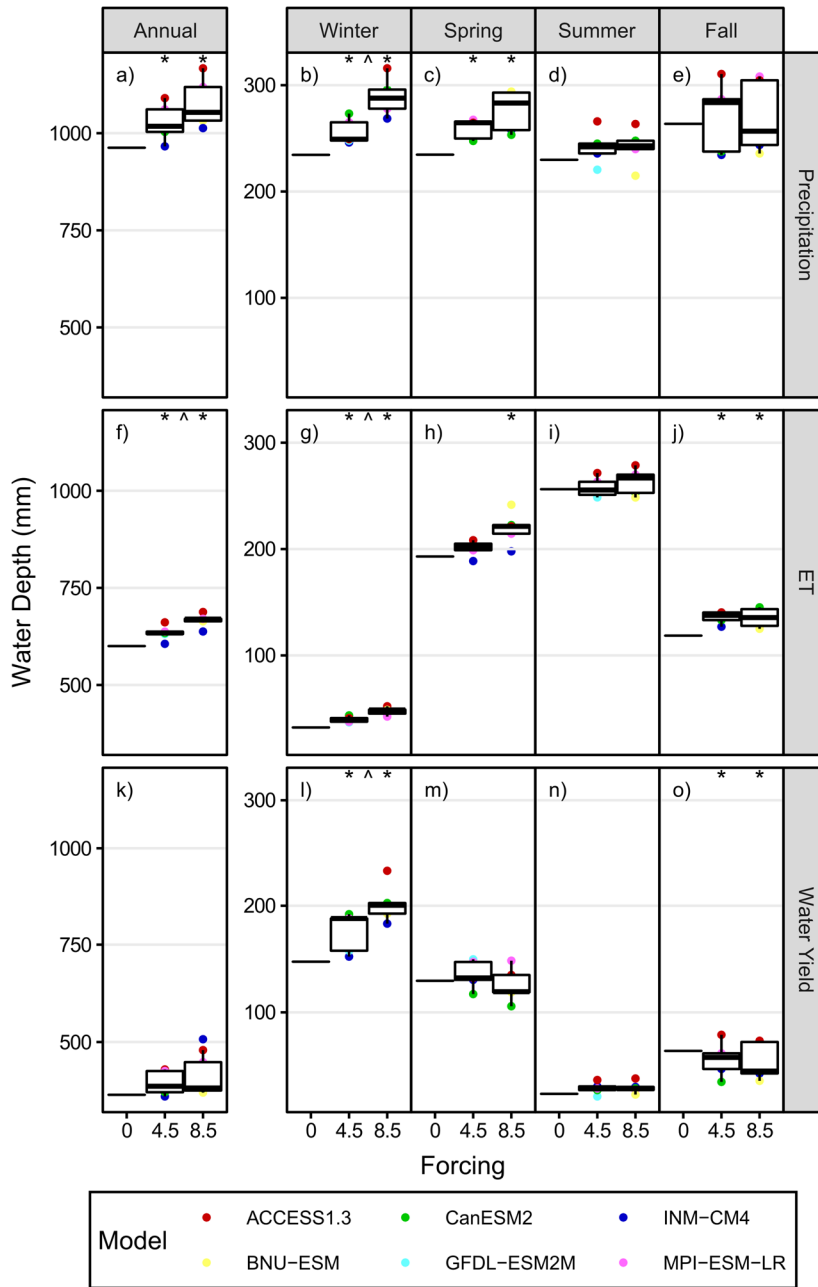


Figure 3-3. Annual and seasonal precipitation, ET, and water yield for the historic (0 forcing; 1990-2010) and future climate periods (RCP4.5 and 8.5 forcing; 2080-2100). Color indicates the climate model, when outside of the interquartile range. * indicates significant difference ($p < 0.05$) from historic model based on two-tailed Student t-test and ^ indicates significant difference ($p < 0.05$) between forcings from unpaired two-sample Student t-tests.

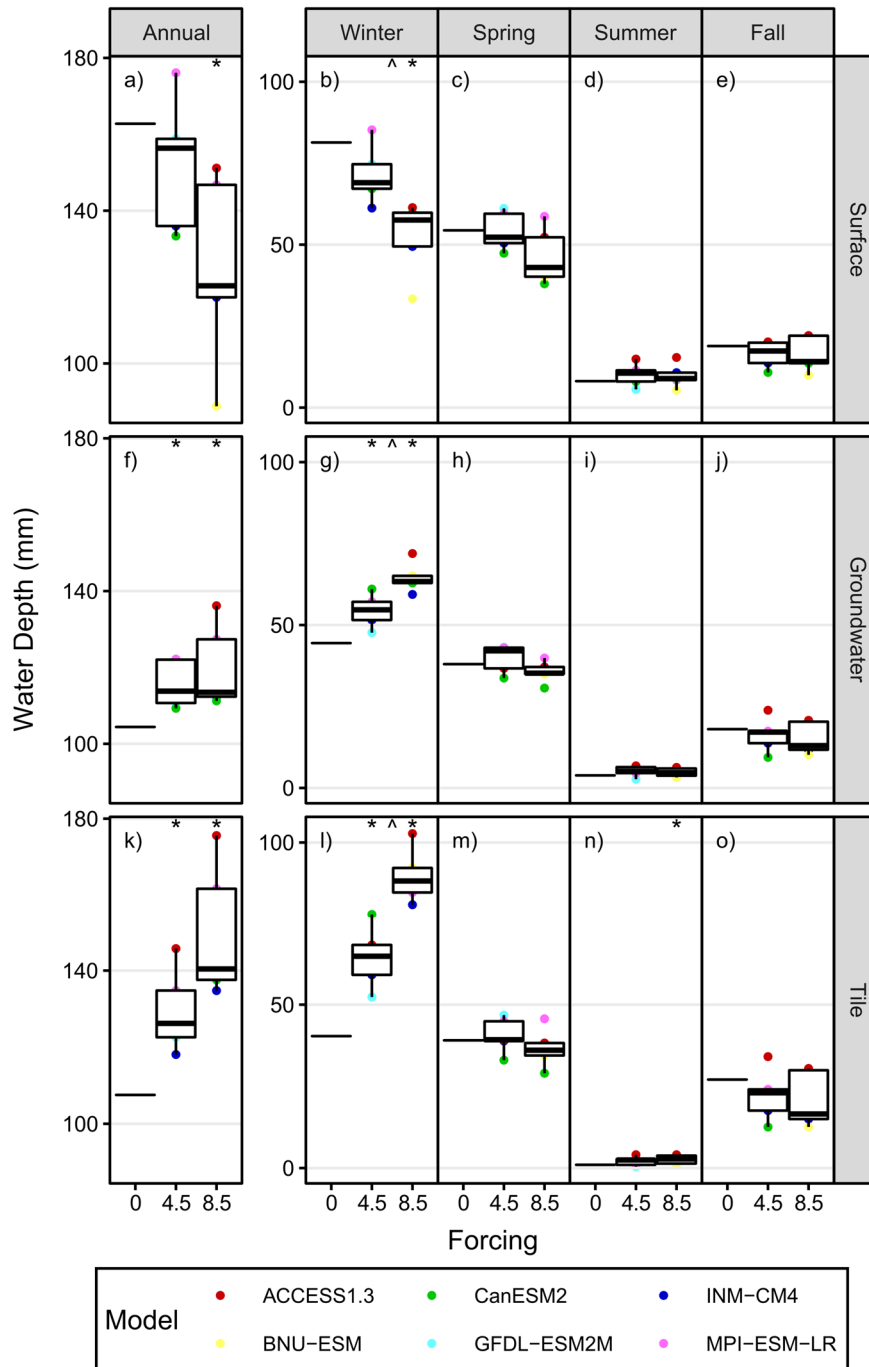


Figure 3-4 Annual and seasonal surface runoff, tile flow, and groundwater for the historic (0 forcing; 1990-2010) and future climate periods (RCP4.5 and 8.5 forcing; 2080-2100). Color indicates the climate model, when outside of the interquartile range. * indicates significant difference ($p < 0.05$) from historic model based on two-tailed Student t-test and ^ indicates significant difference ($p < 0.05$) between forcings from unpaired two-sample Student t-tests.

Overall, results indicate that there will be a definitive but varying flow magnitude increase for the high stream flow regime and decrease for the low flow regime in all seasons (Figure 3-5). This corresponds to an average annual flow decrease (12%), which has been similarly projected in another study (Cousino et al., 2015). For all scenarios in winter and spring, flows occurring at 50% exceedance probability will decrease relative to the baseline period, indicating a reduction in the median flow (8% and 12% decreases respectively) and average flow (Figure 3-5). In summer, for all scenarios there will be much higher flows occurring up to 15 percent exceedance when compared to the the baseline period, with all scenarios less than the baseline not until 40 percent exceedance. The extent of high stream flow regime increases are reflected by variability in the average flow projections (Figure 3-5). Fall behaves similarly to summer except there is a bit more variability for the flow magnitudes occurring from 30 to 80 percent exceedance (Figure 3-5). In this range, most of the flows become higher at around 50 percent exceedance indicating an overall median flow increase, which is contrary to the average flow (Figure 3-5), and therefore also indicative of variability.

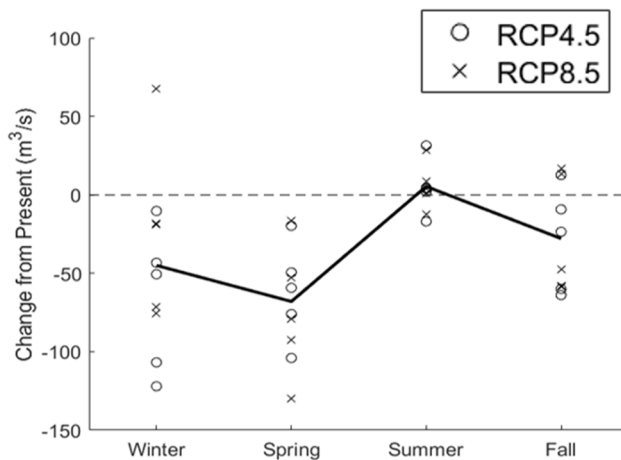


Figure 3-5 Average stream flow changes by season for all scenarios (black line) with each individual scenario grouped by RCP. All were during the period 2080-2100 and values are the difference between the projected and the modelled baseline data from 1990-2010.

In winter, considering the overall decrease in surface runoff and increase in subsurface flow, this will result in attenuation of the stream response time to a precipitation event, reducing stream flows. In spring, stream flow decreases the most due to the previously mentioned causes of the change in the winter and spring water balance combined with the changing precipitation patterns. In winter and spring, increased frequency and magnitude of more extreme daily precipitation events, will increase runoff intensity and the magnitude of the infrequent peak flows, which is opposing for the low flow regime that responds to smaller precipitation events decreasing in magnitude and frequency, but generally have a greater probability of occurring.

In summer, the precipitation magnitude and frequency changes seen in Figure 3-2 are not the only factors influencing the high flow regime given that all scenarios show increases over a large range of exceedance probabilities. Due to changes in the timing of precipitation, there could be potential for a greater segregation of extremely wet (increased precipitation) and dry periods resulting in surface runoff pattern changes. This corroborated by the large discrepancy between the baseline and future scenarios at low flow conditions, which indicates a potential increase in the risk of drought conditions and decrease in soil storage (Figure 3-6). SWAT uses the SCS curve number updated daily based off daily plant evapotranspiration (PET) to estimate direct surface runoff. Therefore, in fall, the projected increase in ET greater than precipitation will result in water deficiency, reduced surface runoff volumes, and average flow. As a result, in comparison to summer, surface runoff will have less influence on the high stream flow regime, and the precipitation pattern changes will reduce the percent of time during which all of the scenarios have high flows that are greater than the baseline period from 15 to 3.5 percent of the time.

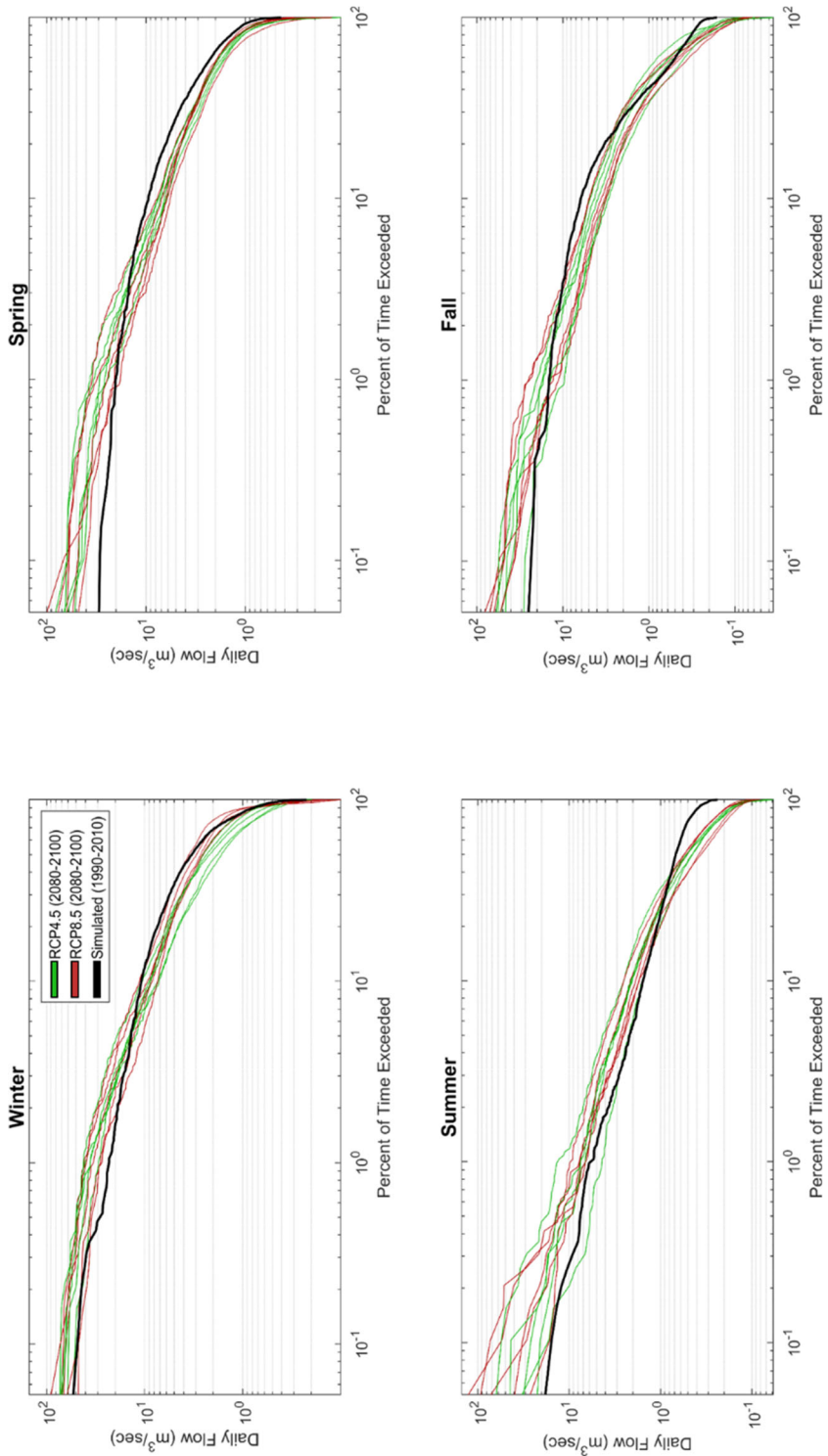


Figure 3-6. Flow duration curves for the watershed outlet with daily flow in 1990-2010 and for 2080-2100 in each season and future climate scenario

3.1.7 Model Results: Nutrient and sediment loads in the future climate

3.1.7.1 Nitrate Loading from the MCW

The model projected a significant increase in annual nitrate loads and flow-weighted mean concentrations (FWMC) (Figure 3-7a and f). In winter, median nitrate loads increased from 8 Kg ha⁻¹ to 14.1 Kg ha⁻¹ (77% increase), and FWMCs from 4.5 mg/L to 8.6 mg/L (91% increase) in the 2080-2100 period. The median spring loads decreased from 9.2 Kg ha⁻¹ to 8.8 Kg ha⁻¹ (4.2% decrease), and increased FWMCs from 5.3 mg/L to 6.8 mg/L (28.3% increase), with changes in load varying from -3.6 to 2.6 Kg ha⁻¹ between scenarios (Figure 3-7c). In summer and fall, we see increases in the NO₃⁻ loads, (1.1 and 1.5 Kg ha⁻¹ increases respectively), but these are much smaller changes than are projected in winter.

The increase in the annual and seasonal loads and FWMCs can be attributed to the changes occurring in the NGS. Since NO₃⁻ is highly mobile in the subsurface, tile drains are known to contribute a large proportion of the total NO₃⁻ loads to streams (Arenas Amado et al., 2017). This results in increased NO₃⁻ losses (Figure 3-7b) due to the large tile flow increase in winter (Figure 3-4l) and a shift in the timing of residual soil nitrogen (RSN) remobilization towards the winter months. In spring, results suggest that extent of tile flow increases and soil water depletion in winter will cause the variability in spring loads. For example, the RCP 4.5 GFDL-ESM2M scenario had the smallest winter tile flow increase (Figure 3-4l), which corresponds with the largest spring tile flow (Figure 3-4m) and NO₃⁻ load increase (Figure 3-7c).

In summer, NO₃⁻ loads increase slightly due to tile flow, small median flow increases at the outlet, and large increases in the FWMC because of potentially longer periods between precipitation events initiating subsurface flow and high flow conditions. This could cause greater accumulation of NO₃⁻ in the soil before it is flushed during the next storm event and exported via tiles (Van Meter et al, 2016; Vidon et al., 2009). In fall, load and FWMC increases are similar to summer, yet most flow pathways are decreasing, which indicates that the interactive effects of mineralization and decomposition of organic matter, a dominant NO₃⁻ process in SWAT (Mehdi et al., 2016), and timing of high flow conditions are important. However, more analysis is needed to understand changes in export patterns and the exact contribution each pathway or process is contributing to the majority of these changes throughout the season.

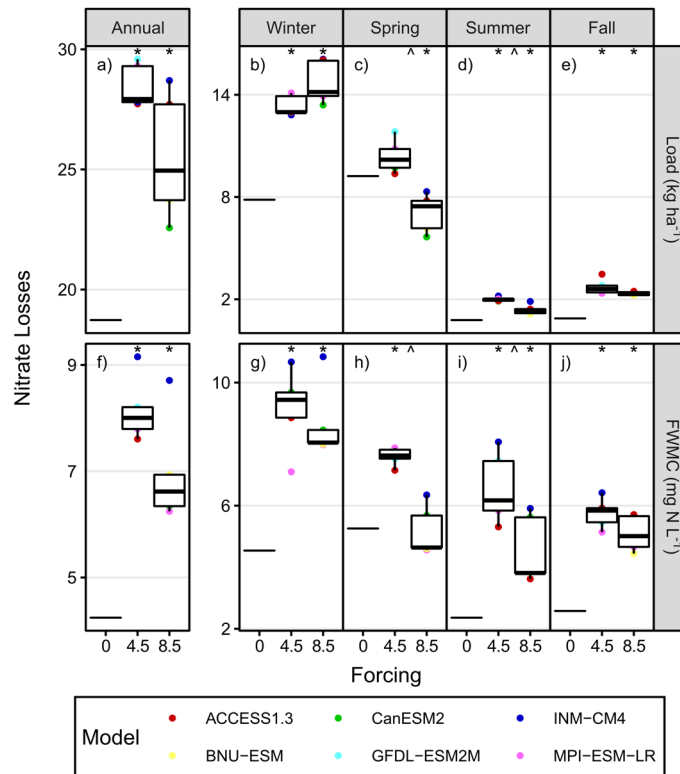


Figure 3-7. Boxplots for NO₃- loads and FWMC at the watershed outlet in 2080-2100 grouped seasonally, annually, and by GCM forcing (RCP4.5 and 8.5). With forcing “0” representing the historic period (1990-2100). Color indicates the climate model, when outside of the interquartile range. * indicates significant difference ($p < 0.05$) from historic model based on two-tailed Student t-test and ^ indicates significant difference ($p < 0.05$) between forcings from unpaired two-sample Student t-tests.

3.1.7.2 Suspended Sediment

In contrast to NO₃- loads, which the model projected would increase in winter and decrease in spring by the 2080-2100 period, SS loads were projected to decrease in both winter (8.1 Kg ha⁻¹; 10%) and spring (16.1 Kg ha⁻¹; 24%) (Figure 3-8) along with FWMC. This reduction is mostly driven by reduced surface runoff and stream flow, which decreases hillslope sediment supply and sediment transport capacity in the stream. Within the model, surface runoff increases SS export from the HRUs. It is interesting to note that the model projected that spring would have a substantial decrease in SS loads compared to winter, despite the smaller decrease in surface runoff. This may be partially driven by earlier crop growth in spring, which would lessen SS losses from fields. However, winter SS loads vary from -32 to 18 Kg ha⁻¹ despite the fact that a substantial decrease in surface runoff is projected, which suggests that streamflow may be a more important controlling factor.

In contrast to the projected reductions in SS loads in winter and spring, the model projected that summer and fall SS loads will increase, offsetting the winter/spring increases and resulting in

no significant annual change (Figure 3-8a). In summer, there will be significant increase in the median SS loads (20 Kg ha⁻¹; 340%) and FWMC by the 2080-2100 period. This should be expected given the combination of increased surface runoff and average stream flow. In fall, loads have a significant median increase of 17.5 Kg ha⁻¹ (195%) and this corresponds to a 25 mg/L (95%) FWMC median increase for all scenarios by the 2080-2100, despite the fact that flow and water balance changes are small and variable, which makes the reason for the fall changes less clear. These changes may be driven by higher intensity rainfall and shifts between wet and dry periods, which would not lead to an increase in overall flow but could lead to elevated losses of SS during peak flow events.

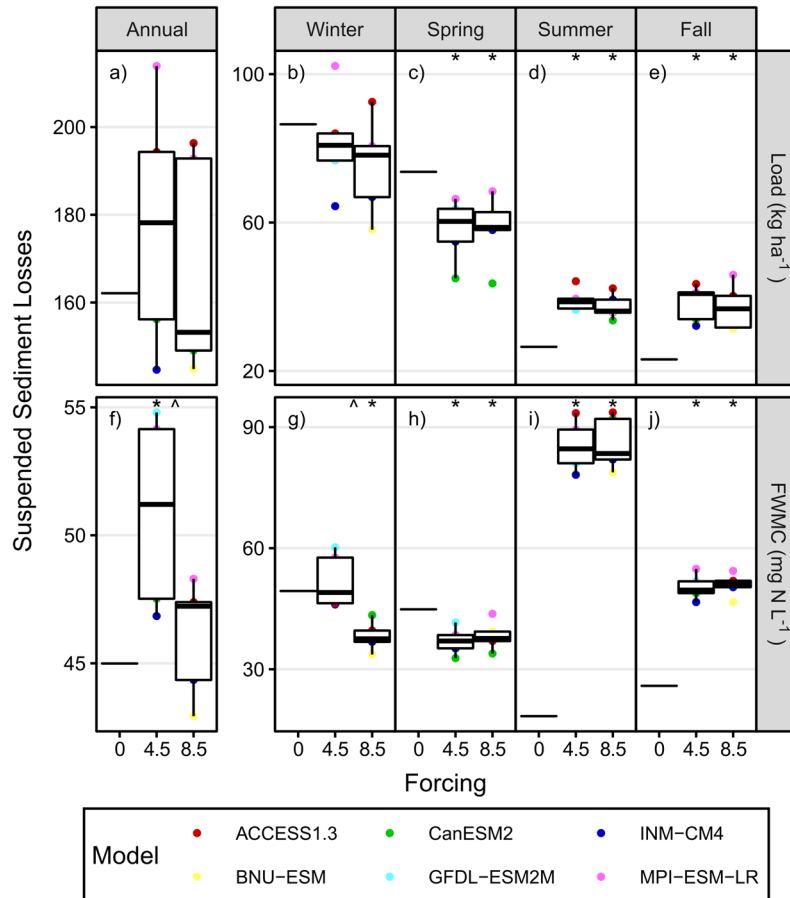


Figure 3-8. Boxplots for SS loads and FWMC at the watershed outlet in 2080-2100 grouped seasonally, annually, and by GCM forcing (RCP4.5 and 8.5). With forcing “0” representing the historic period (1990-2100). Color indicates the climate model, when outside of the interquartile range. * indicates significant difference ($p < 0.05$) from historic model based on two-tailed Student t-test and ^ indicates significant difference ($p < 0.05$) between forcings from unpaired two-sample Student t-tests.

3.1.7.3 Total Phosphorus

In winter and spring, the model projected a median increase in TP loads for all scenarios by 0.07 (31%) and 0.025 (19%) Kg ha⁻¹ respectively (Figure 3-9b and c). Changes in TP would be expected to behave similarly to SS and surface runoff given that the SWAT model lacks a subsurface P transport component (Neitsch et al., 2011). Although TP loads and FWMC did not decrease, some similarities are found between SS and TP export. For example, the model scenario with the smallest decrease (or an increase) in SS and surface runoff were associated with increased TP export. Overall, results suggest an increased potential for changing climate to alter TP:SS export ratios in winter and spring, causing median FWMC in winter to increase by 0.05 (39%) and 0.033 (37%) mg/L in spring (Figure 3-9g and h). A plausible reason for these changes would be the increase in high flows, which are known to increase P transport (Royer et al., 2006). Large surface runoff and precipitation events associated with these increased peak flows could flush P accumulated in the soil between smaller events. It is possible that more fine-grained material, which is enriched in P, or, dissolved P species are being mobilized, which would not lead to an increase in SS. This is supported by the fact that there is a sensitivity of solution P export in SWAT to increased precipitation intensity (Michalak et al., 2013), and, there may be an increase in solution P resulting from increased decomposition and mineralization of organic residue due to temperatures and soil moisture increases.

In summer and fall, load changes are significantly greater relative what is typically found in these seasons with increases of 0.023 (200%) and 0.02 (121%) Kg ha⁻¹, respectively. Although these increases are large, they are considerably smaller than what is found in the winter (200% greater). Results suggest that TP will be primarily exported with SS due to their coordinated increase. Within the MCW, water quality conditions are ranked using a standardized grading system developed by Conservation Ontario. The current overall surface water quality condition has a score of D with not much change occurring since 2005; however, P levels have improved but are still at levels 4 times the provincial aquatic life guidelines (0.03 mg/L). In the final period (2080-2100) concentrations are expected to increase by 0.042 mg/L in winter and spring, which is almost 1.4 times water quality guidelines.

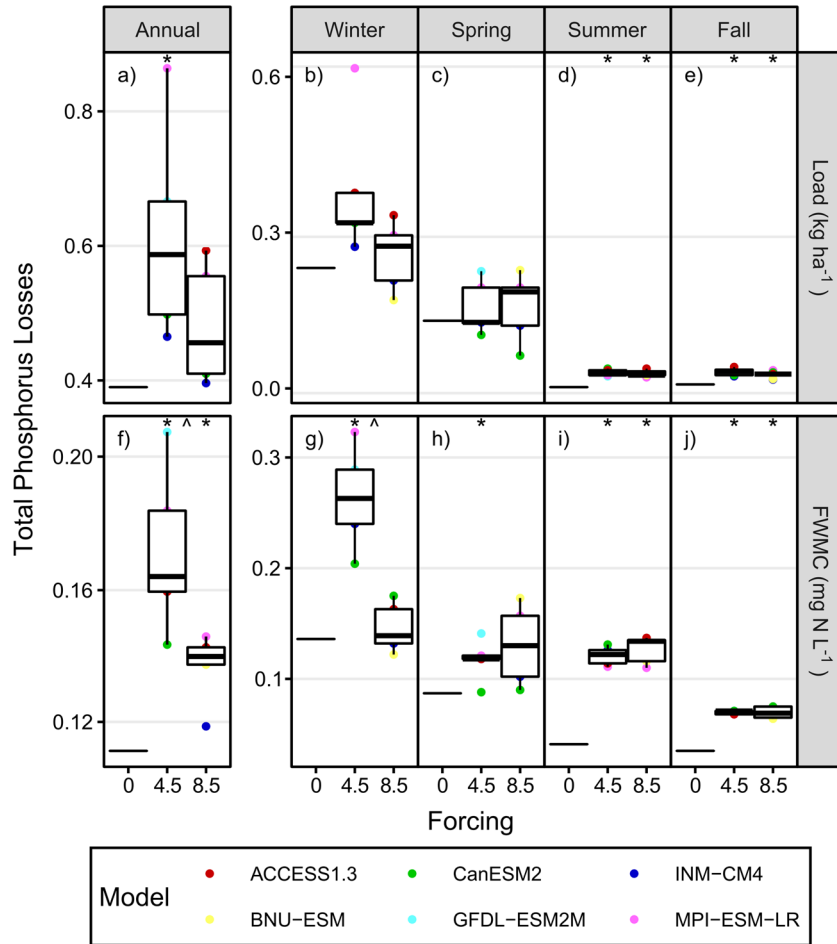


Figure 3-9. Boxplots for TP loads and FWMC at the watershed outlet in 2080-2100 grouped seasonally, annually, and by GCM forcing (RCP4.5 and 8.5). With forcing “0” representing the historic period (1990-2100). Color indicates the climate model, when outside of the interquartile range. * indicates significant difference ($p < 0.05$) from historic model based on two-tailed Student t-test and ^ indicates significant difference ($p < 0.05$) between forcings from unpaired two-sample Student t-tests.

3.1.8 Conclusions for Medway Creek Study

In this study, the SWAT model coupled with an ensemble of future climate change scenarios were used to evaluate the implications of seasonal changes in climate on water quality in the MCW, in southwestern Ontario. Given increased temperatures and precipitation, seasonal shifts in temperature, and increased frequency of extreme rainfall, the model projected annual increases in runoff, NO₃⁻ and TP but a decrease in SS by the 2080-2100 period. Generally, these changes were controlled by changing precipitation characteristics and flow paths in the NGS that also affected stream flow regimes, increasing peak flows. There were also shifts in seasonal patterns in terms of flow and pathways, which will shift nutrient export timing towards winter.

3.2 Londesborough Field Site Study.

3.2.1 Context and Objectives

Some managers and land stewards have recommended the use of controlled tile drainage (CD) to mitigate P losses. Controlled drainage permits control of water table position and soil water storage using a series of gates installed near the tile network outlet that can be raised or lowered. This results in decreased tile flow, which leads to a reduction in P and NO₃ loads from tiles (Ale et al., 2012; Lalonde et al., 1996; Lavaire et al., 2017; Skaggs et al., 2012; Sunohara et al., 2016; Tan & Zhang 2011; Wesström et al., 2014; Williams et al., 2015; Youssef et al., 2018). Additionally, when using CD during the growing season, this can decrease plant water stress, which increases crop yields (Poole et al., 2013; Sunohara et al., 2016), thereby providing economic benefits (Crabbé et al., 2012). Although CD has the potential to improve water quality in subsurface drainage, few studies have considered potential water quality tradeoffs such as increased surface runoff, which may increase total phosphorus (TP) loads and impact SRP:TP ratios (Riley et al., 2009; Ross et al., 2016; Tan & Zhang 2011; Zhang et al., 2017). Moreover, in cool temperate climates such as the Great Lakes region, many landowners do not employ controlled drainage during the non-growing season (NGS) due to the potential for ground frost to damage tile drains. Given that the majority of annual runoff and P loss in the Great Lakes region of North America occur during the NGS (Macrae et al., 2007b; Van Esbroeck et al., 2017; Williams et al., 2016), it is unclear if and how CD may affect year-round runoff and nutrient losses from fields. The objectives for this study were to: (1) Calibrate a single HRU SWAT model of a field site in southern Ontario, Canada to demonstrate the capability of the SWAT and the H-K-DC routines to accurately simulate tile flow and surface runoff; and (2) Simulate the impact of CD on flow path partitioning using the SWAT HRU model and estimate the impacts of these changes on edge-of-field TP and SRP losses using field data.

3.2.2 Field Site Description

The Londesborough site (LON) is a small ~8.1 ha field located in southwestern Ontario, Canada (43°38'33.0"N 81°24'42.6"W; Figure 3-10), within the Maitland Valley watershed that drains in to Lake Huron. Londesborough has a humid continental climate with an elevation above sea level of ~350 m. Long-term (1981-2010) climate normal for the region are mean temperatures of -5.3 °C in winter (December to February), and 19.2 °C in summer (June-August), with mean annual precipitation amounts of 1245 mm (374 mm as snowfall from October to April) (ECCC, 2018a). The current study uses a dataset collected over the 2012-2015 water years (Oct 1 – Sept 30). Weather over this period was variable, with 3 of the 4 years receiving an average of 187 mm less than the 30-year average and one year receiving 241 mm more. Temperatures occurring throughout the study period were also variable, but consistent with long-term normals for the region.

Soil in the field is classified as a Perth clay loam (Plach et al., 2018), which is imperfectly drained. The average slope of the field site ranges from is 0.2 to 3.5%. Tile drain laterals (10 cm) are installed within the field at ~ 75-90 cm depth with a spacing of 14 m, and connected to a single tile main line that exits at the field edge. The tile drainage system is restricted to the field site and does not receive inputs from adjacent fields. The crop rotation is a corn (*Zea mays* L.), soybean (*Glycine max* L.), and winter wheat (*Triticum aestivum* L.). The field is managed with a rotational shallow conservation till (vertical tillage to 5 cm depth). Soil test P concentrations are 16 ppm (Olsen P) in the top 15 cm of soil. P is applied as monoammonium phosphate (MAP) via subsurface placement prior to corn (15 Kg P ha⁻¹), and via surface broadcast following winter wheat harvest (92 Kg P ha⁻¹), concurrent with the rotational till. Cover crops (red clover; *Trifolium pretense* L.) are planted in the spring (air seeded in April) in years during which winter wheat is cropped, and killed in October using an herbicide.

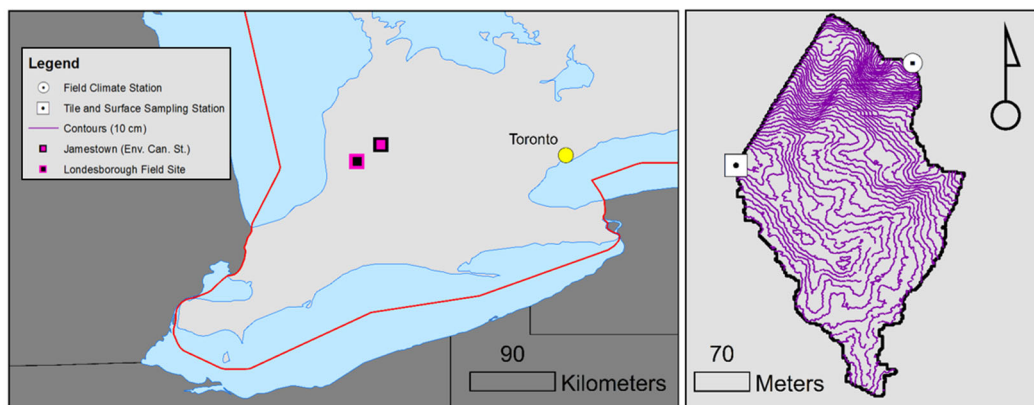


Figure 3-10. Location of LON in Canada (left) and other field site details (right; topography, observation station locations, and boundary). Also shows the location of the climate station used to supplement missing data at the field site (Jamestown).

3.2.3 Field Data Collection

Hydrometric data are collected continuously (15-min intervals) at the field edge, year-round. Meteorological data (rainfall, air temperature, windspeed and direction, relative humidity, soil temperature and moisture) are recorded on-site using a standard meteorological tower (Onset Ltd.). Because the on-site weather station does not measure snowfall, precipitation data was obtained from a nearby weather station (ECCC, 2018). Water table position is monitored continuously at the field edge using a pressure transducer in a 2 m deep well (ID 5 cm) (U20, Onset Ltd.). Surface runoff drains from the field via a single culvert (ID 45 cm) and tiles drain via a single header tile. Flow in both surface drainage and tile drainage are measured using depth-velocity sensors (Flo-tote, Hach Ltd.) and recorded on FL900 data loggers (Hach Ltd.). Water samples of surface and subsurface runoff are collected at high frequencies (2-8 hr intervals) during storm and thaw events, and periodically during baseflow (when tiles are flowing) using automated field samplers (ISCO) that are triggered by a flow response. Unfiltered samples are acidified to 0.2% H₂SO₄ (final concentration) and digested using acid persulphate digestions and colorimetric analyses in the Biogeochemistry Lab at the University of Waterloo. Filtered samples (0.45 micron) are analyzed for DRP using colorimetric methods. For more detailed information on the field site and data collection, refer to Van Esbroeck et al. (2017).

3.2.4 SWAT model description

For the study, the SWAT2012, rev. 664 was used. Within the most recent versions of SWAT, a new tile drainage routine (H-K-DC routine) was added by the developers that uses a combination of either the Hooghoudt or Kirkham equations depending on the water table depth (Moriasi et al., 2013). Tile flow only occurs once the perched water table rises above the drains (Neitsch et al., 2011). To create the SWAT model for LON consisting of only one HRU and subbasin all input files needed for a single HRU model were created and altered to ensure the model was representative of the field site. Some initial modifications were made to parameters usually initialized in the ArcSWAT model builder based on the available field data. For example, in the sub input file the subbasin area (SUB_KM) was set to be equivalent to the field site surface runoff area (8.1 ha) and the input files linked with the subbasin file (.sub) were set to one of each input type. In the HRU input file (.hru), the fraction of subbasin area contained in HRU (HRU_FR) was set to one and the slope (HRU_SLP) was changed to 1.6%. This value is the mean slope of the field site calculated using the SWOOP digital elevation model (Ministry of Natural Resources and Forestry, 2015).

The soil input file (.sol) parameters were set and representative of the field soil type (Perth clay loam), which was determined using the Ontario Soil Survey Complex data (1:50000 scale) obtained from the Land Information Ontario (LIO) database (Ministry of Agriculture, Food and Rural

Affairs, & Canadian Soil Information Service, 2015). Soil layer data was available to a depth of 1100 mm, and had a bulk soil texture consisting of 27% clay and 25% sand. The pedotransfer function developed by Saxton and Rawls (2006) was used to estimate available water capacity, saturated hydraulic conductivity, and bulk density for each soil layer using the available texture data.

Climate input data sets were made using rain and temperature data collected at the field site. During the months with snow and the part of the year in 2015 when there was no precipitation data, more was obtained from a nearby climate station to supplement the field site data and make a continuous precipitation data set (Jamestown, ON, 25 Km away; Figure 3-10; 43°48'09.1"N 81°11'01.0"W, ECCC, 2018b). Agricultural management practices were input using reported field activities at the site (noted above), with the remainder of the parameters used in SWAT set to default before calibration.

In this study, the Optimization Software Toolkit for Research Involving Computational Heuristics (OSTRICH) was used to auto-calibrate the SWAT model. This toolkit is able to function with any model that operates using text files and has many options to choose from with respect to the calibration and optimization algorithms available (Matott, 2017). During calibration, the Dynamically Dimensioned Search (DDS) algorithm was selected due to its computational efficiency and ability to determine a globally optimum solution within a selected number of iterations (Tolson and Shoemaker, 2007). To auto-calibrate the model both the percent bias (PBIAS) and the Nash–Sutcliffe model efficiency coefficient (NS) within OSTRICH, the general-purpose Constrained Optimization Platform (GCOP) were used. Within the GCOP module, the multiplicative penalty method (MPM) was selected to calculate the overall objective function, which is a combination of the system cost and the penalty function (Chan-Hilton and Culver, 2000). To determine the system and penalty cost associated with the applied constraints a MATLAB script was developed to extract model outputs and calculate response variables to use within OSTRICH after each iteration.

3.2.4.1 Calibration and validation approach

Monthly tile (2012-2015) and surface runoff (2013 and 2015) were determined from the 15-minute field site data. Surface runoff (2013 and 2015) and tile flow (2012-2014) were calibrated together at a monthly time step using the field site data with a three-year warm up period. During calibration, the average NS for tile flow and surface runoff was used as the system cost, and the penalty cost was calculated by constraining the surface runoff and tile flow PBIAS to ± 25 and 20 percent respectively. The perturbation factor and maximum number of iterations were set to 0.2 and 1500 respectively, and after calibration, tile flow was validated using the data in 2015.

Some parameters that control calculation methods within the model were changed from default. These were the daily potential evapotranspiration calculation (PET), which now uses the

Hargreaves method (IPET=2) and the Soil Conservation Service (SCS) curve number (CN), which now varies with accumulated plant ET (ICN=1; Arnold et al., 2012a). To use the new tile flow routine mentioned above, ITDRN was set to one. Additionally, the default value for the Manning's overland flow roughness (OV_N) was too low so it was increased to 0.15 to be representative of the site, which used either no-till or vertical tillage, and leaves crop residue.

Parameters known to affect HRU runoff were included in the calibration (Abbaspour et al., 2007, 2015; Arnold et al., 2012b, Guo et al., 2018; Wang & Melesse, 2005), as well as additional parameters required by the new H-K-DC routine. Site-specific information and collected agricultural management data were used to fix some of the parameters to improve the model. For example, the distance between drains (SDRAIN) was set to 14 m, pump capacity (PC; mm h⁻¹) was set to 0, and based on the results of Golmohammadi et al. (2016a) in Ontario, the effective radius (RE) was set to be 15 mm. The depth to drains (DDRAIN) was known to be between 750 to 900 mm and allowed to vary during calibration. Other tile specific parameters used in calibration include the drainage coefficient (DRAIN_CO; mm d⁻¹) and multiplication factor to determine lateral saturated hydraulic conductivity (LATKSATF; mm h⁻¹).

Due to the lack of soil data past 1100 mm, an unknown depth to the impervious layer, high sensitivity of the impervious layer depth, and its control over shallow aquifer seepage (Bauwe et al., 2016; Neitsch et al., 2011), an iterative approach was used to define reduced ranges for calibration. To ensure a realistic impervious layer depth after calibration, tiles were removed (DDRAIN = 0) and the layer depth was increased until the shallow aquifer recharge was between 15 to 20 percent of the average annual precipitation, which is typical in Ontario clay and silt soils (David Rudolph, personal comm.). This value was used as the maximum limit during calibration of the impervious layer depth (DEPIMP; range of 1500-3000 mm) and was similar to the ranges used by Guo et al. (2018). Additionally, some soil parameters were added due to the uncertainty in actual conditions with depth and their importance in percolation and water table depth calculations (Neitsch et al., 2011). Using the available data, saturated hydraulic conductivity (SOL_K), bulk density (SOL_BD), and the available water capacity (SOL_AWC) were allowed to vary \pm 25 percent of the initial value for the layers.

3.2.4.2 Tile drainage scenarios and TP load estimation

To determine the effect that tile drains have on the flow paths contribution to runoff two tile drain scenarios were created. The calibrated HRU model was used as the free tile drainage (FTD) scenario (DDRAIN= 840 mm). Tile height was subsequently raised (DDRAIN = 500 mm) to be representative of depths typically used for CD in southern Ontario (Upper Thames River Conservation Authority, personal comm.) for the continuously raised tile drainage (RTDcont) scenario over the study period. Each height was run during the calibration period (2012-2015) with

no other modification of the parameters. Since SWAT is unable to change tile heights during a simulation, pseudo CD data sets were created for two typical management scenarios found in southern Ontario. Where HRU model outputs from the RTDcont and FTD scenarios were joined together based on the planting and harvest dates for the crops reported at the field. Monthly TP and SRP FWMCs were calculated for each flow path during the study period using field site data obtained using the methods mentioned in Van Esbroeck et al. (2017). TP and SRP loads were then determined by multiplying the monthly FWMC by the corresponding surface runoff and tile flow volumes output in each scenario because nutrient reductions have been shown to be primarily driven by flow (Sunohara et al., 2010) and SWAT lacks the capability to model P subsurface losses through tile drains (Qi & Qi, 2017).

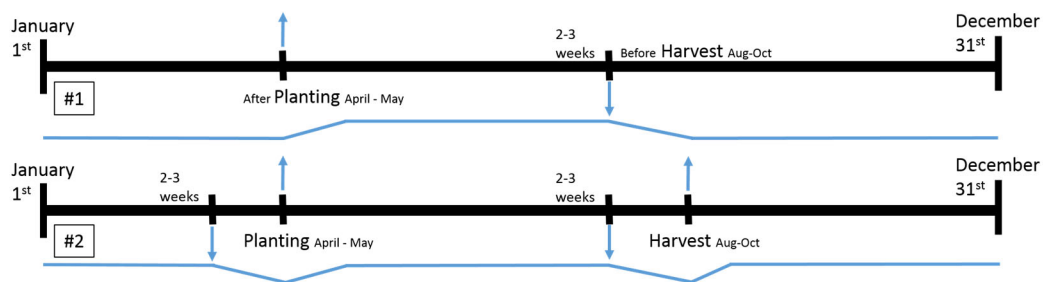


Figure 3-11. Shows two typical CD management approaches used in southern Ontario (#1 = RTDGS; #2 = RTDNC). Blue arrows represent the raising or lowering of the drain gate 3 weeks before planting and harvest, while blue lines represents a simplified representation of the water table depth changes. Major difference is the management during the NGS, which typically occurs from late fall to early spring for most crops.

3.2.4.3 HRU performance evaluation

To evaluate the performance of the HRU flow pathways, the NS (Nash & Sutcliffe, 1970), PBIAS (Gupta et al., 1999), and coefficient of determination (R^2) statistics were used in conjunction with graphical methods. The model evaluation criteria developed by Moriasi et al. (2007b) and based on the streamflow outputs, were used to provide performance ratings for NS and PBIAS statistic. For the R^2 , performance was considered good if it was higher than 0.6 (Santhi et al., 2001).

3.2.5 Results: SWAT HRU performance: Surface runoff and tile drainage

Following calibration, the model performance was good (Table 3). The model simulated surface runoff more precisely than tile flow, despite the fact that there were fewer surface runoff events. The model evaluation criteria developed by Moriasi et al. (2007b) that uses NS and PBIAS to rate model performance, the ratings for surface runoff were very good and good respectively, while tile flow was satisfactory for both, with R^2 performance also well within the acceptable range (>0.6 ; Santhi et al., 2001; Table 3). Tile flow during the validation period slightly underperformed with respect to the NS and R^2 , but had a satisfactory PBIAS.

Table 3.3. Performance statistic values (NS, PBIAS, and R^2) after calibration for surface runoff and tile flow.

Performance Measure	Monthly Surface Runoff	Monthly Tile Flow	
	2012 and 2015	Calibration (2012-2014)	Validation (2015)
NS	0.79	0.60	0.23
PBIAS	-12.7	17.3	15.6
R^2	0.81	0.64	0.46

Through visual assessment, the model reasonably captured the timing and magnitude of monthly surface runoff peaks, with slightly decreased performance for tile flow. Although the model generally simulated NGS surface runoff well, there were some irregularities in October of 2013 and 2015. The model simulation of tile drainage was erratic in summer and winter but was generally good in the spring and fall. There were several tile drain responses that the model had difficulty simulating (February 2013, January 2014, March 2014, and June 2012 and 2013). The winter events were associated with cold conditions/snowmelt. Despite these events that were missed by the model, runoff coefficients in 2013 and 2015 simulated by the model were 0.29, which is close to the observed runoff coefficients of 0.33.

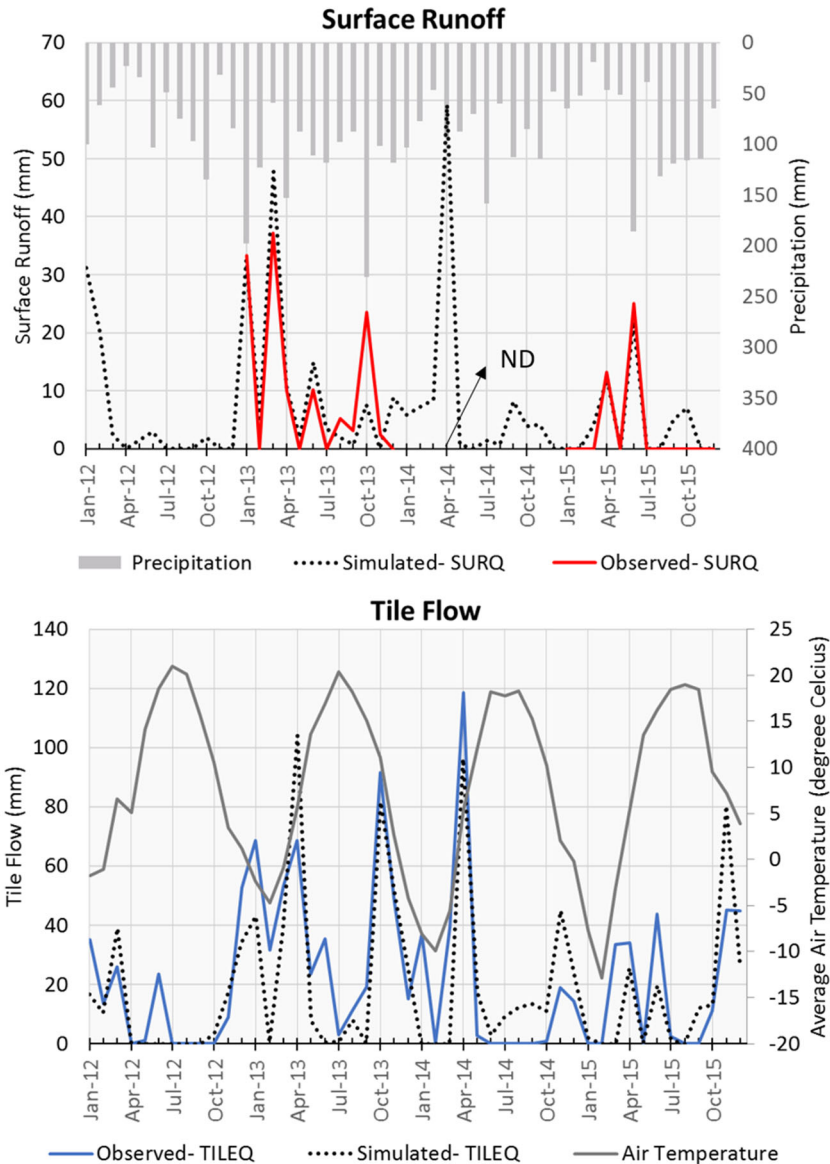


Figure 3-12. Graphical performance of surface runoff (top; SURQ) and tile flow (bottom; TILEQ) after calibration of the LON HRU model. In addition to performance, it shows monthly precipitation (top) and average air temperatures (bottom) over the 2012 to 2015 period. Arrow with ND indicates no data due to sensor failure.

Other water balance components were representative of southern Ontario conditions, where evapotranspiration (ET) was ~54% (42 to 66%) of the average annual precipitation over the 2012-2015 period (Table 3.4), which was within the range reported by Parkin et al., 1999. With tiles shallow aquifer recharge is 7% and when removed ~11.3% (range: 10 to 15%) of the annual precipitation over the 4 years, which is close to the ~15% expected for silt and clay soils in Ontario (David Rudolph, personal comm.).

3.2.6 Results: Effects of modified tile depths on runoff and flow paths

The depths of tile drains were modified in the model to simulate the effects of (a) no tile drainage and (b) continuously controlled drainage (RTDcont) on both runoff magnitude and the reallocation of precipitation among the pathways (e.g. surface runoff, tile drainage, groundwater recharge). Altering the tile drain depths modified both the total water yield (RTDcont, 4% decrease) as well as the flow paths through which the runoff moved. Raising the tile drain depths from 84 cm to 50 cm resulted in reduced tile drainage by 41 mm (22%), of which 55% was redistributed to surface runoff and 24% to aquifer recharge, with minor changes in ET and lateral flow. A similar reallocation was found when tile drains were removed from the model altogether, with the 224 mm change in tile flow largely redistributed to surface runoff (57%) and lateral flow (5%). However, there was a 4% decrease in the shallow aquifer redistribution, and 3% increase in tile flow redistributed as ET compared with the raised tile scenario.

Table 3.4. Average annual water balance with permanent changes in the tile height for the 2012 to 2015 period.

Water Balance	Free Tile Drainage (FTD; 840 mm)		Raised Tile Drainage (RTD _{cont.} ; 500 mm)		No Tiles (0 mm)	
	mm	%	mm	%	mm	%
Precipitation	1097	100	1097	100	1097	100
Surface runoff	86	8	109	10	214	20
Lateral soil Q	14	1	16	1	25	2
Tile Q	224	20	183	17	0	0
Total aquifer recharge	77	7	87	8	124	11
Total water yield	342	31	328	30	268	24
ET	594	54	594	54	604	55

There were seasonal trends in how the reduced tile drainage was reallocated. For example, in general, most tile flow was redistributed to surface runoff during the winter, early spring, and late fall months (i.e. the NGS), whereas during the GS, the reduced tile flow was typically redistributed to aquifer recharge and rarely resulted in increased surface runoff. Although this general pattern existed, there was variability among years within the NGS, demonstrating the complexity

associated with simulating winter runoff generation. For example, more surface runoff was found in the winter (JFM) months of 2012 (a dry year with 871 mm annual precipitation) than during a wetter year (2015, 1003 mm annual precipitation) due to the fact that temperatures were warm in 2012 (9 oC) and 71 mm more precipitation was received during the winter months of 2012 than 2015, despite the fact that both years received less winter precipitation than normal (ECCC, 2018a).

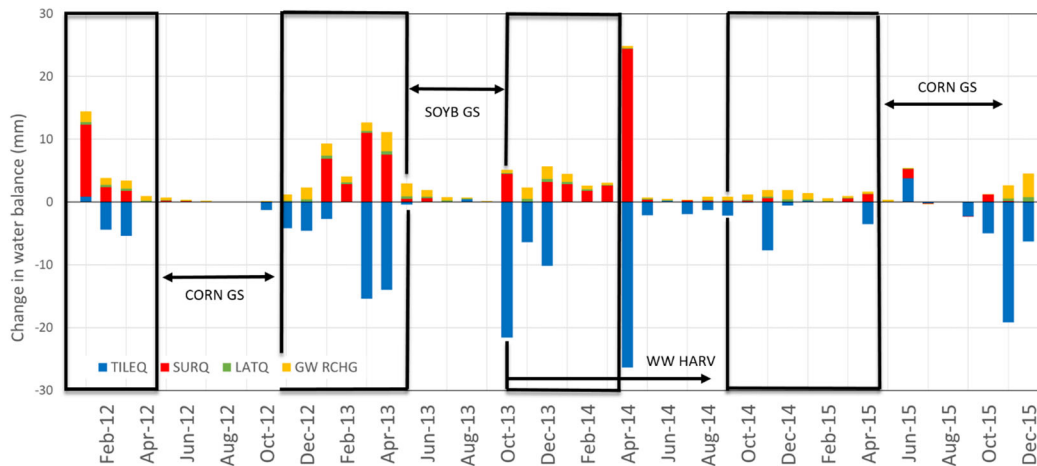


Figure 3-13. Monthly changes in the water balance over the 2012 to 2015 period with continuously raised tiles (RTDcont). Bars show the difference between RTDcont and the free tile drainage (FTD) scenario . A positive value denotes an increase in flow and a negative denotes a reduction in flow. Black bars indicate the growing season over the study period and boxes showing the NGS.

3.2.7 Results: Effects of controlled tile drain management on runoff and phosphorus export

The patterns discussed previously in this study had the same treatment year-round (i.e. free-drainage, raised tiles or no tile). However, as noted earlier, controlled drainage can be managed differently across seasons. In the model, the RTDGS scenario (free drainage within the NGS but raised to 500mm in the GS) and RTDNC scenario (drainage controlled year-round near continuously, with tile depths raised to 500mm) both resulted in very small decreases in annual runoff (RTDGS = 2%, RTDNC = 5%) relative to the FTD scenario. The subtle difference in flow reduction between the RTDNC and RTDGS scenarios was because the increase in surface runoff (44 mm cumulative total over study period, largely during the NGS) offset the decrease in tile flow (cumulative decrease 84 mm over study period) (Figure 3.14).

Because the SWAT model cannot yet simulate P in tile drainage, hypothetical changes in edge-of-field TP loss under different controlled drainage scenarios were estimated using measured field data (seasonal average flow-weighted mean concentrations, FWMC, Table 3 3.5) applied to the different flow paths (Figure 3.15, Table 3.5). At the study site, FWMC of TP in surface runoff were typically ~10x greater than in tile flow (e.g. Van Esbroeck et al., 2017; Plach et al., 2018). Consequently, given that RTDGS and RTDNC have surface increases they have a 0.2 Kg TP ha⁻¹ (8%) and 0.32 Kg TP ha⁻¹ (13%) load increase respectively in runoff relative to the FTD scenario.

Given that tile drainage P export was a smaller component of the edge of field loss to begin with and FWMC were smaller, tile flow reductions did little to reduce TP losses, whereas small increases in surface runoff increased TP losses considerably. Of the two CD scenarios, RTDNC increased surface runoff and TP export by more compared to RTDGS because this mostly occurred in the NGS. The increase in surface runoff under the RTDNC scenario compared to the RTDGS scenario resulted in a cumulative increase in TP in surface runoff of 0.18 Kg TP ha⁻¹ than was simulated under scenario RTDGS, Figure 3-15). In contrast, the tile flow reduction associated with scenario RTDNC (Figure 3-15) only led to a cumulative reduction in tile flow TP export of 0.06 Kg TP ha⁻¹ relative to RTDGS. While cumulative SRP losses were on average 29 and 45 percent of TP in tile flow and surface runoff for all scenarios, with runoff losses increasing almost correspondingly to TP (RTDGS 12% and RTDNC 15% increase relative to FTD).

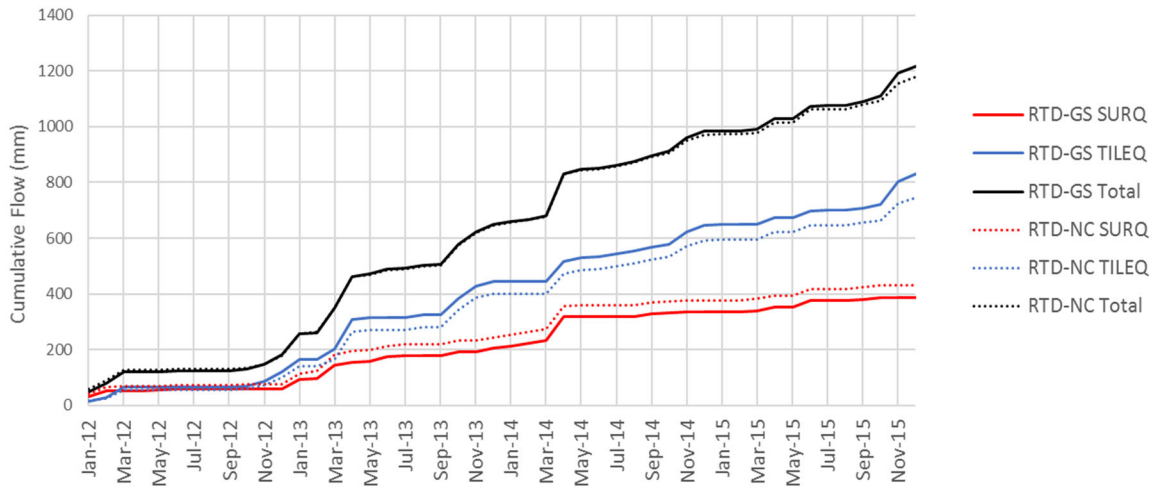


Figure 3-14. Cumulative tile flow (TILEQ; blue), surface runoff (SURQ; red), and total runoff (black) for RTDGS (solid line) and RTDNC (dotted line) over the 2012 to 2015 period.

Table 3.5. Summarized TP and SRP FVMCs from the field site used to create estimates of TP export from the surface runoff and tile flow paths.

Surface Runoff FVMC			
Season	TP (mg/L)	SRP (mg/L)	SRP:TP Ratio
Winter	0.54	0.10	0.18
Spring	0.68	0.41	0.60
Summer	0.80	0.24	0.30
Fall	0.25	0.12	0.47

Tile Flow FVMC			
Month	TP (mg/L)	SRP (mg/L)	SRP:TP Ratio
Jan	0.037	0.004	0.11
Feb	0.004	0.003	0.72
Mar	0.074	0.020	0.27
Apr	0.102	0.045	0.44
May	0.025	0.001	0.05
Jun	0.024	0.003	0.13
Jul	0.016	0.0001	0.01
Aug	0.023	0.007	0.32
Sep	0.050	0.003	0.06
Oct	0.054	0.018	0.33
Nov	0.105	0.066	0.63
Dec	0.170	0.034	0.20
Average	0.057	0.017	0.274

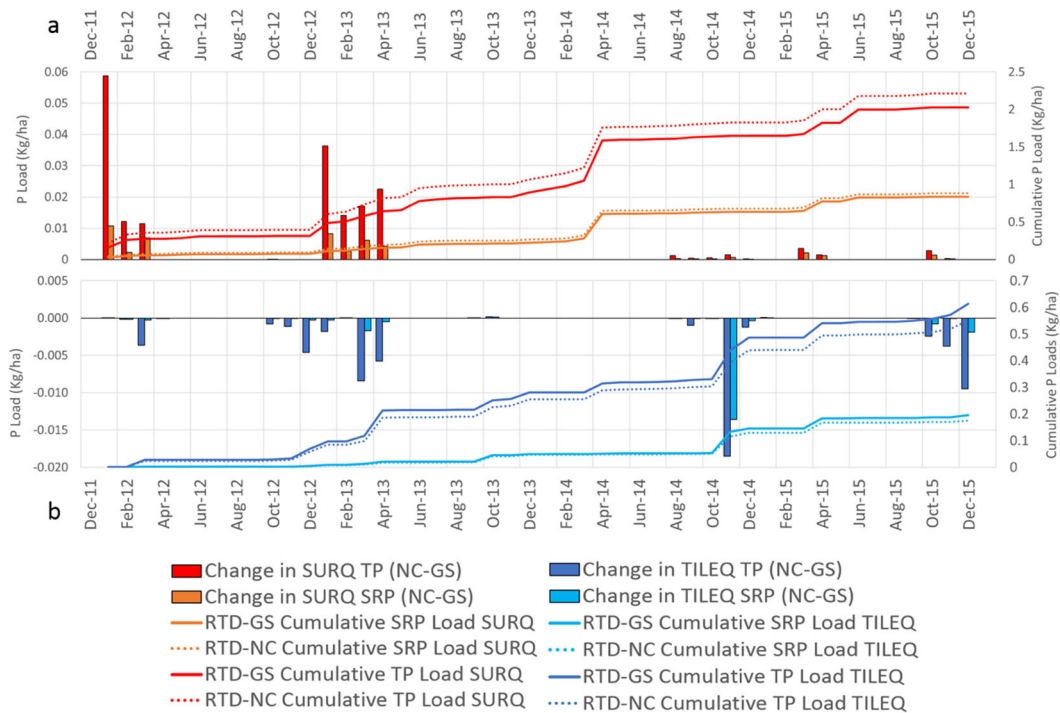


Figure 3-15. Monthly cumulative loads (lines) and change in loads between RTDGS and RTDNC from 2012 to 2015 for TP and SRP in surface runoff (SURQ; a) and tile flow (TILEQ; b).

3.2.8 Discussion

3.2.8.1 SWAT HRU performance

The model performed adequately with respect to tile flow and surface runoff to perform the subsequent analysis. These results are comparable to a study by Guo et al. (2018) where tile flow performance with respect to the NS ranged from 0.53 to 0.61 and 0.50 to 0.81 for surface runoff. Some of the performance issues may be explained by model inputs. The uncertainty associated with soil conditions at depth and the location of the impervious layer impacted the calculations of percolation, water table depth, and tile flow (Neitsch et al., 2011). In winter, precipitation data was supplemented by the nearby Jamestown station data (43 km away from site) because snowfall was not measured continuously at the field site, and consequently, may have varied slightly from what occurred at the site. Tile performance issues could also be explained through model structure. For example, in February 2013 there is no surface runoff probably because of precipitation being added to the snowpack. This should increase the soil temperatures and allow for the tile flow response that was found because winter soils are typically at field capacity or saturated (Lam et al., 2016). However, within the model, when soil layer is frozen, water movement does not occur (Neitsch et al., 2011). This indicates that there might be issues with the soil temperature calculations in SWAT. The model is unable to capture this response due to the known simplicity of the empirically based soil temperature algorithm, and its inability to simulate soil temperatures in cold regions with regular of freeze-thaw conditions (Qi et al., 2016). As well, SWAT had performance issues in summer due to underperforming soil water estimation (Rajib & Merwade, 2016) and erratic water table estimation related to dryer soils (Moriassi et al., 2009).

In summer, it is uncertain if macropore flow is a large contributor to tile flow at the field site, which is a clay loam. Furthermore, there was no surface runoff data from the summer of 2014 to confirm if infiltration was overestimated. In October 2015, it is uncertain what caused the overestimation of surface runoff since precipitation data was from the nearby Jamestown station, which cannot be validated using field site data. However, similar precipitation events in October 2013 were validated with field data, and the small 4% difference indicates another reason. The poor validation performance is most likely due to the limited time span of the dataset that did not capture a range of wet, dry, and average years for validation.

3.2.8.2 Impact of CD on flow paths and TP export

The results of this study suggest that the use of CD throughout the NGS may increase annual TP losses in runoff and could exacerbate eutrophication; however, the use of CD during the

GS has relatively little effect on TP losses. These results are in contrast to Tan and Zhang (2011) who projected a 12% decrease in annual TP losses over their study period. The primary difference between the current study and the work of Tan and Zhang (2011) is that the current study was conducted in coarser textured soils on sloping ground, whereas the study by Tan and Zhang (2011) was conducted in lacustrine clays. Indeed, the current study reported a very different water balance distribution than Tan and Zhang (2011) who reported that 97% of runoff occurred as tile flow with FTD. Other differences between the two studies include narrower tile spacing (3X narrower) and the use of sub-irrigation at the clay site.

The current study has shown that any decrease in tile depth (either no tiles, RTDNC, or RTDGS) will lead to decreased tile flow; however, this flow will be redistributed, leading to increased surface runoff. This finding is consistent with what has been shown in other studies (Ross et al., 2016; Skaggs et al. 2012; Tan & Zhang, 2011). Given the greater P concentrations in surface runoff at the site (Van Esbroeck et al., 2016), this will exacerbate the P loading from the site.

In our study, RTDGS exported less TP in runoff than RTDNC relative to FTD because of reduced surface runoff in the NGS. Surface runoff increases in the RTDNC scenario during the NGS resulted from the higher soil water levels, decreasing the water table depth from the surface and making saturation excess surface runoff a greater risk. This response was typically spread out over the entire winter or did not occur in every year, because the southern Ontario climate facilitates multiple snowmelt events with a wide range of pre-event soil conditions and precipitation form variability in the NGS (Van Esbroeck et al., 2017). In the summer, surface runoff does not increase much, because the model calculates the surface runoff using the SCS-CN method (Soil Conservation Service, 1972) where the curve number (CN) and retention parameter is updated using PET and the previous day's parameter (Neitsch et al, 2011). Therefore, high PET values result in a reduction of the CN compared to winter, increasing the infiltration for the day. As a consequence of increased PET, soil water levels are initially very low and even though precipitation intensity might be greater, it requires substantially more rain and reduced PET to trigger surface runoff.

How tiles are managed during the winter NGS will be increasingly important since they can increase surface runoff and TP loads, contrary to the GS where there are clear benefits of using CDs (Sunohara et al., 2015, 2016). Furthermore, in humid climates, most N leaching occurs during the winter (Bohne, Storchenegger, & Widmoser, 2012) and P losses as well (Macrae et al., 2007b; Van Esbroeck et al., 2017; Williams et al., 2016).

3.2.8.3 Potential for CD to Mitigate Runoff and P Loss Under Future Climates

In this portion of the study, the field scale SWAT model was combined with the MCW historical and future climate to speculate on what may occur to nutrients and sediment at the edge of field if CD were used in a future climate.

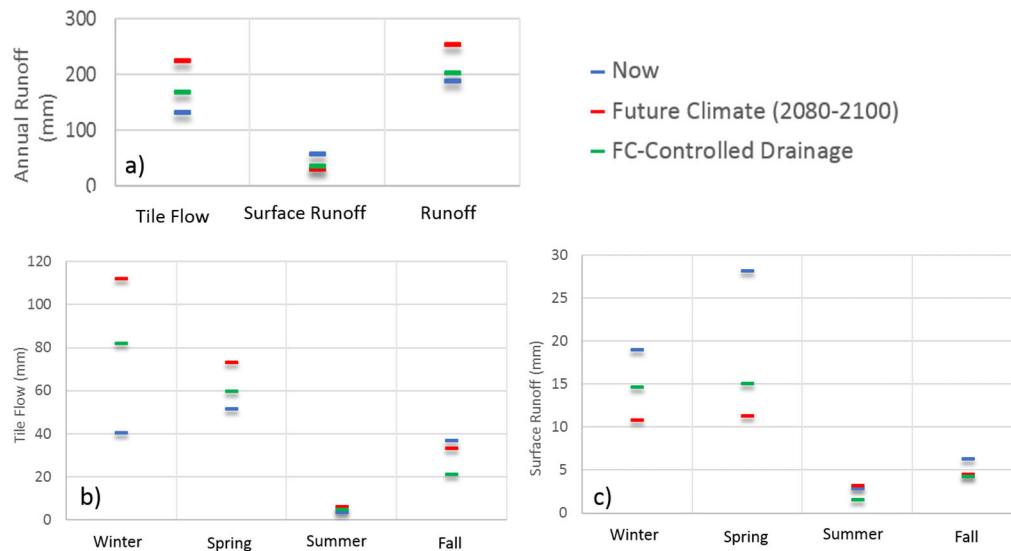


Figure 3-16. (a) Changes in the tile flow, surface runoff, and runoff annually in the LON field site transplanted into the MCW during the 1990-2010 period (blue), 2080-2100 period (red), and 2080-2100 period with continuous CD (green). Also, shows tile flow seasonally (b) and surface runoff seasonally (c).

On an annual basis, water balance changes due to CD and climate change are very similar to what was reported in the Medway Creek and Londesborough studies. The change in climate will lead to greater runoff in future, and this will occur despite the presence of CD, CD will most likely exacerbate annual TP export trends by enhancing surface runoff during peak flows. Indeed, the increase in surface runoff caused by CD will only increase the potential for greater and more occurrences of saturation excess overland flow events, which is a major factor in TP export from fields. In the case of NO_3^- , average NO_3^- concentrations were almost equivalent between tile flow and surface runoff pathways at Londesborough. Therefore, because the decrease in tile drainage is greater than the increase in surface runoff, there could be a net reduction in NO_3^- export with CD under a future climate. Although, CD promotes anaerobic conditions that increase the potential for denitrification (Skaggs et al., 2010; Wesström & Messing, 2007) the exact effect of climate change on denitrification is unknown (Barnard et al., 2005). When combined, we could expect further decreased nitrate losses due to increased denitrification rate from increased soil moisture and temperature; however, there are many other complex feedbacks to consider (Karmakar et al., 2016; Singh et al., 2010; Veraart et al., 2011). Consequently, either CD management scenario will provide nitrate reductions and near continuous management (RTDNC) will have the greatest reduction due to larger tile flow reductions throughout the year.

More work is needed on this topic as the precise responses of fields and watersheds to CD and climate change will be spatially variable given that runoff and nutrient loss are dependent on many field specific characteristics such as tile spacing and depth, NGS management depth, FWMC runoff ratios, slope, soil characteristics and specific land management practices. Therefore, future work should confirm the effect of large-scale adoption of CD and climate change on TP export in watersheds that have fields with different characteristics (i.e. tile layouts and NGS management) and in combination with other BMPs. However, in order to do this, SWAT needs some improvement, mainly to the soil temperature and TP tile routing algorithm given the winter season responses found in this study.

3.2.9 Conclusions

In this portion of the study, the SWAT model was assessed at the HRU scale and the impact of CDs on flow pathways, SRP, and TP export were analyzed for a clay loam soil in southern Ontario. Results indicate that the SWAT model still needs improvement simulating soil temperatures in the NGS. Overall, year-round tile management (RTDNC) causes an increase in average annual surface runoff (26%) and edge of field TP losses (13%) over the study period, specifically due to the increase in NGS (January to April) surface runoff. Tile management practices that keep the water table lower most of the year (RTDGS) may not have as great an impact on TP losses in runoff (4 to 8% increase) or surface runoff volumes (8 to 13% increase). Controlled drainage may provide many benefits with respect to tile drainage water quality; however, care should be taken when deciding on how to best manage the tile drains in the NGS considering the effects it can have on surface runoff P export.

4 QUEBEC REGION STUDIES

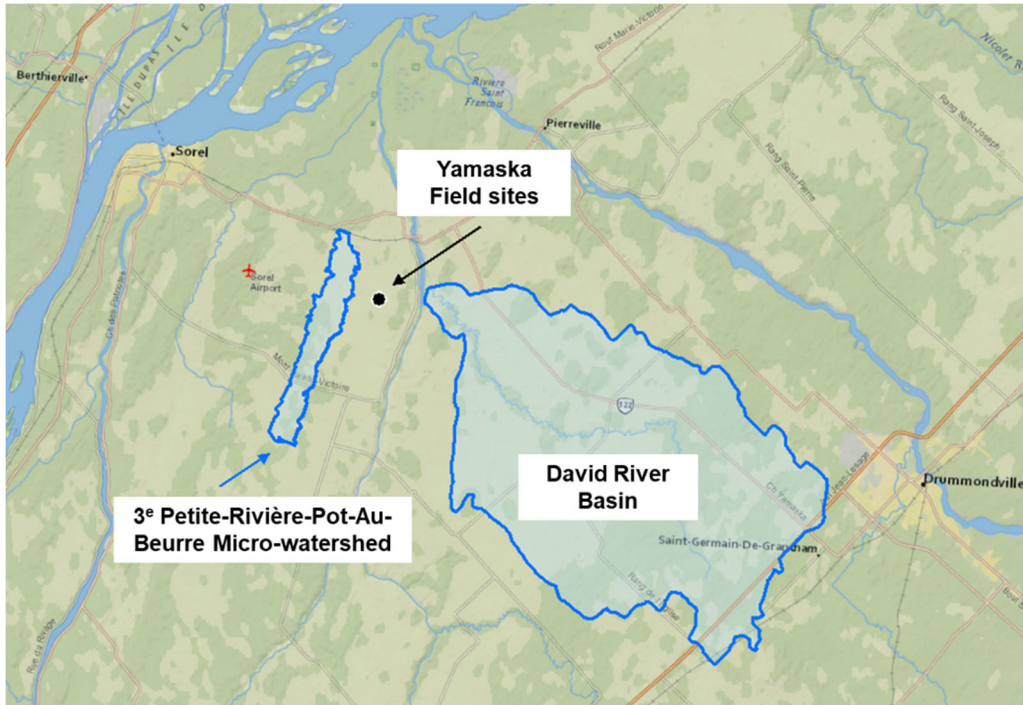
The following sections present successively the methodology and experimental results from the three nested scales of study from Montérégie region, Quebec, namely the 3rd Petite-Rivière-Pot-au-Beurre micro-watershed (20 km²), Yamaska field sites (< 10 ha) and David river basin (230 km²).

4.1 Micro-watershed study: 3rd Petite-Rivière-Pot-au-Beurre

From a multi-scale experimental approach, the hydrometric monitoring of the 3rd Petite-Rivière-Pot-au-Beurre (PRPB) micro-watershed complements both the Yamaska field scale study and the David basin scale study in several ways. The PRPB study provided a detailed portrait of water yields and pathways, as well as historic sediment and nutrient fluxes from the study region, which are critical inputs for the interpretation of the environmental and agronomic feasibility of controlled drainage scenarios. The coupling of the separated (surface vs subsurface) water yields from the micro-watershed with the water yields from the field site tile drainage systems was also important in describing the partitioning of subsurface flow pathways at field scale (tile vs return/resurgent flow). Finally, the monitoring of the micro-watershed, including hydrograph separation using geochemical methods, provided benchmark information on the intensity and temporal distribution of surface runoff and subsurface transfers within the study region. These guidelines were useful to the hydrologic modeling of the David river basin, as they ensured that the model adjustment of stream discharge reflected a realistic hydrologic balance and distribution of flow pathways.

4.1.1 Site description

The 3rd Petite-Rivière-Pot-au-Beurre subwatershed (20.0 km²), hereafter referred to as PRPB subwatershed, is located within the Baie Lavallière watershed, tributary to the Yamaska river basin which flows into the Saint-Lawrence river, upstream of Lake Saint-Pierre. The Baie Lavallière's downstream wetland was designated in 2000 as part of the Saint-Pierre Lake UNESCO World Biosphere Reserve. The PRPB subwatershed is located entirely within the *Municipalité régionale de Comté* (MRC) de Pierre-de-Saurel, flowing across the Saint-Robert municipality, and partially through Saint-Aimé (upstream portion) and Yamaska (downstream portion) (Figure 4.1).



Figure

4-1. Location of project experimental sites including 3e Petite-Rivière-Pot-Au-Beurre (PRPB) micro-watershed, Yamaska field sites and David River Basin.

In the cold, humid temperate climate of the study region, the monthly air temperature ranges from -10.0°C in January to 20.5°C in July with 1132 mm of precipitation in the form of rain (931.7 mm yr⁻¹) and snow (200.5 mm yr⁻¹; ECCC, 2018). The PRPB subwatershed landscape is flat, with an average slope of 0,65%, and elevations ranging from 15 to 28 m above sea level. Surface soils are sandy podzols (upstream) to dominantly clayey gleysols (downstream), overlying poorly-drained clay subsoils of marine origin (Michaud et al., 2012a). The soil map of the watershed is presented within figure 4.2a. Properties of individual soil series are reported in Michaud et al.(2012a) .

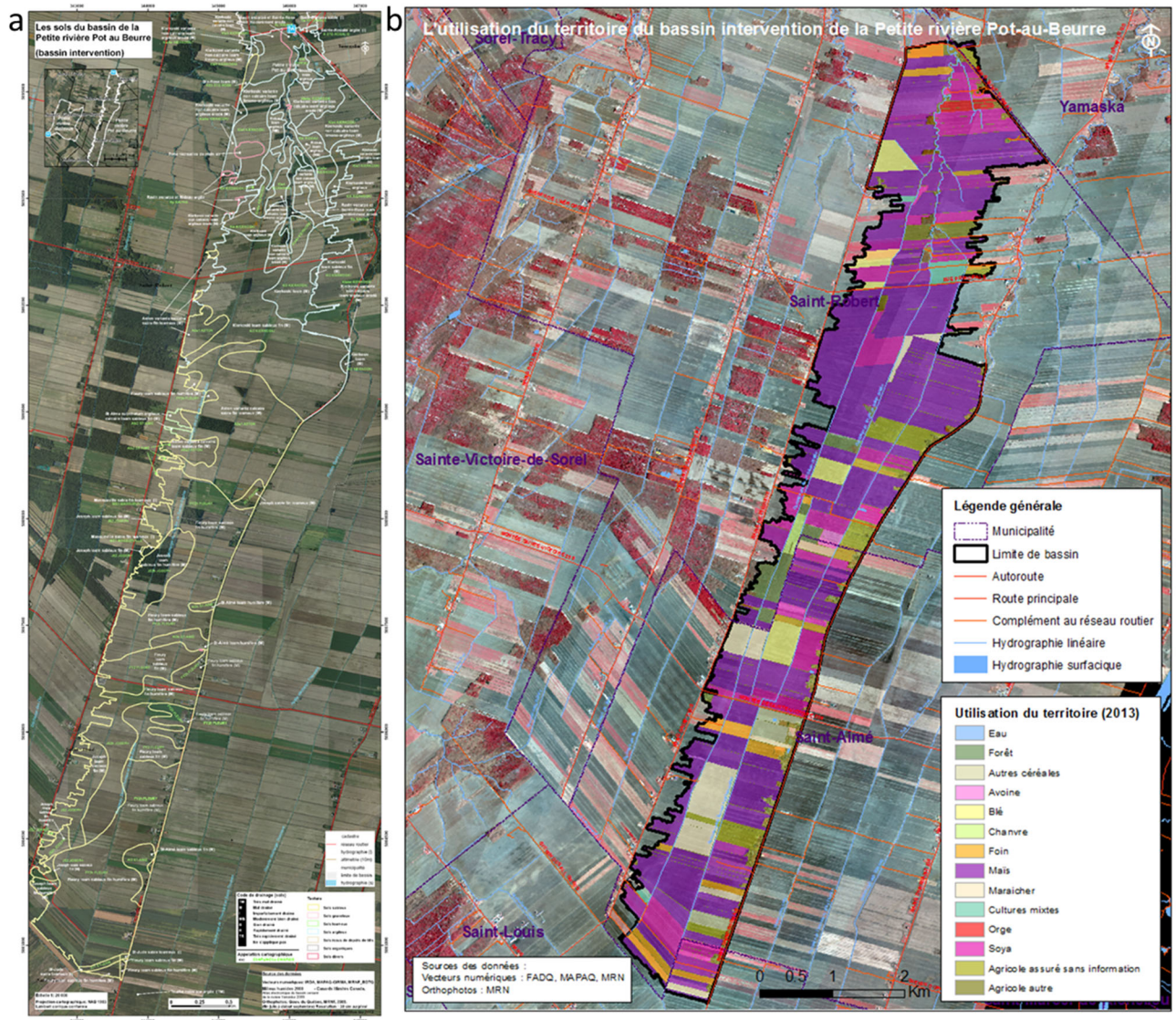


Figure 4-2. Soil map (a) and land use map (b) of PRPB micro-watershed (Michaud et al., 2012).

Agriculture accounts for 97% of the PRPB sub-watershed land use and is dominated by annual corn production (58% of fields surface area), soybean (12%), small grains (7%) and horticultural crops (5%). Hayfields with perennial forages occupy the remaining 13% of agricultural land in the subwatershed (Michaud et al., 2012a). Most cropland (approximately 80%) within the subwatershed is systematically tile drained and municipal drains have been installed to reach approximately a density of 2 km/km². Figure 4.2 illustrates the land use of the PRPB subwatershed.

Hydrograph separation. The hydrograph separation method relied upon the continuous EC monitoring of stream water, following a mass balance approach. The rationale behind the method is that tile drainage and resurgence flow have a higher EC than surface runoff due to more contact time with electrolyte-rich soil. The continuous monitoring (every 15 min) of stream water temperature, turbidity and electrical conductivity (EC) were supported by a multi-parameter probe (YSI 600XL, YSI Incorporated, Yellow Springs, OH, USA). During base flow conditions, groundwater resurgence typically generated a base flow with EC from 0.75 mS cm⁻¹ to 1.0 mS cm⁻¹ (Fig. 4.4).

For individual high flow events, subsurface flow at time i (QD_i , in mm d⁻¹) in the stream was calculated using Eq. 1:

$$QD_i = \frac{(EC_i - EC_s)}{(EC_{TD,i} - EC_s)} \times Q_{peak,i} \quad [1]$$

where EC_i is the measured EC in streamflow at time i , EC_s is the reference EC of surface runoff water (0.0012 mS cm⁻¹), $EC_{TD,i}$ is the estimated EC of the subsurface streamflow contribution at time i , and $Q_{peak,i}$ represents the water discharge (mm d⁻¹) at time i , after subtracting the contribution of groundwater resurgence to discharge.

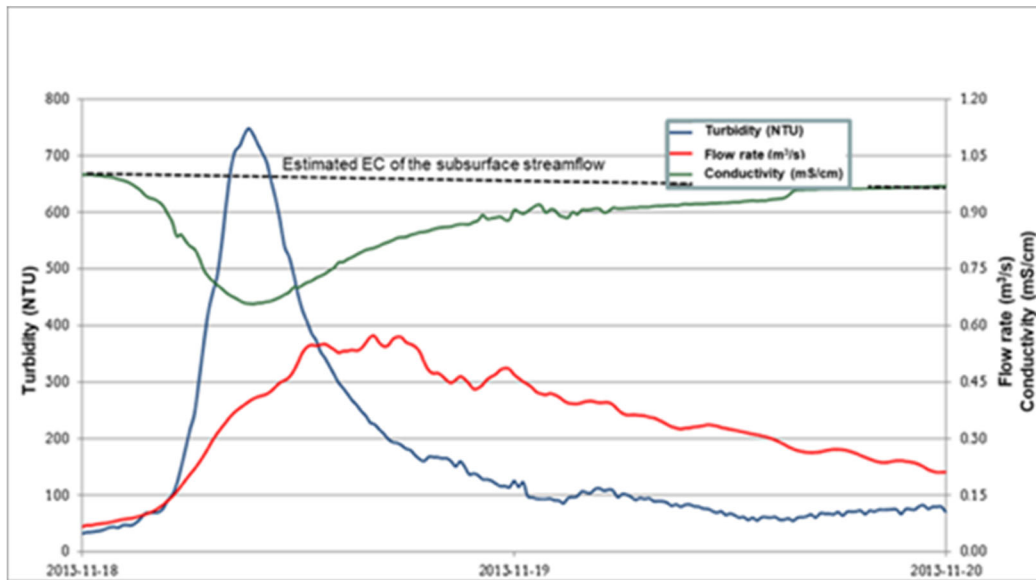


Figure 4-4. Temporal variability in instantaneous (15 min.) stream flow rate, electrical conductivity and turbidity signals at PRPB monitoring station for a single late fall rainfall event.

The estimated EC of the subsurface streamflow contribution was determined for each individual runoff event from the linear relationship relating the initial stream flow rate corresponding to maximum EC prior to initiation of the hydrograph rising limb, to the final flow rate when EC has returned to its pre-event value, following completion of the hydrograph recession limb (Fig 4.4). Changes in stream water EC during a peak flow event were attributed to the volume and EC of water entering the stream from fields via surface runoff and tile drainage pathways. Surface runoff reference EC was estimated from the stream observed EC minima, corresponding to the highest stream peak flow rates, after subtracting the contribution of the tile drainage systems to the global stream EC (specific daily water yield of 9 mm).

Sediment and nutrient fluxes. Sediment loading was estimated from the turbidity signal (15 min) following a calibration of the linear relationship between turbidity and TSS estimates in water samples. Nutrient fluxes were determined from a total of 162 grab water samples collected throughout the 2009-2014 period at the PRPB hydrometric station, using a sampling strategy favoring elevated and peak flow events. All water samples were kept at 4°C until analysis for Total suspended solids (TSS) were determined by filtration through a 0.45 µm filter (Greenberg et al., 1992a). Dissolved reactive phosphorus (DRP) was determined colorimetrically on filtered samples (< 0.45 µm) using the molybdenum-blue method of Murphy and Riley (1962), while total phosphorus (TP) concentration was measured using the persulphate digestion technique (Greenberg et al., 1992b). Nitrogen (ammonia and nitrates) were determined by the Cadmium Reduction Method (Greenberg et al., 1992c). Bioavailable phosphorus (BioP) was also determined on a subset of samples using the 0.1 N NaOH extraction method of Sharpley et al. (1991) to document the bioavailability of P with respect to flow pathways.

Daily nitrogen and phosphorus fluxes from the subwatershed were computed using the FLUX 5.0 software (Walker, 1998). The two flow-strata and two seasonal strata regression was based on the log concentration/flow (log C/Q) relationship of the mean daily flow (Q) and water quality concentrations (C) from the 162 grab samples. The coefficients of variation of TP, DRP and NO₃, and TSS export estimates, calculated using the cross-validation (jack-knife) procedure reported by Walker (1987), were close or below 10%, which indicate an excellent model adjustment for such small flashy watersheds (Walker, 1998). The concentration and load residuals provided by FLUX 5.0 were independent of flow, date, season, concentration, and export, with no outliers being detected at a confidence level of $\alpha = 0.05$.

4.1.3 Results

4.1.3.1 Historic water, sediment and nutrient yields

Annual water yields ranging from 440 to 460 mm were dominated by subsurface flow paths according to the geochemical flow separation. Surface runoff events were concentrated within the recharge period, in late winter and early spring (figure 4.5). The systematic tile drainage of the cropped area and the relatively deep and high-density network of (approximately 2 km /Km²) municipal drains accounted for the efficient and rapid drainage of the micro-watershed.

Approximately 25% of annual discharge occurred during the growing season (May-September), essentially all through subsurface flow (table 4.2). This seasonal water yield averaged 108 mm, which could be considered, in theory, as the inherent capacity of the watershed to supply additional water to the cropping systems, excluding an hypothetical minimum ecological flow rate.

Nitrate yields from the micro-watershed averaged 26 kg N/ha (22-28 kg N/ha). Relatively high N loadings are explained by the importance of corn crop (Table 4.3), typically requiring large N inputs (approximately 180 kg N/ha from fertilizer recommendations grid). As reported in the literature and from PRPB hydrometric records, nitrate loadings are essentially driven by subsurface flow paths. The relative importance of resurgent and tile flow pathways of N cannot be determined from the outlet monitoring protocol. On average, 30% of the annual nitrate export occurred during the growing season (May-September), which represents a yearly specific loading of 7.7 kg N/ha.

With respect to phosphorus, up to 80% of the Total P yield occurred during the recharge period and was driven by peak flow events, presumably associated with surface runoff and preferential subsurface flow paths. The stream outlet monitoring protocol did not enable the quantification of P in surface vs subsurface flow paths. For similar edaphic environment and cropping systems in the Monterégie region, Total P loads were apportioned from 58-65% to surface runoff and 26-37% to tile drainage, dominantly through preferential, macropore flow (Michaud et al., 2019).

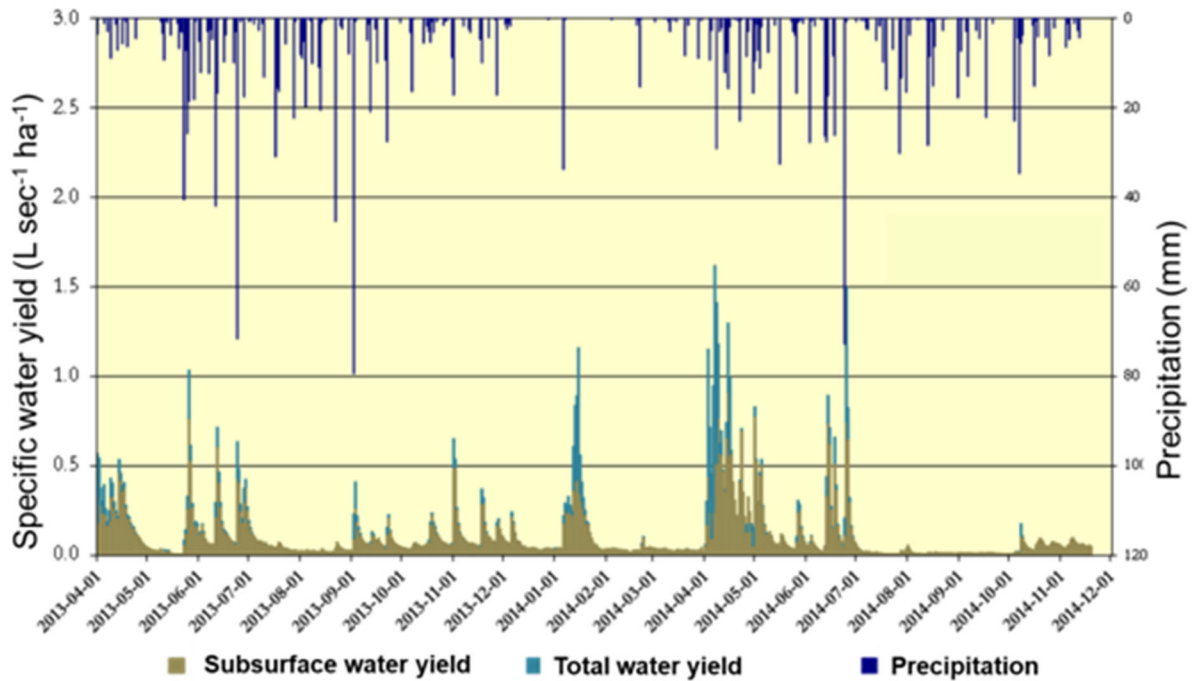


Figure 4-5. Daily precipitation and specific water yields separated according to the geochemical signal at PRPB micro-watershed outlet for the april 2013 to November 2014 period.

Table 4.1. Average annual specific water yields, sediment and nutrient fluxes monitored at PRPB micro-watershed outlet for the September 2009 to October 2011, and the April 2013 to October 2014 period.

	September 2009 to october 2011			April 2013 to october 2014		
	Spec. Load	Conc.	CV ¹	Spec. Load	Conc.	CV ¹
	(kg ha ⁻¹ yr ⁻¹)	(µg l ⁻¹)		(kg ha ⁻¹ yr ⁻¹)	(µg l ⁻¹)	
TSS²	575	124 672		429	97 230	
Total phosphorus	0.93	203	0.114	0.89	202	0.10
Dissolved total pohosphorus	0.14	30	0.075	0.28	64	0.09
Nitrates	28	5 973	0.106	22	5 031	0.11
Calcium	337	73 242	0.029	333	75 554	0.06
Water yield	460 mm			441 mm		

(1) Coefficient of variation of loadings estimated by crossed validation procedure (jack-knife).

(2) Estimation derived from the turbidity signal (multi-parameter probe).

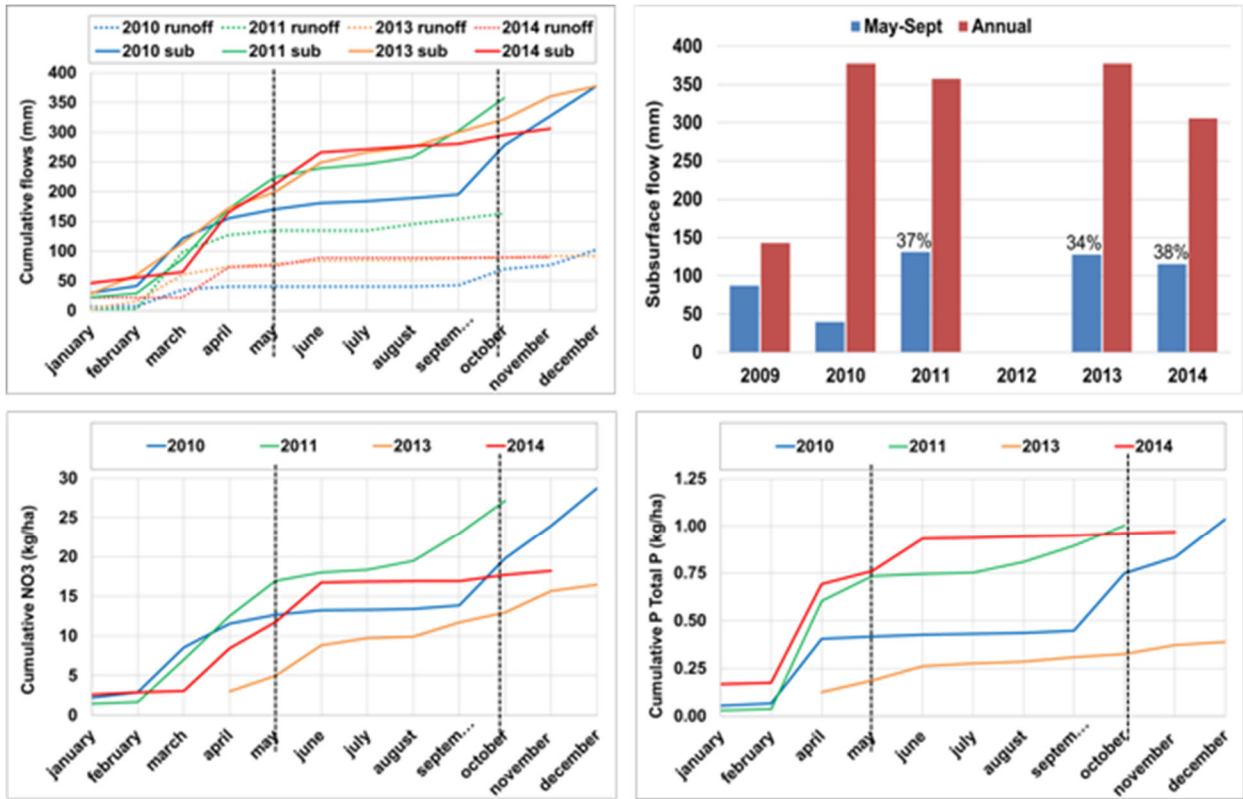


Figure 4-6. Cumulative surface runoff and subsurface flow (a,b), nitrates yields (c) and Total phosphorus yields (d) monitored at PRPB micro-watershed outlet for the 2010-2014 period.

Table 4.2. Cumulative stream discharge, subsurface flow, TSS and nutrient exports monitored at the PRPB micro-watershed outlet for the growing season and recharge periods (averages for the 2010-2014 period).

	Growing season (May-Sept.)	Recharge Period (Oct.-April)	% Growing Season/Annual
Total stream discharge (mm)	108	320	25%
Subsurface flow path (mm)	107	270	28%
Total P export (kg/ha)	0.21	0.78	21%
Reactive soluble P export (kg/ha)	0.06	0.15	29%
Bioavailable P export (kg/ha)	0.07	0.27	20%
TSS export (kg/ha)	128	459	22%
Mineral nitrogen export (kg/ha)	7.7	17.8	30%
Calcium export (kg/ha)	92	241	28%

4.1.3.2 Hydrograph separation during the 2015-2017 period

During the 2015-2017 monitoring period, when both field and micro-watershed sites were simultaneously monitored, PRPB micro-watershed water yield totaled 1282 mm (Table 4.2). Figure 4.7 illustrate the temporal variation in the instantaneous (15 min.) electrical conductivity signal for the 2016 annual cycle. During the growing season, base flow EC plateau fluctuated between 0.5 and 0.9 mS/cm, with a typical inflection around 1.1 mm/day stream flow rate. During the recharge period, the base flow reference EC tended to be lower, and plunged down to 0.153 mS/cm during peak flow events with maximum contributions from surface runoff to total water yield. Figure 4.8 illustrates the daily flow separation between surface and subsurface components estimated by the hydrograph geochemical separation method for the 2016 annual cycle.

Significant surface runoff events occurred during mild spells and snowmelt events in the late winter and early 2016 and 2017 periods. Stream flow during the growing season totalled 231 mm, dominantly through subsurface pathways, with a marginal surface runoff contribution (33 mm). Conceptually, the subsurface water yield monitored at the micro-watershed cumulates both resurgent and tile flows. The coupling of the observed time series of tile flow rate from the Yamaska field sites with the PRPB subsurface series is expected to generate an approximation of the relative importance of resurgent vs tile flow.

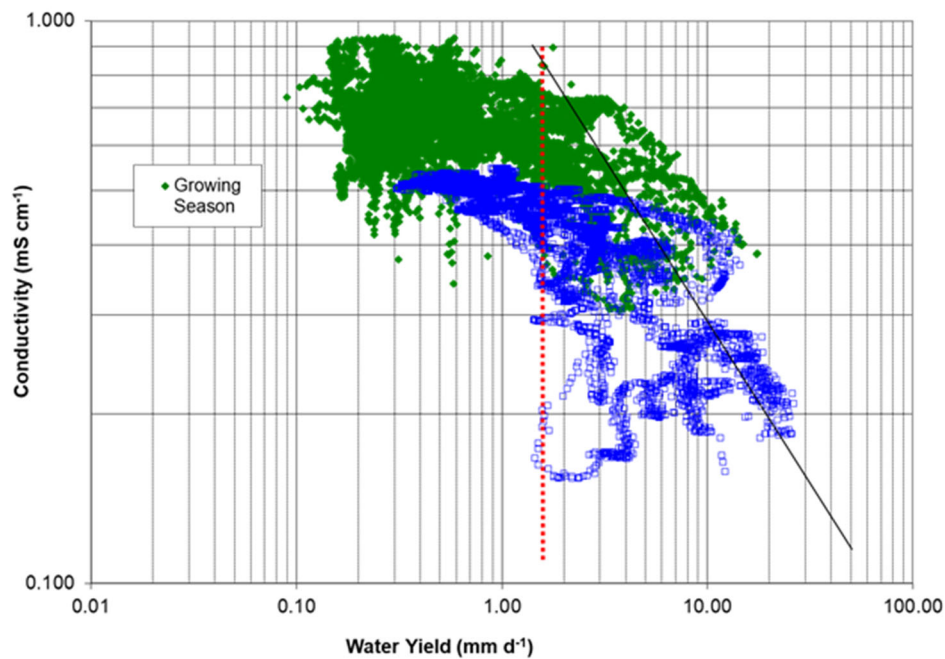


Figure 4-7. Temporal variability in the instantaneous (15 min.) electrical conductivity signal at PRPB monitoring station (Green: growing season; Blue: recharge period), shown as a function of stream flow rate and season for the 2016 monitoring period.

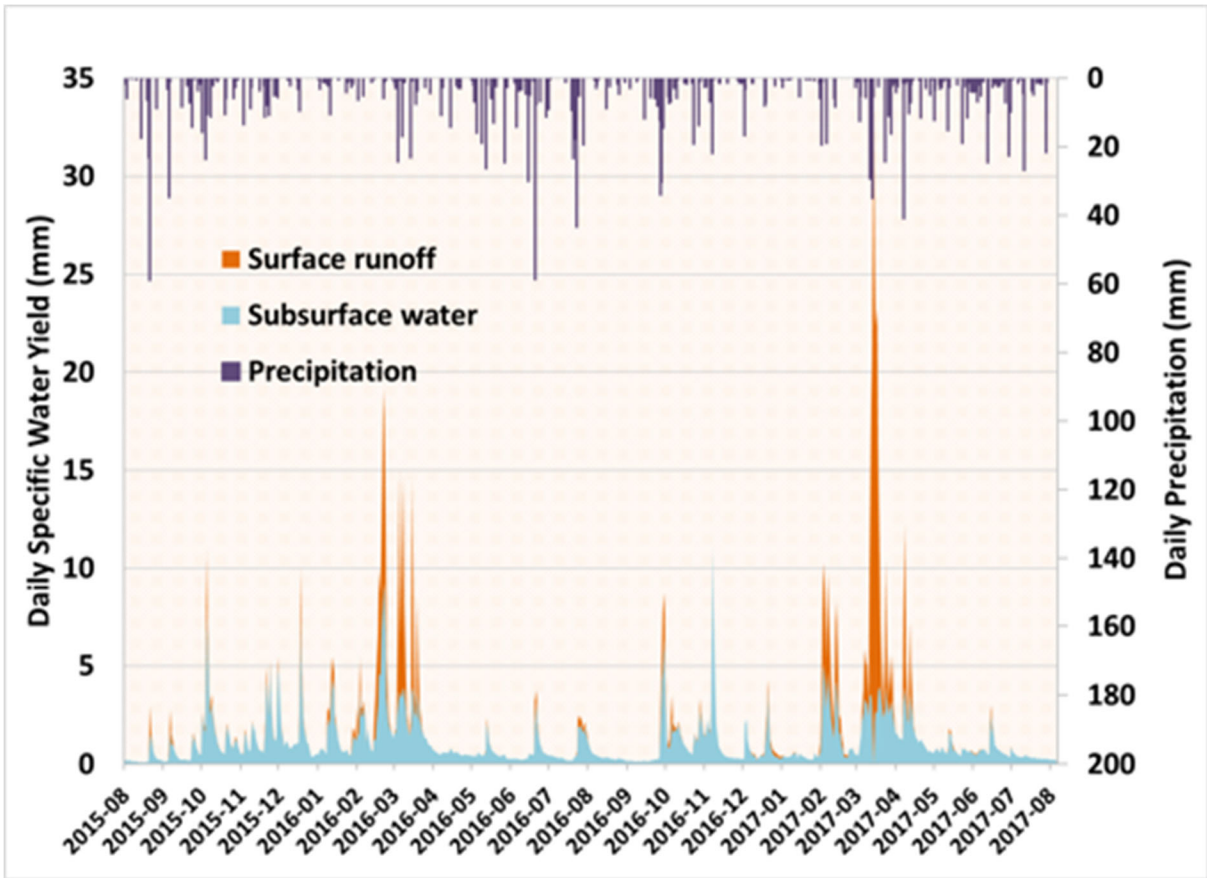


Figure 4-8. Daily precipitation and specific surface and subsurface water yields, estimated using geochemical signals at the PRPB micro-watershed outlet for the Controlled drainage project period (July 2015 to September 2017).

Table 4.3. Cumulative stream discharge, subsurface flow and surface runoff for the Controlled drainage project period (July 2015 to September 2017).

	Total stream discharge (mm)	Subsurface flow path (mm)	Surface flow path (mm)	Ratio Sub/Total
Total period (2015-2017)	1 282	856	426	0.67
Growing season (May-Sept.)	231	198	33	0.86
Recharge Period (Oct.-April)	1 051	658	393	0.63

4.2 Yamaska field site study

4.2.1 Introduction

The main objective of the Yamaska field study in the Montérégie region, Québec, was to evaluate the agronomic and environmental feasibility and benefits of controlled drainage. Water table stage, drainage water, sediment and nutrient yields from tiles, as well as crop yields were monitored during three growing seasons on two fields, including a controlled drainage treatment and a free drainage site. The coupling of the field sites and 3e Petite-Rivière-Port-Au-Beurre (PRPB) hydrometric data provided additional insights on the partition of subsurface flow pathways (tile vs resurgent flow) within the study region.

4.2.2 Methodology

4.2.2.1 Site description

The experiment was conducted on two fields from GenLouis farm, owned and managed by by Mr Louis Joyal and his family in Yamaska, Montérégie region, Québec. The fields have a history of row crop production, namely corn, soya and wheat rotation, under liquid hog manure and mineral fertilization. Currently, the farm is being converted to organic farming.

Both fields have a very flat landscape (50 cm gradients in elevation), as pictured in Figure 4.8, which is typical of the Saint-Lawrence lowland landscape. The clayey texture of top- and subsoil is a result of the former Champlain sea deposits. The fields have been systematically subsurface drained to 1.0-1.4 m depth by the farm owners and control chambers were installed at each field's tile drain collectors. Two deep municipal drains (>3.0 m) and ditches (1.5 m) surround the fields.

4.2.2.2 Experimental design and monitoring protocol

The eastern field was designated as the Controlled drainage treatment (Figure 4.9). The tile drain collector was blocked during the growing season, triggered by a flow device that engaged when the water table reached the 50 cm critical depth. The western field was used as a control site, where the tile drain collector remained open during the three growing seasons and was monitored during that time.

Monitoring stations were installed within the controlled chambers of both fields to monitor water yields and quality coming from the tile drain collectors. Acoustic dopplers and barometric probes (ISCO Teledyne 2150 Area Velocity Module) were used to monitor the stage and the speed of the current within the collectors, and calibrated against discharge from flow rate measurements at the

collectors outlets. Water samples were collected by manual and automated samplings (ISCO Teledyne 6712 Full-size Portable Sampler) from a schedule based on cumulative water discharge. Respectively, 47 and 69 water samples were collected from the Controlled drainage and Free drainage monitoring stations and brought in the lab for analytical determinations.

Total suspended solids (TSS) of water samples were determined by filtration through a 0.45 μm filter (Greenberg et al., 1992a). Dissolved reactive phosphorus (DRP) was determined colorimetrically on filtered samples ($< 0.45 \mu\text{m}$) using the molybdenum-blue method of Murphy and Riley (1962), while total phosphorus (TP) concentration was measured using the persulphate digestion technique (Greenberg et al., 1992b). Nitrogen (ammonia and nitrates) was determined by the Cadmium Reduction Method (Greenberg et al., 1992c). Bioavailable phosphorus (BioP) was also determined on a subset of samples using the 0.1 N NaOH extraction method of Sharpley et al. (1991) to document the bioavailability of P with respect to flow pathways. TSS, P fluxes were computed from the product of instantaneous (15min) flow rates and estimated nutrient concentration derived from concentration: flow rate linear models. Nitrogen fluxes were computed from flow rate measurements and time-interpolated concentration values.

Water table stage from both fields was monitored using a series of twelve observation wells. The experimental design, as pictured in figure 4.9, is composed of the three pairs of wells (one overlying the drain and the other one mid-spaced), that were installed at incremental distance from the tile collectors. Barometric probes (HOBO U20L-04 Water Level Data Logger; 13 ft) were placed on the bottom of each perforated tube (1.6 m) and protected from silting by nylon nets (Figure 4.9).

The soil physico-chemical properties at 0-20 cm and 20-40 cm depth increments of the water stage monitoring site were determined from core (N=24) and composite samplings (N=12) and analytical determinations at IRDA's laboratory. Bulk density, macroporosity (100 cm tension) and saturated hydraulic conductivity were performed on the core samples. Soil pH, cation exchange capacity, organic matter content and nutrient levels (N, P and macro-elements) were determined on composite samples.

Crop yields were determined from manual local harvest on individual observation wells sites (N=12) from 7.62 m² plots, with mass and moisture determined in the lab. The crop yields were also derived from the combine's yield monitor, operated by the farm managers.

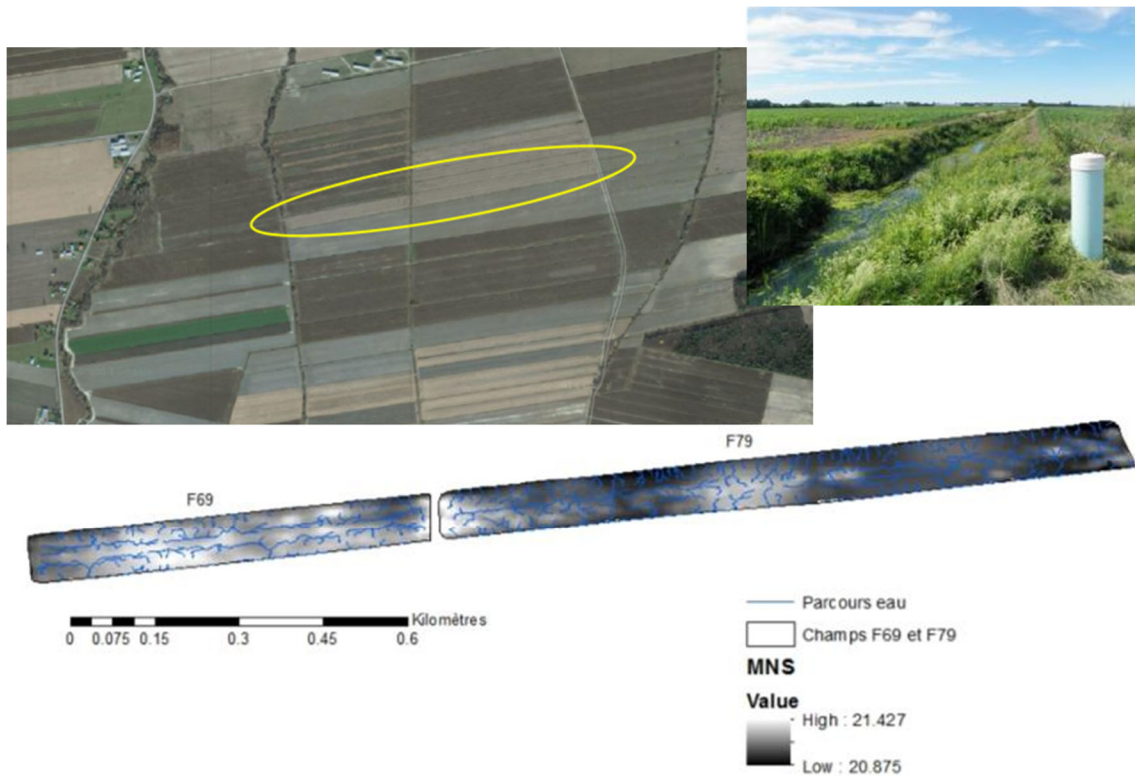


Figure 4-9. Aerial photograph, Lidar-derived elevation model and surface flow paths of experimental field sites.

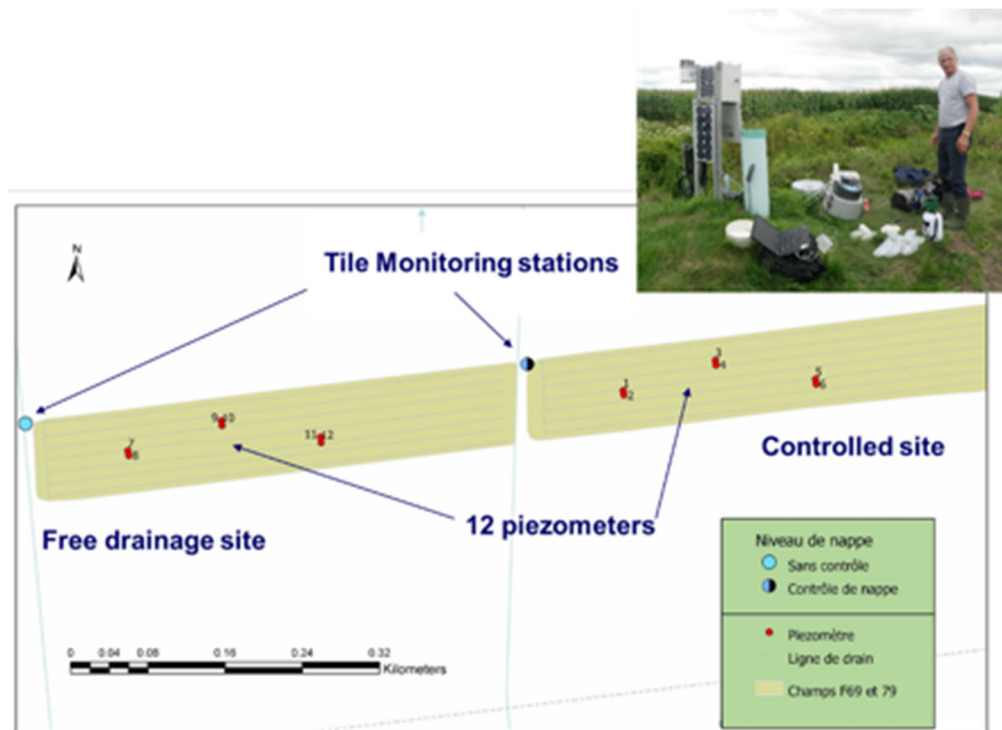


Figure 4-10. Location of the 12 observation wells and monitoring stations of the subsurface drain collectors.



Figure 4-11. Installation of the observation wells.



Figure 4-12. Monitoring stations of the subsurface drain collectors.

Table 4.4. Soil physical properties of field sites.

Treatment	Depth (cm)	Texture	Bulk density g / cc		Macroporosity 100 cm g/cc		Saturated hydraulic conductivity cm / min	
			Average	Std	Average	Std	Average	Std
Control	0-20	Clay loam	1.215	0.219	0.177	0.024	0.445	0.033
Control	20-40	Clay	1.553	0.077	0.057	0.016	0.033	0.045
Free	0-20	Clay loam	1.348	0.056	0.148	0.026	0.211	0.182
Free	20-40	Silty clay	1.560	0.056	0.048	0.013	0.038	0.086



October 2015

Table 4.5. Soil chemical properties of field sites.

Traitement	Site	Depth (cm)	pH*	CEC Calcul mEq/100g	M.O. %	P mg/kg	N-NH4 mg/kg	N-NO3 mg/kg
Control	1-2	0-30	7.18	19.20	2.85	38.2	3.36	8.42
Control	3-4	0-30	6.73	18.00	2.83	31.6	2.7	6.39
Control	5-6	0-30	6.79	19.90	2.88	32.5	3.2	5.29
Free	7-8	0-30	6.37	18.60	3.24	27.9	2.5	4.57
Free	9-10	0-30	6.57	17.10	2.95	30	2.15	5.21
Free	11-12	0-30	6.62	19.00	2.52	23.9	2.95	3.31
Control	1-2	30-60	6.98	22.30	2.09	11.2	3.69	4.48
Control	3-4	30-60	6.98	21.90	1.4	3.92	2.26	2.93
Control	5-6	30-60	7.08	21.00	0.99	2.88	2.54	1.67
Free	7-8	30-60	7	19.20	1.61	9.12	2.76	2.32
Free	9-10	30-60	7.26	18.70	1.09	5.56	2.57	1.58
Free	11-12	30-60	7.51	22.10	1.07	4.91	3.13	1.96

4.2.3 Results

4.2.3.1 Soil properties

Table 4.4 provides the results from the physical determinations on the core soil samples. Overall, the fields are homogeneous in texture, with clay contents in topsoils (0-30 cm) ranging from 33 to 39%, with a notable exception of 47% percent clay on free drained sites no. 11-12. Clay content typically increases in subsoils, with levels ranging from 41% to 53%. The saturated hydraulic conductivity is relatively higher within the sampled Controlled site topsoils, together with an higher macropore volume (Table 4.5.)

The field sites do not show significant gradients in soil chemistry (Table 4.5), with relatively similar pH, CEC, %C and P status. A gradient in nitrate levels was however detected in October 2015 samples, favoring the Controlled site. This contrast is not explained by the soil organic matter levels of individual sites or N inputs (none for soya in 2015). Indications of a better soil physical condition at Controlled site, and its anticipated effect of N pool mineralization, may explain the residual nitrate contrast.

Significant differences in surface drainage were also observed during the visits to the field sites. Ponding was observed within the free drainage site in late winter and early spring, especially around the sites no. 11 and 12, which impacted on the subsurface drainage and crop yields, as discussed within the following sections.

4.2.3.2 Water table stage and water yield monitoring

Figure 4.13 illustrates the variability in water table elevation (absolute values, relative to surface benchmark), monitored at the 12 observation wells for the 2015-2017 monitoring period. Globally, the rise and decline of the water table at the six wells of the Controlled site appear in phase. The nearly constant elevation gradient amongst the sites reflects the position of the wells according to the tile drain position, with relatively lower water table over the tiles (sites 1,4,5) as compared to mid-spaced (sites 2,3 and 6). Also, for a common position with respect to tiles (over or mid-spaced), the water table elevation is consistently higher for the sites further away from the collector, which reflects the relative elevation of the tiles.

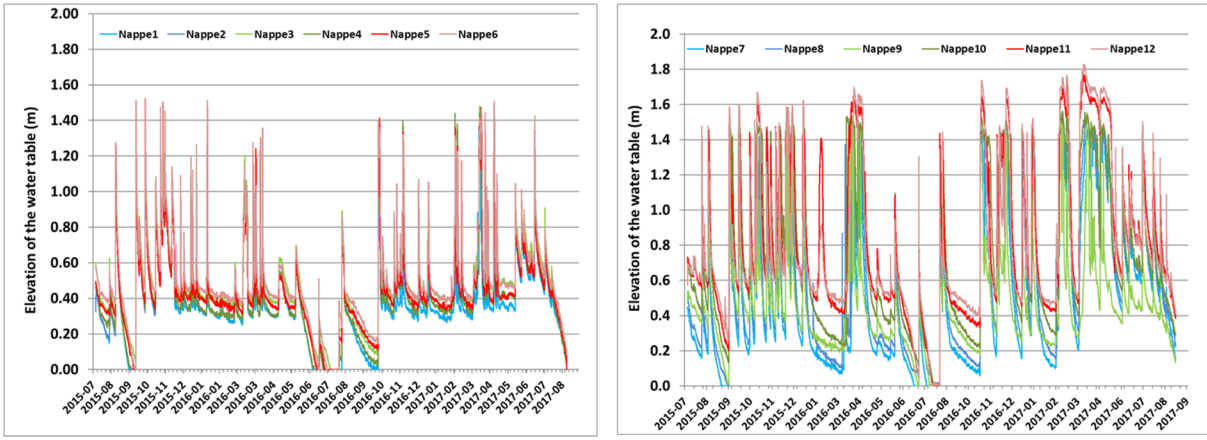


Figure 4-13 Water table stage variability monitored within individual observation wells for the controlled drainage site (no. 1 to 6) and Free drainage site (no. 7 to 12) for the 2015-2017 period.

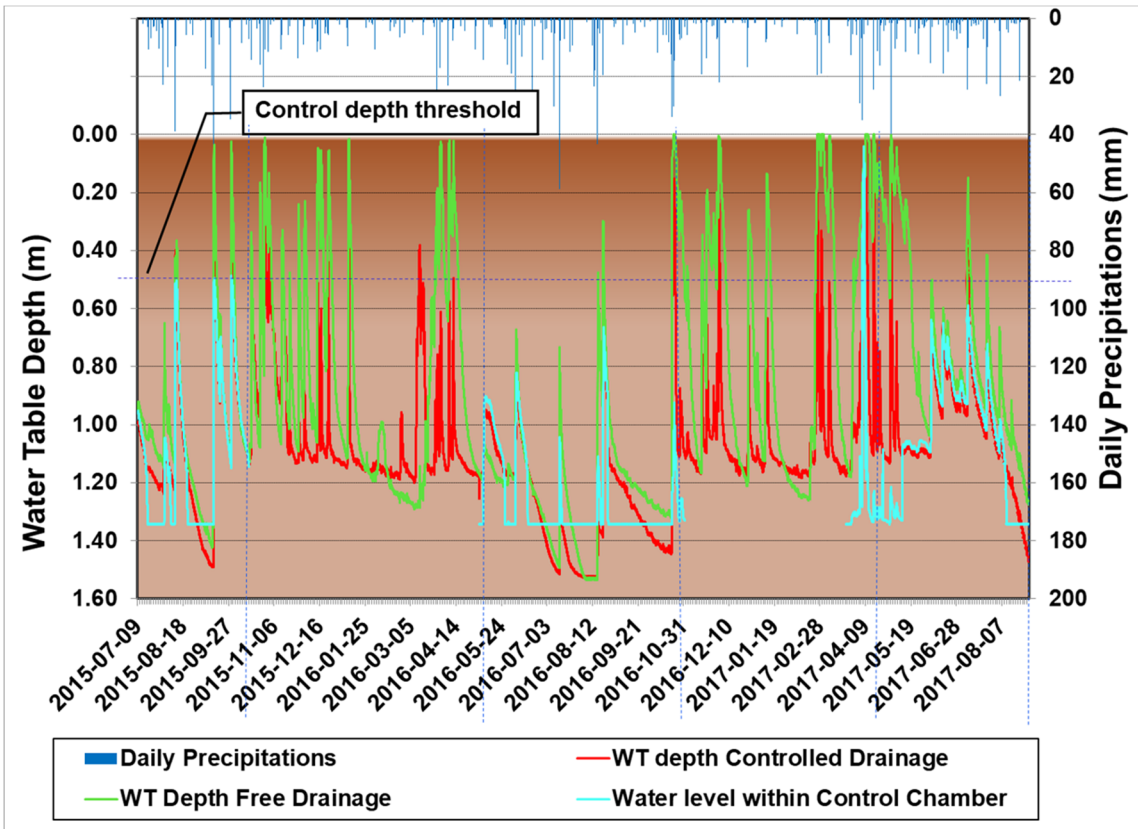


Figure 4-14. Precipitation, and averaged water table depth variability for the observation wells from the Controlled drainage site (no. 1 to 6) and the ones from Free drainage site (no. 7 to 12) for the 2015-2017 period.

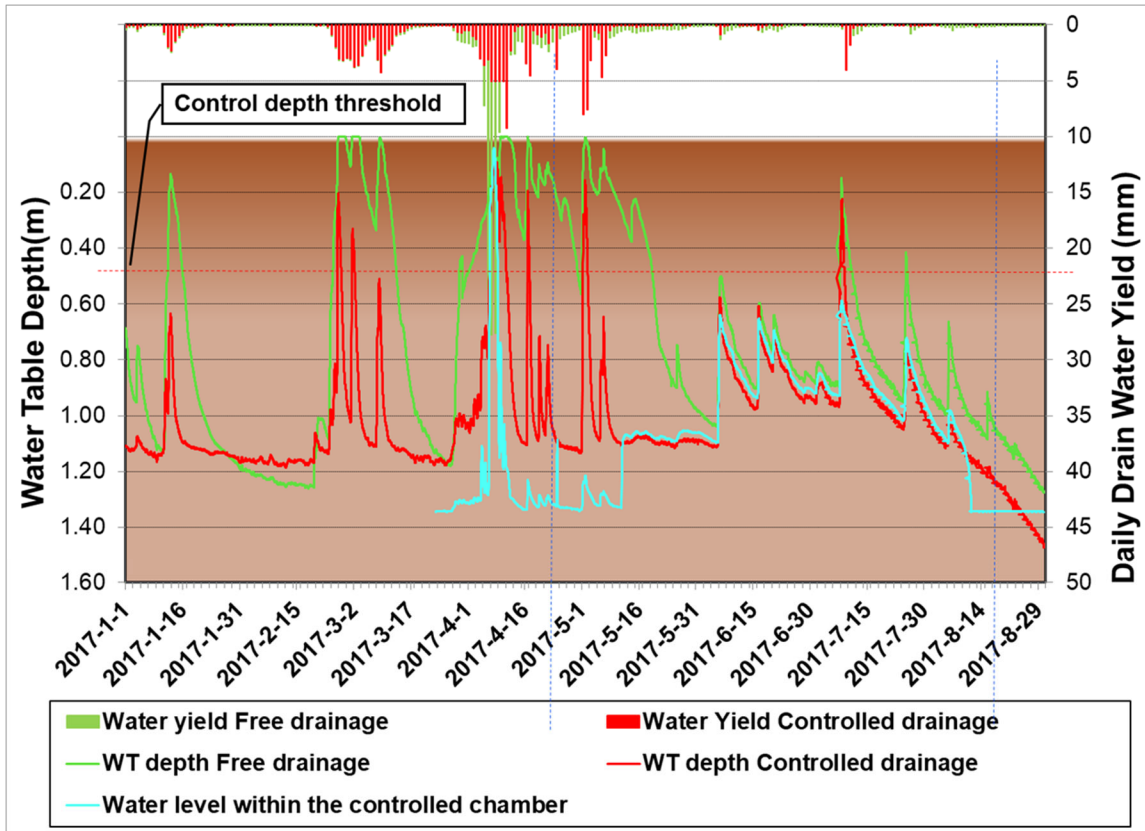


Figure 4-15, Tile drainage water yield and averaged water table depth variability for the observation wells from the Controlled drainage site (no. 1 to 6) and the ones from Free drainage site (no. 7 to 12) for the 2015-2017 period.

The water table elevations observed within the wells of the FD site, as well as the WT recession rates, are highly contrasted, as opposite to the CD. The elevation of the water table from wells 12 and 11 noticeably departed from the other wells. The contrast in water table stages among observation wells is more pronounced during the recharge period. In March 2016 particularly, the water table reached the surface at sites 11-12, in response to surface ponding and related infiltration of runoff water.

Table 4.6 Tile water specific yields for the Yamaska field sites, together with PREB micro-watershed water yields separated into surface and subsurface contributions for the corresponding free drainage and controlled drainage periods.

Periods	Tile water yield (mm)		Surface runoff (mm)	Subsurface water yield (mm)	Total water yield (mm)
	Controlled	Free drainage	Microwatershed estimates		
2015-07-09 to 2015-10-15	15	41	4	18	22
2015-10-16 to 2016-05-07	156	233	144	365	509
2016-05-08 to 2016-08-25	1	6	5	69	75
2016-08-26 to 2017-04-24	206	287	249	296	544
2017-04-25 to 2017-08-11	38	54	24	103	127
2017-08-12 to 2017-08-30	0	2	0	5	5
Total - Control Periods	54	101	33	191	224
Total - Free Drainage	362	523	393	666	1059
Total (784 days)	416	623	426	857	1282
%Total - Control Periods	0.13	0.16	0.08	0.22	0.17
%Total - Free Drainage	0.87	0.84	0.92	0.78	0.83

The contrasting behavior of the water table of experimental sites FD and CD is highlighted in Figure 4.14. The variation of the water table depth, averaged from individual field observation wells (N=6) is plotted against time for the overall monitoring period. The water level elevation from the control chamber at the Controlled site is also illustrated, together with daily precipitation. During the recharge period, when both sites are under free drainage (the WT control is non effective), higher WT elevation and lower water table recession rates are consistently observed within the free drainage site (FD) in response to precipitation and snowmelt events. The water table of the FD site also reached consistently (15 times) the surface during the recharge period, resulting in saturation of the topsoil and presumably in an increased surface runoff volume (not monitored). In contrast, the water table of the Controlled drainage site (CD) never reached the surface during the 2015-2017 monitoring period.

Figure 4.15 illustrates the variation in WT tables elevation, together with water yields monitored at individual tile collector outlets for the 2017 recharge and growing season. The corresponding totals in water yields for recharge and growing season (when the control is activated at CD site) are reported in Table 4.4. During the recharge period, the relatively higher WT at the free drainage site is associated to higher tile water yields. For the overall monitoring period, 50 % more tile water is exported from the FD site (623 mm) during the recharge period as compared to the CD site (416 mm). Higher water yields are consistent with relatively higher water table elevations and lower recession rates documented for the FD site. Two factors are proposed here to explain the strong inter-site gradients in water table stage and recession rates, as well as tile water yields. First, the

surface ponding of the FD site, especially within the sector of wells 11 and 12 is the most probable driver of contrasting water table behavior and water yields amongst field sites. At the FD site, more water was available to infiltrate and contribute to tile flow, for a longer period. Also, the gradient in soil physical properties amongst field sites, namely relatively higher bulk density, lower macroporosity and lower saturated hydraulic conductivity of FD topsoil (Table 4.4) possibly triggered the contrasted WT stage and water yields during the recharge period. In turn, it is hypothesized that inter-site gradients in surface drainage and indicators of internal drainage are related. In short, poor surface drainage of the FD site triggered the development of unfavorable soil physical conditions.

During the controlled drainage period, the contrast in the water table depths among sites is less apparent. For most of the 2015 and 2016 growing seasons, the WT elevation at CD site remained below the tile lines. There is no noticeable effect of the controlled drainage at CD site, since there was no water table to hold early in the growing season, as a result of relatively dry climate conditions. In 2017, contrasting with the preceding growing seasons, a relatively higher water table elevation is observed at CD site, above or near the tile depth. The fluctuations in the water table elevation of CD site appear in phase with the FD site. Considering the highly contrasted profiles of WT stages and recessions rates during the non-growing season, the relative synchronicity of the water table stages at CD and FD sites during the 2017 growing season is interpreted as a controlled drainage effect. The water table of the CD site was retained to levels equivalent to the FD sites.

From an experimental design perspective, the data from the free drainage site (FD) could not be used as a control to quantify a controlled drainage effect on CD site, considering the highly contrasting hydrologic responses of the field sites. In this situation, a state-of-the-art design would require a *Reference period*, documenting the site-specific hydrologic responses within both sites under free drainage, prior to water table control treatment. In turn, a relative effect of the controlled drainage on water elevation and yield would be detected under a following *Treatment period*, through a covariance analysis approach, using the data from the free drainage site as covariable. The application of this approach was not possible considering the duration of the current project.

The apparent, very limited effect of the Controlled drainage treatment on water table elevation and yield is explained by the drawdown of the water table, early in spring, below the tile lines at the CD site. The typical land development from the study area, including high density (2 km/km²), deep municipal drains (over three m), systematic subsurface drainage systems (80% of cropped area) and narrow, elongated field configuration, has been in fact designed to rapidly draw down the water table in early spring. During the following growing season, the deep and relatively dry municipal drains exert an important hydraulic head in the soil profiles, which favors the resurgence of excess precipitation to the stream. The coupling of the hydrometric data from the FD field site with the data from the neighboring 3e Petite-Rivière-Pot-au-Beurre (PRPB) micro-watershed (10 km²)

illustrate the relative importance of the resurgent and tile flow pathways for the study region (Figure 4.16). The cumulative separated water yields (tile vs resurgent) according to recharge and growing season are also documented in Table 4.6.

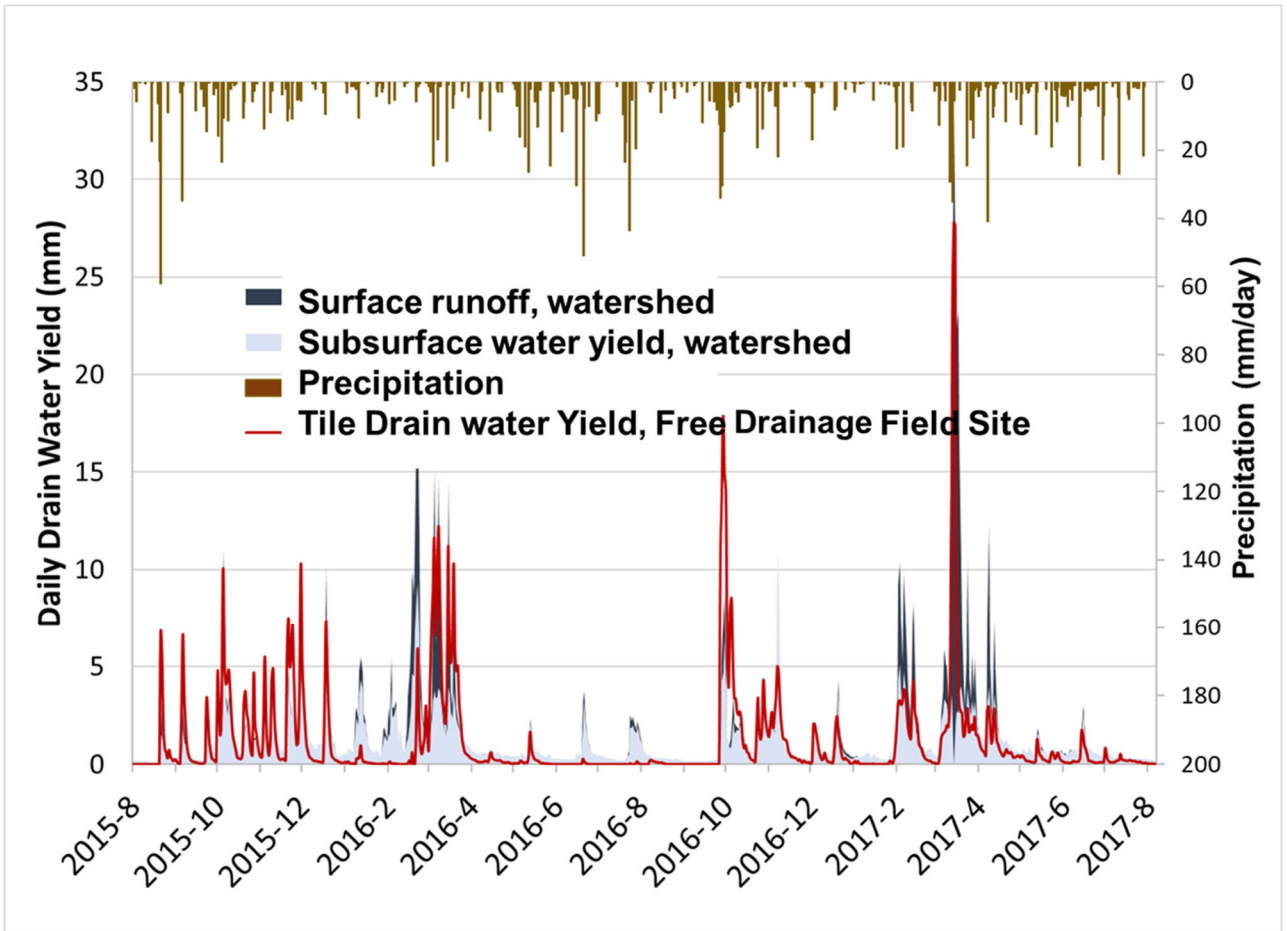


Figure 4-16. Specific tile drain flow from the Yamaska free drainage site coupled with the hydrometric data from the 3rd Petite-Rivière-Pot-au-Beurre micro-watershed.

During the period under controlled drainage, the cumulative tile water yields reached 58 and 102 mm, respectively, at the Controlled and Free drainage sites. The tile water yield from the CD site is indebted essentially to two runoff events during the 2017 growing season (May 2nd and July 8th; Figure 4.15), when the water table raised over the 50 cm depth threshold and yielded 42 mm of tile flow. The tile water yield differential among sites thus cumulates at 46 mm over the 2015-2017 monitoring period, which is indicative of a marginal effect of the controlled drainage on global tile water yield at CD site. During the same period (growing season), total subsurface water yields cumulates at 192 mm at PRPB micro-watershed outlet (Table 4.3), which is approximately two to four times the tile water specific yields at FD and CD sites, respectively. The subtraction of the

seasonal tile flow from the total subsurface flow components gives an indication of the amplitude of the resurgent (return) flow path, by-passing the tiles, which ranges between 90 to 134 mm on an annual basis.

4.2.3.3 Sediment and nutrient fluxes

Figure 4.17 and 4.18 illustrate the distribution of instantaneous concentration in TSS, N, P and Ca observed at the field site tile outlets with respect to time and tile flow rate. Observed TSS and total phosphorus concentration values are flow rate dependent for both field sites. At the free drainage site, TSS and total phosphorus (TP) respectively peaked at 488 mg TSS/L and 595 ug P/L for peak 1.00 L/sec-ha specific flow rate on September 14th 2015 (Figure 4.17.) The temporal distribution of the TP concentrations indicates that the elevated concentrations are synchronous to the peak tile flow rates in late fall 2016 and 2017 wet spring. The distributions of TSS and TP concentrations at the controlled drainage site also exhibit a similar dependency on season and tile flow rate, but reached lower maxima, namely 249 mg TSS/L and 425 ug TP/L (Oct. 22nd 2016), for a peak flow rate of 1.09 L/sec-ha.

The overall flow dependency of TSS and TP concentrations at both sites is interpreted as an indication of preferential transfers active during the most intense tile flow events. Similar flow-dependent gradients in P and TSS are reported by Michaud et al. (2019) for ten field sites from the same physiographic region (Saint-Lawrence lowlands). Conceptually, the highest TP and TSS concentrations observed at tile outlets are attributed to rapid flow through the soil profile macropores, with relatively short contact time with the soil matrix and elevated transport capacity of fine sediments. Poirier et al. (2012) provided a detailed description of the sediment and phosphorus speciation from tile fluxes for similar edaphic conditions.

The effect of water table retention at CD site on phosphorus concentrations during the controlled period was also investigated by comparing the P speciation and flow-weighted concentrations during Control Vs Non-control periods at both sites. In theory, increases in tile water P concentrations can in fact result from waterlogging by favoring the development of reducing conditions and related P desorption. As reported in Table 4.8, the flow-weighted P concentration at CD site, for all P species (total, dissolved, bioavailable and reactive), were lower during the controlled period than during the free drainage period. From a plot study on a clay site in Ontario, Zhang et al. (2017) reported also a reduction in soluble P concentration resulting from the implementation of CD with sub-irrigation. For the current field site study, the contrasted water yields observed at CD and FD sites, together with the common flow dependency of P observed P concentrations, indicate that the hydrodynamic conditions (flow rate) were the dominant driver of P concentrations, rather than reduced conditions that could have developed from waterlogging. In short, highest concentrations during the recharge period, as compared to the controlled period,

were driven by higher flow rate and related transport capacity of P through preferential flow pathway. Also, no significant increase in soluble P concentration was observed at CD site in response to controlled drainage. The short period of water table retention apparently did not cause significant anoxic conditions, which has been linked to soluble P concentration increases in other studies. (Stämpfli and Madramootoo, 2006; Sanchez Valero et al., 2007).

Table 4.9 reports the TSS and nutrients loadings (N and P) for both field sites. The P TSS fluxes have been compiled using the concentration:tile flow rate models (Figures 4.17 and 4.18), while nitrogen fluxes are based on the interpolation of concentration based on time. Figure 4.19 illustrate the resulting sediment and nutrient fluxes in time. Globally, TSS and TP fluxes are highly discriminated in time, reflecting the tile flow rate distribution. Higher specific yields of TSS (688 kg/ha-yr) and TP (0.87 kg/ha-yr) are observed for the FD site, as compared to CD site (232 kg TSS/ha-yr and 0.55 kg TP/ha-yr), which reflects its higher tile water yield. Flow-weighted concentrations in TSS and TP are also relatively higher for FD site, which support the theory of preferential transfers. In short, higher concentrations are positively related to the highest tile flow rates.

Considering annual loadings within the 1.0 kg P/ha range for the 3e Petite-Rivière-Pot-au-Beurre micro-watershed (previous section 4.1), a practical implication of the field site study is that the phosphorus export from the drainage tiles (0.55 and 0.87 kg P/ha for the CD and the FD sites, respectively). likely accounts for most of the phosphorus transferred from the field to the stream within the study region. From a land and river stewardship perspective, the effective reduction of P loadings to the stream thus calls for mitigations measures on subsurface P transfers, together with surface runoff abatement.

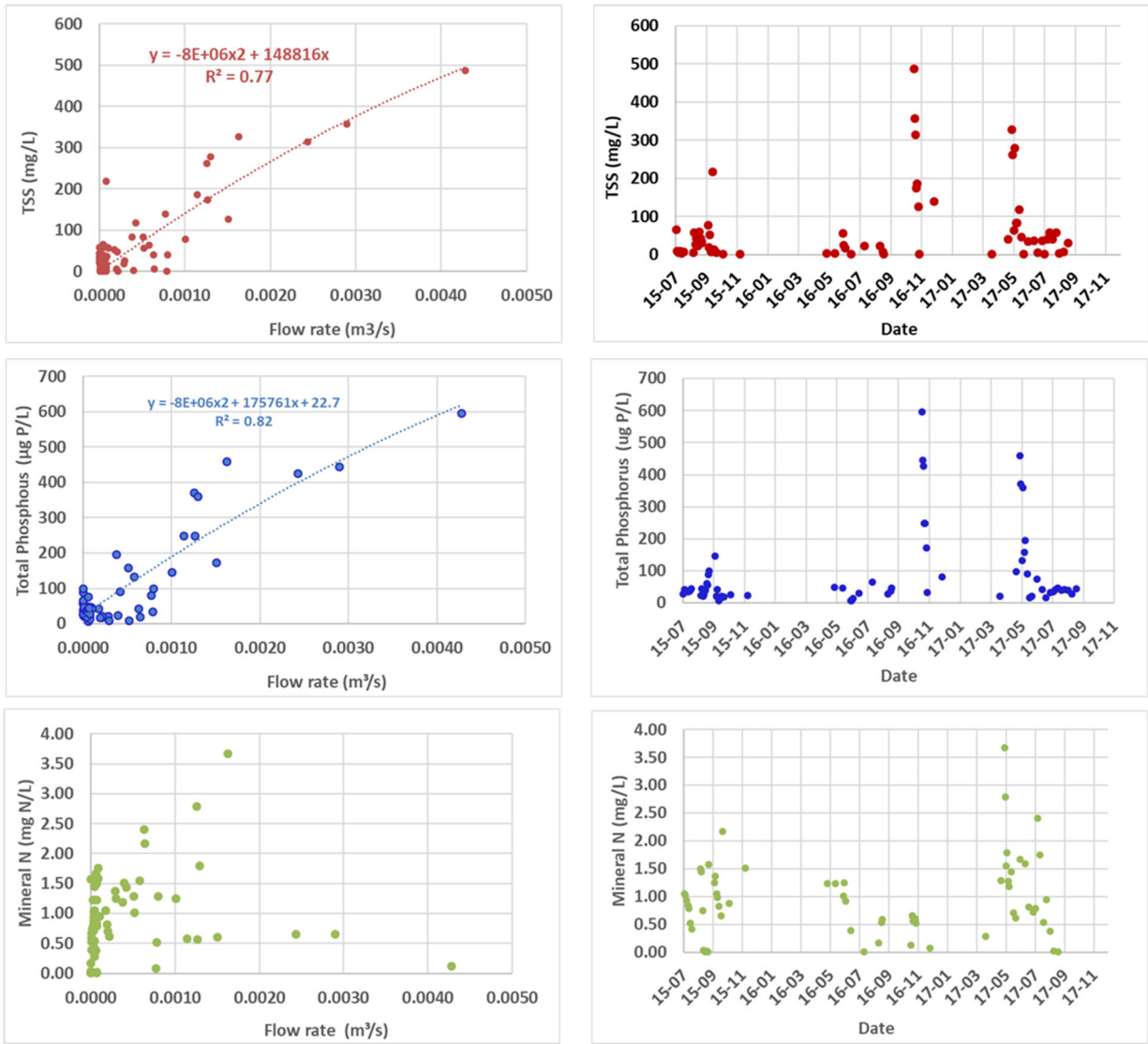


Figure 4-17. Variability in total phosphorus and nitrates concentrations of tile drainage waters from the free drainage site with respect to instantaneous discharge and date.

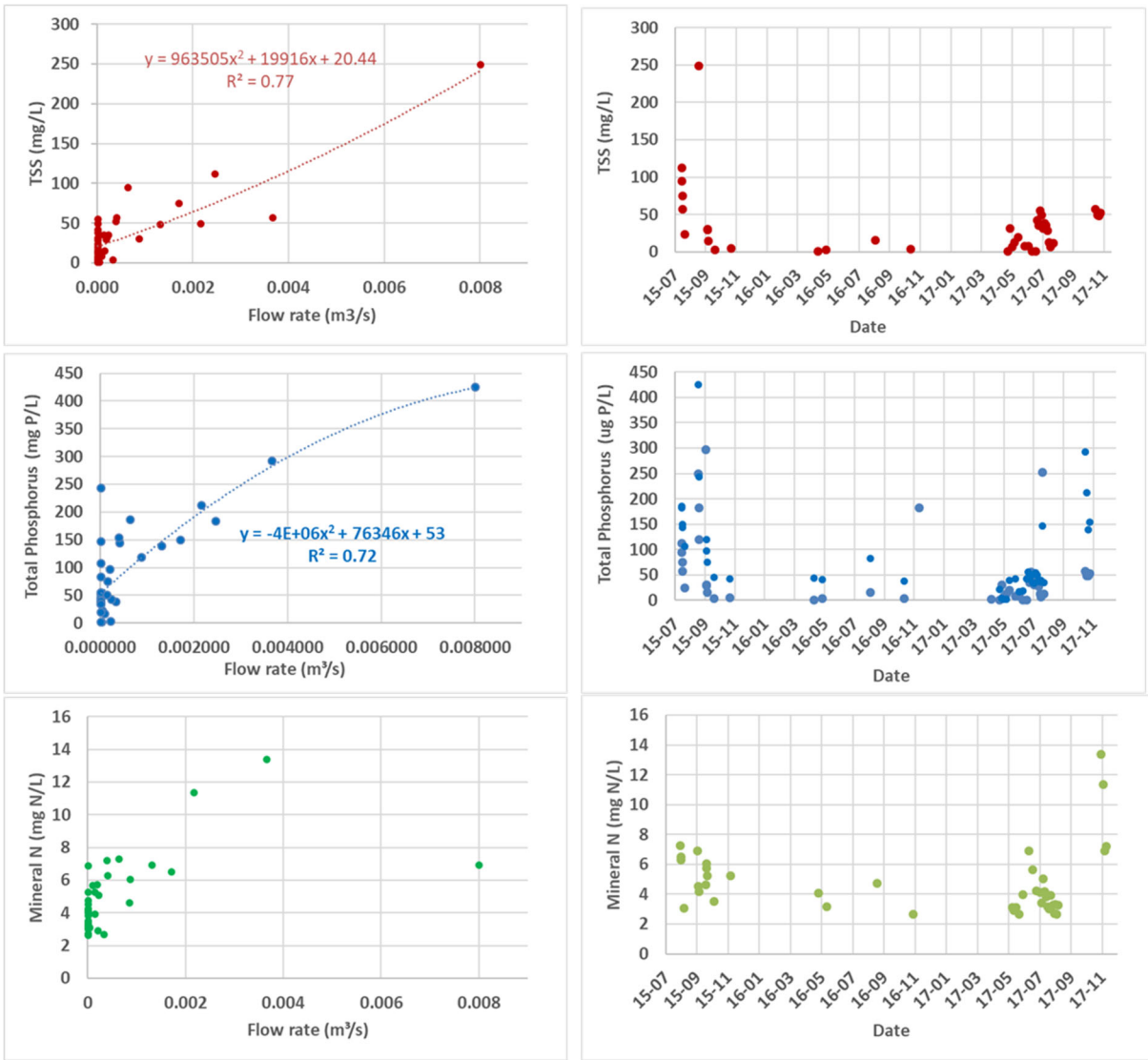


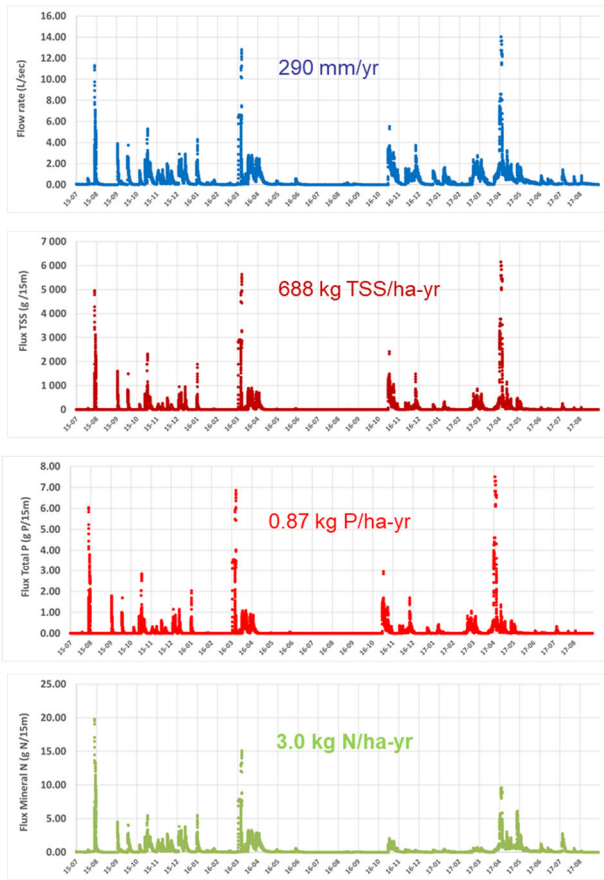
Figure 4-18. Variability in total phosphorus and nitrates concentrations of tile drainage waters from controlled drainage sites with respect to instantaneous discharge and date.

Table 4.8. Phosphorus speciation and flow-weighted concentration monitored at tile drainage outlets of the free drainage and controlled drainage site. (Growth period effect = Control-No control/No control).

Period	TSS mg/l	Total P ug/l	Diss. P ² ug/l	Bioavail. P ug/l	RSP ³ ug/l	Diss. P Ratio	Bioavail. P Ratio	RSP Ratio
Free drainage site								
Control period¹	138	189	37	94	29	0.19	0.50	0.16
Without control	195	251	24	127	22	0.10	0.51	0.09
Growth period effect	-0.29	-0.25	0.51	-0.26	0.34	1.01	-0.02	0.79
Controlled drainage site								
Control period	92	155	27	58	23	0.18	0.37	0.15
Without control	74	191	92	119	79	0.48	0.62	0.41
Growth period effect	0.25	-0.19	-0.70	-0.52	-0.70	-0.64	-0.41	-0.64
¹ Period according to the schedule at the controlled drainage site								
² Diss P: Dissolved P (0,45 um)								
³ RSP: Reactive soluble P (dominatly ortho-phosphates)								

Regarding mineral nitrogen yields in tile waters, the fluxes observed (CD: 6.14; FD: 2.91 kg N/ha-yr) at tile outlets of field sites (Table 4.9) are relatively low, considering the range of 20-30 Kg N/ha-yr monitored at proximal PRPB micro-watershed (Figure 4.6). The mineral N concentrations tend to be higher within the tile water from the CD site, with flow-weighted concentration reaching 3.17 mg N/L as compare do 1.0 mg N/L for the FD site. This gradient is consistent with the residual soil N levels after soya harvest monitored in October 2015 (Table 4.5), which indicates relatively higher available N within topsoil of the CD site (5.3-8.4 ug/g) as compared to the FD site (3.3-4.6 ug/g). Considering the homogeneous N management provided to the field sites during the study, the gradient in tile N fluxes is more likely determined by the inherent soil properties. Since the field sites have nearly equivalent organic matter levels ranging from 2.5 to 3.3 % O.M. (Table 4.5), better drainage conditions of the CD site are interpreted as the driver of relatively higher N yields from tile waters, which were favorable to mineralization of organic N stock.

Free drainage site



Controlled drainage site

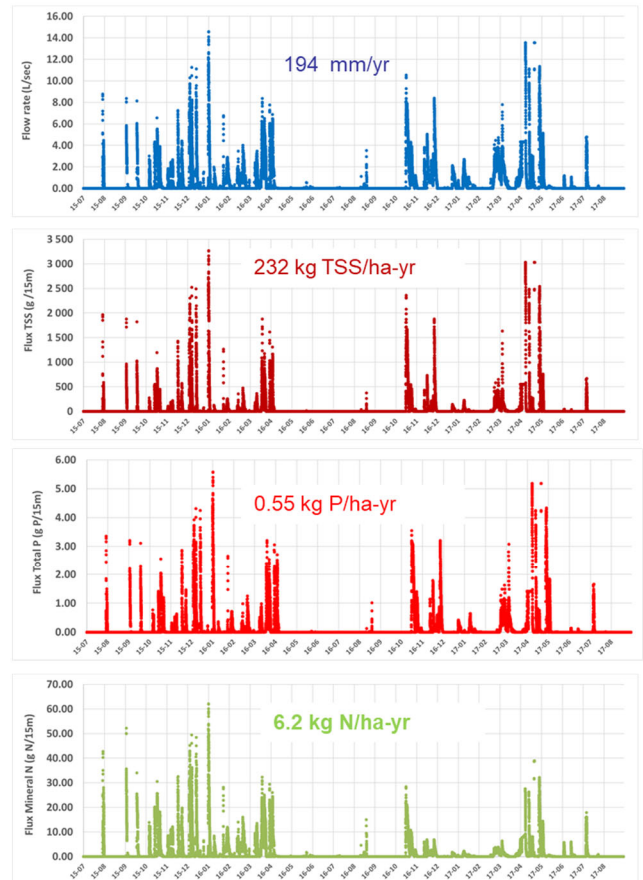


Figure 4-19. Sediment, phosphorus and mineral nitrogen loading time series estimated for the free drainage and controlled drainage sites according to controlled drainage and free drainage periods (Note that scales differ among sites).

Table 4.9. Sediment, phosphorus and mineral nitrogen specific loadings estimated for the free drainage and controlled drainage sites according to controlled drainage (growing season) and free drainage (recharge) periods.

Periods	Total suspended sediments (kg TSS/ha)		NO ³ + NH ⁴ (kg N/ha)		Total Phosphorus (g P/ha)	
	Control Site	Free Site	Control Site	Free Site	Control Site	Free Site
2015-07-09 to 2015-10-15	19	101	0.89	0.66	48	123
2015-10-16 to 2016-05-07	185	569	7.29	3.09	443	717
2016-05-08 to 2016-08-25	0	1	0.04	0.06	1	2
2016-08-26 to 2017-04-24	240	761	3.67	1.53	578	953
2017-04-25 to 2017-08-11	54	46	1.30	0.91	119	62
2017-08-12 to 2017-08-30	0	0	0	0	0	0
Total (784 days)						
Total (Control period)	74	149	2.24	1.63	168	188
Total (Without control)	425	1 330	11.12	4.79	1 022	1 671
Total (All periods)	498	1 479	13.36	6.42	1 190	1 859
Total (Base 365 days)						
Total (Control period)	34	69	1.04	0.76	78	87
Total (Without control)	198	619	5.18	2.23	476	778
Total (All periods)	232	688	6.22	2.99	554	865

4.2.3.4 Crop yields

Table 4.10 and figures 4.20 and 4.21 illustrate the crop yields of soya (2015 and 2017) and spring wheat (2016) determined manually and from the yield monitoring on the producer combine for the field zones 1 to 12. Globally, manual and combine harvesting results indicate higher yields for the CD site for the three crop yields, with gradient ranging from 10-12 % for wheat in 2016 to 10-39% for soya in 2017. This yield advantage for the CD site, however, cannot be attributed to an effect of the controlled drainage on reducing water stress. In 2015, the water table from the CD site did not rise over the tile drains until august 8th, followed by a recession similar to the water table at the FD site. Similarly, in 2016, the water table did not rise over the tile drain prior to august 22nd, without a noticeable effect of the controlled drainage on the recession rate of the water table (Figure 4.14). The situation differed in 2017 as the water table raised over the tile drain on both sites during June

and July. However, as pictured in figure 4.15, the variation of the water table elevation of both field sites appeared in phase, without a distinct, slower recession within the CD site. Clearly, the closure of the tile drain collector was not effective in maintaining the water table within the CD site soil profile and thus could not provide a yield benefit to the spring and soya crops related to moisture stress. As presented earlier, the water table draw down past the tile line was presumably controlled by the hydraulic head maintained by the deep municipal drains, while the stream discharge was fed essentially by resurgent flow.

Since the water table elevation monitored during the three crop years cannot explain a yield advantage of CD site (with respect to moisture stress), the relatively lower yields at FD site result most likely from excess moisture. The relatively lower soya yields from field zones 11-12 in 2015 and 2017 (Table 4.20), particularly, were related to surface ponding, with the water table rising up to the soil surface (Figure 4.14). This excess moisture likely explains the spatial gradient in soya yields across the field, as supported by the yield monitor data and illustrated in Figure 4.21. In contrast, in 2016, the spring wheat yields from the same zones (11-12) turned out higher than the other ones (7 to 10) suggesting a soil moisture advantage.

Table 4.10. Crop yields of soya (2015 and 2017) and spring wheat (2016) determined manually and from the combine yield monitor for the field zones 1 to 12.

	2015 - Soya		2016 - Spring Wheat		2017 - Soya
	Monitor	Manual	Monitor	Manual	Monitor
Wells 1-2	4.60	3.61	2.64	3.66	5.33
Wells 3-4	4.59	3.52	4.03	2.97	4.84
Wells 5-6	4.33	3.10	3.28	3.43	4.96
Average Controlled	4.51	3.41	3.32	3.35	5.04
Wells 7-8	4.17	3.09	2.72	2.77	4.09
Wells 9-10	4.17	3.30	2.73	3.07	4.06
Wells 11-12	2.89	2.71	3.42	3.31	2.77
Average Free drainage	3.74	3.03	2.96	3.05	3.64
Gradient¹	0.20	0.12	0.12	0.10	0.39
¹ (Controlled-Free)/Free					

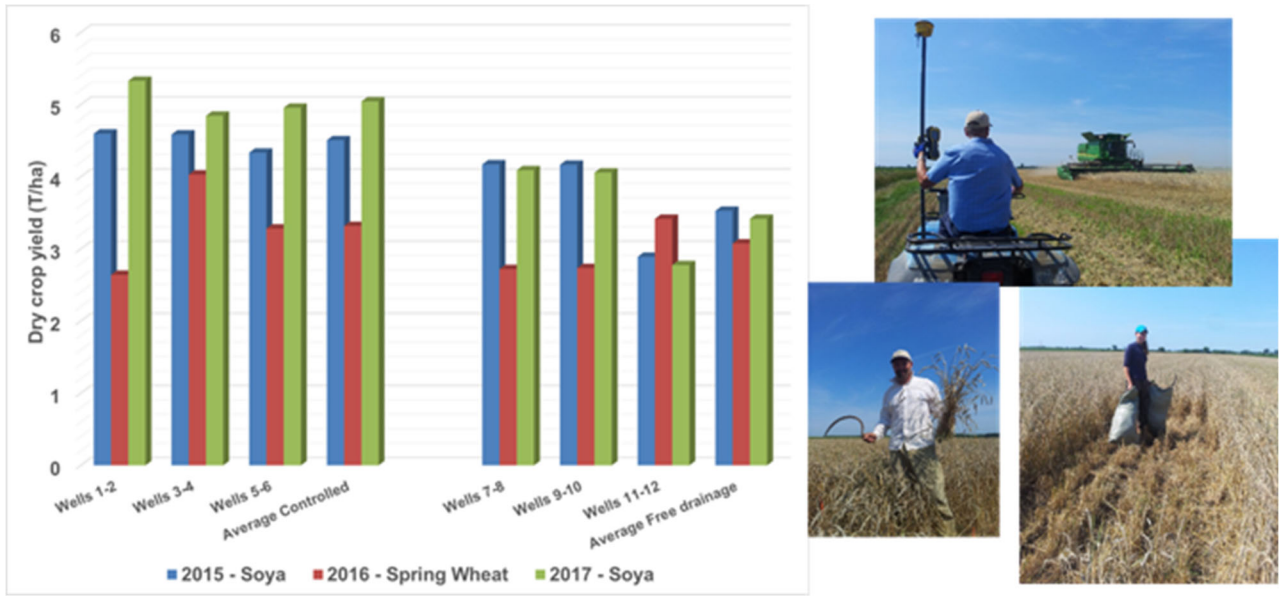


Figure 4-20. Crop yields of soya (2015 and 2017) and spring wheat (2016) determined manually and from the combine yield monitor for the field zones 1 to 12.

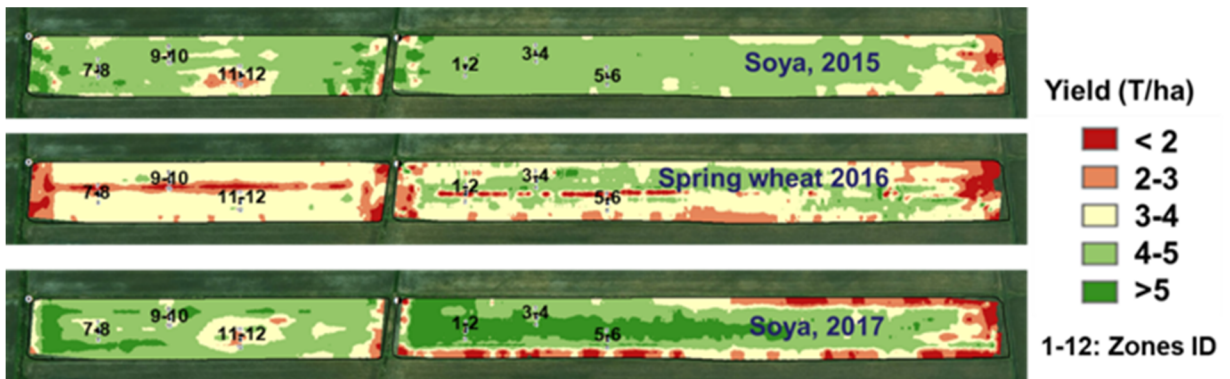


Figure 4-21. Spatial variability in crop yields data captured by the yield monitor for soya in 2015 and 2017, as well as for spring wheat in 2016.

4.2.4 Conclusions of the micro-watershed and field scale experiment

The effect of controlled drainage on tile water yield during the growing season was marginal, with a potential retention in the order of 50 mm over the 2015-2017 three growing seasons monitoring period. The monitored water table stages indicate that some retention was effective during one growing season (2017) out of three but cannot be quantified due to contrasting hydrologic responses of field sites and absence of pre-treatment reference period.

Yield benefits on CD site were monitored over the three growing seasons, which cannot be attributed to a controlled drainage effect. In fact, relatively lower crop yields within the free drainage site are attributed to deficient surface drainage conditions and related, unfavorable soil physical conditions. In short, the wetter soil, despite free drainage, had lower yields. A practical implication of these observations is that surface and internal drainage are determinant drivers of the agronomic feasibility and benefits of controlled drainage

From an environmental perspective, the water table monitoring of the free drainage site indicated frequent saturation of the soil surface, which presumably lead to surface runoff events (not monitored). It is anticipated that a controlled drainage scenario in this situation could exacerbate runoff losses, and be counter-productive from an environmental perspective. It is apparent that surface drainage is linked with subsurface drainage. A lesson learned from the monitored water and nutrient fluxes is that deficient surface drainage, which leads to an increased tile drained water volume, results in higher phosphorus export through preferential flow to tiles.

Considering the marginal effect of controlled drainage observed on the water table and yields at the CD site, the results of this study suggests two options to increase the effects of tile drainage control on water table retention, namely a different scheduling for the activation of controlled drainage, and complementary water retention within the municipal drain through weirs. These precision water management options have to be site-specific, giving primary consideration to the surface and internal drainage condition of the site. The most important issue here is to avoid an increased generation of surface runoff, as it has P concentrations within a tenth order of magnitude of the tile water.

Evidence of phosphorus export triggered by preferential flow pathways to tiles suggest that the maintenance of the WT above the tile could be an effective way to limit preferential transfers of phosphorus to the stream, during both the growing season and recharge period. Part of the reduction of the phosphorus yield would result from a relative increase in the return flow path to the stream, and corresponding lower tile flow. As indicated by the PRPB water quality data during base flow, higher contact time of the water with the subsoil matrix during return flow favors the immobilization of P. Considering the elevated, flow rate-dependent P concentration in tiles observed within this study, it is also anticipated that the limitation of preferential transfers through

elevated WT overcomes the potential increases in soluble P concentration related to reduced conditions within the subsoil matrix.

Notwithstanding the management scenario, the feasibility of effective control on the WT elevation is limited by the water levels in surrounding municipal drains. As inferred by the results of this field scale study, elevated hydraulic heads draw down the water table below the tiles. A practical approach to maintain more water in soil profiles would be to concurrently manage the water level within the municipal drains. The conservation of water within the stream could provide additional benefits to the agronomic ones, namely by promoting habitat biodiversity in riparian ecosystems, as well as reducing nutrient and toxics export to downstream water bodies. The concept of concurrently managing the subsurface and the surface drainage systems make even more sense, both from agronomic and environmental perspectives, considering the expected increase in summer evapotranspiration and moisture stress in future climate documented for the the study region (Gombault et al., 2015; This study, section 4.3.3). The David Basin scale hydrologic modeling study provides more insights regarding this issue of adapting water management to future climate.

4.3 David basin study

The main objective of the David basin scale study was to evaluate the feasibility of controlled drainage under present and future climates. The study was conducted by coupling climate change scenarios with hydrologic models, based on over 30 years of hydrometric data time series, in order to describe the effects of drainage scenarios and future climate on water yields and pathways (surface runoff, tile flow, return flow to stream and aquifer recharge). From an environmental perspective, the main research question was to evaluate the risk of increased surface runoff emission resulting from the closing of the tile drain collectors. An objective of a “zero” increase in surface runoff is inherent to any controlled drainage scenario, given that surface runoff phosphorus concentrations are typically on the order of 10x those from tile drainage. From an agricultural production perspective, the study also provided insights on the pertinence and feasibility of controlled drainage scenarios by estimating hydric budgets for various cash crops under variable soil types and agri-climatic conditions, both historic and future.

4.3.1 Methods

The hydrologic modeling study was conducted through a four-step procedure to investigate the effects of drainage scenarios on historic and future climates:

- The first step consisted in the parameterization and calibration of the model under historic climate using historic (observed) climatic and hydrometric data for the 1983 to 2015 period;
- As a second step, the effect of the drainage scenarios under historic climate were investigated using the calibrated model set-up. The effects of the drainage scenarios on hydric balance and flow pathways were determined from the difference of the model outputs.
- In the third step, climatic data time series for actual (1981-2010) and future climate (2041-2070) were inputted to the calibrated model. The effects of climate change on the watershed hydric balance and flow pathways were projected using a Delta approach; where the difference in modeled outputs (Future – Present) were interpreted as climate change effects.
- Finally, in the fourth step, the drainage scenarios were applied to the calibrated model for the future climate time series data in order to assess the feasibility of controlled drainage in the future.

4.3.1.1 Site description

David River is an important tributary of Yamaska river basin. The river flows northeasterly on the South Shore of the St. Lawrence River, in Quebec, through the municipalities of St. Eugene and St. David. Surrounding watersheds include Saint-François River (East), Saint-Germain River (South) and Black River (West), as illustrated in figure 4.22. The total catchment has an area of 323 km², an approximative main channel length of 33.1 km and a mean annual flow discharge of 5.7 m³/s (DEH, 2018). The surface drainage of the area has been largely modified to account for the implementation of systematic subsurface drainage systems to approximately 71% of cropped area.

The climate of the David basin is characteristic of other snowmelt-dominated watersheds in southern Quebec. The area has an average (1981-2010) annual precipitation of approximately 1000 mm, of which about 200 mm falls as snow. Average mean daily temperatures are 21°C in July and -11°C in January (Environment Canada, 2018). (Table 4.11).

The hydrometric network, elevation model, land use and soil map of the study area are illustrated in Figure x. The landscape of the watershed is relatively flat, with elevations ranging from nearly sea level to 104 m. The average slope of the watershed is 3%, with 95 % of the basin surface area within 0 to 5% slopes (Table 4.12). The soils from the area developed from typical parent materials of the Saint-Lawrence lowlands physiographic region, including marine clays, alluvial deposits and glacial till. The spatial distribution of the soil map units are illustrated in figure 4.23 and respective physico-chemical properties of individual soil series are reported within appendix 1. Regarding land use, cultivated lands cover 81% of the watershed area. Grain corn covers 45% the area of cultivated lands, while soya, small grains and hay are grown over 29, 15 and 8% of cropped area, respectively (Table 4.13 and figure 4.23).

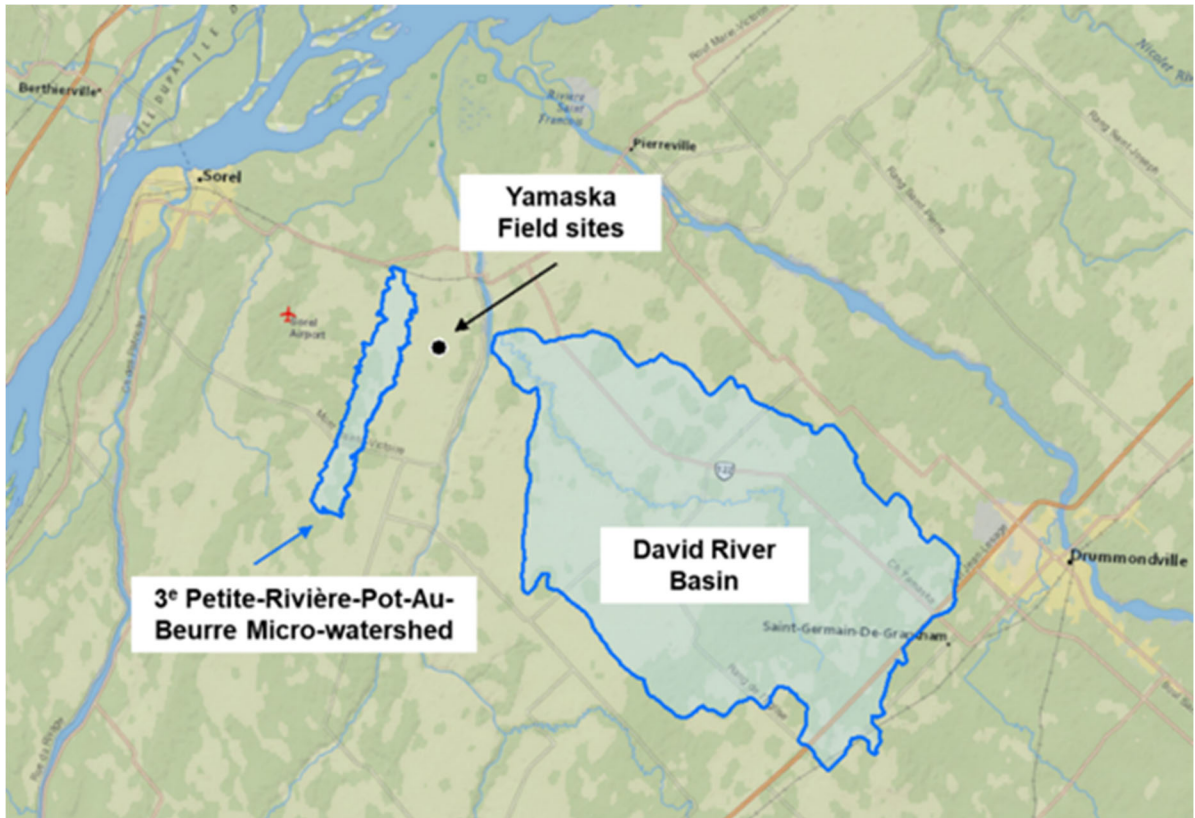


Figure 4-22. Location of the David river basin.

Table 4.11: Monthly precipitation and temperature averages (1981-2010) of the study region (Adapted from Environment Canada, 2018 for Sorel station).

	Janv	Feb	Mar	Apr	May	Jun	Jul	Sept	Oct	Nov	Dec	Year
Daily Mean Temperature (°C)	-10,7	-8,5	-2,7	6,0	13,2	18,7	21,1	15,2	8,2	1,7	-6,1	6,3
St Deviation	3,4	2,5	2,1	1,5	1,7	1,2	1,0	1,5	1,3	1,6	3,1	1,9
Daily Max Temperature (°C)	5,9	-3,4	2,3	11,1	18,8	24,1	26,4	20,2	12,5	5,4	-2,0	11,2
Daily Min Temperature (°C)	15,5	-13,5	-7,6	0,8	7,5	13,2	15,8	10,1	3,8	-2,1	-10,2	1,4
Rainfall (mm)	24,3	19,5	28,1	68,4	86,4	96,8	98,9	80,6	93,5	77,0	31,8	801,2
Snowfall (cm)	49	43	32	9	0	0	0	0	1	15	49	199
Precipitation (mm)	73,6	62,3	60,5	77,7	86,4	96,8	98,9	80,6	94,6	91,8	80,4	999,7

Table 4.12. Slope gradients distribution across the David river basin.

Slope	Area (ha)	% Area
0-2%	13 650	42.26%
2-5%	17 180	53.19%
5-10%	1 221	3.78%
10-34%	245	0.76%

Table 4.13: Land use distribution in the watershed.

	SWAT Land Use Code	Area (ha)	% Area
Agricultural Land-Generic	AGRL	102	0.30%
Barren	BARR	432	1.25%
Corn	CORN	12 746	37.03%
Corn Silage	CSIL	287	0.83%
Forest-Mixed	FRST	6 201	18.01%
Green Beans	GRBN	289	0.84%
Oats	OATS	1 401	4.07%
Pearl Millet	PMIL	164	0.48%
Range-Brush	RNGB	28	0.08%
Rye	RYE	8	0.02%
Soybean	SOYB	8 255	23.98%
Spring Wheat	SWHT	2 497	7.25%
Hay	PAST	1 979	5.75%
Water	WATR	35	0.10%

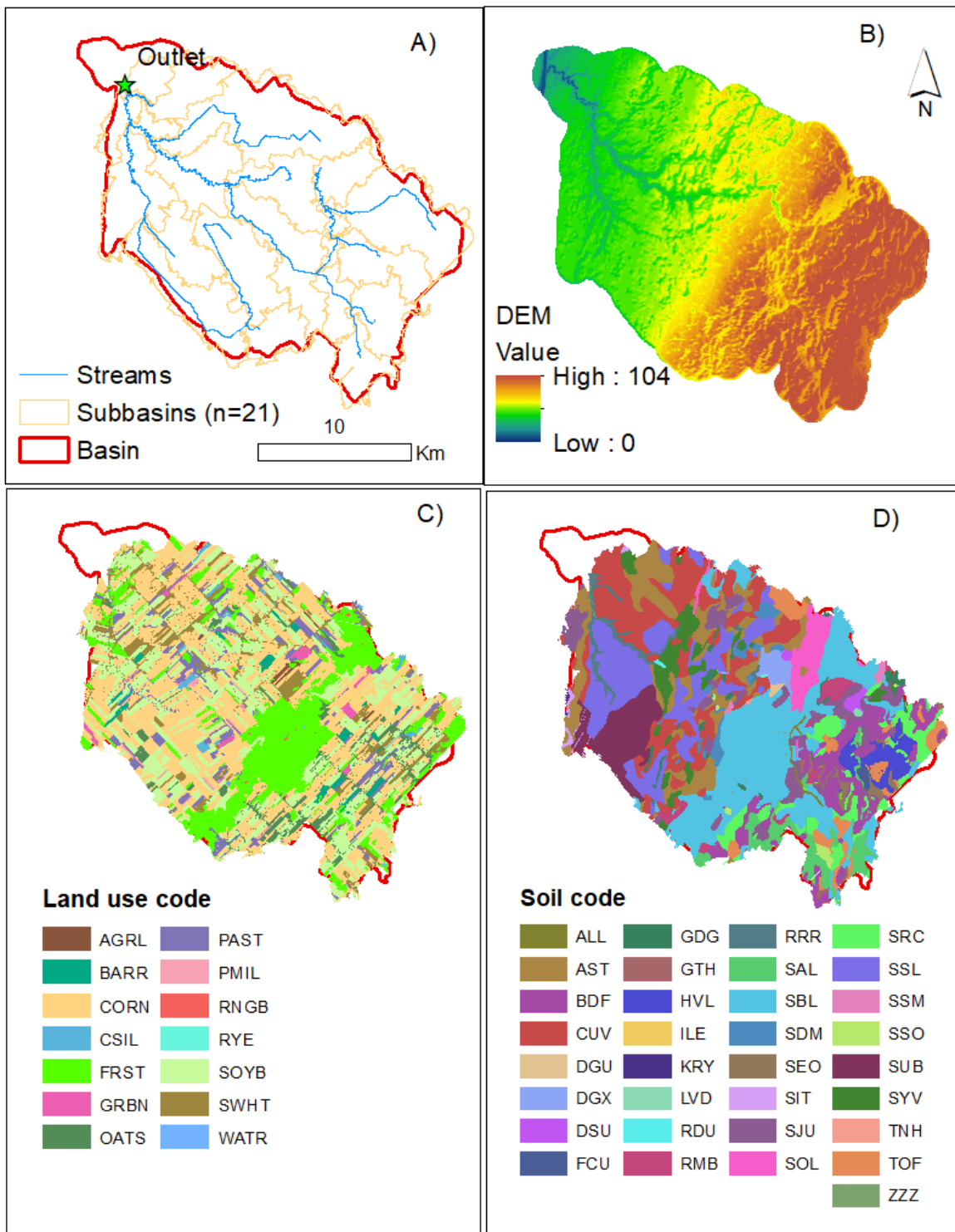


Figure 4-23. Hydrometric network (a), elevation model (b), land use (c) and soil map(d) of David river watershed. The distribution and soil properties of soil map units are described in appendix 1.0.

4.3.1.2 Hydrologic model description

SWAT-MAC model (Poon, 2013) was used to support the modeling of the hydric balance and flow pathways of the David basin in actual and future climate. SWAT- MAC is a modification of SWAT (version 2009), a semi-distributed, watershed-scale hydrologic model that runs on a daily time step. Detailed information on SWAT model functions and capacities are described by Neitsch et al.(2011). In SWAT, sub-basins are delineated based on the stream network and topography (digital elevation model), so that each sub-basin has a main channel. Model inputs and outputs are computed on individual hydrologic response units (HRU), which represent unique combinations of land use, soil, and topography within a sub-basin. Flux components of streamflow including surface runoff, lateral flow, tile drainage, shallow aquifer (return) flow and deep aquifer recharge are calculated in HRUs. The quantity of each flux component flowing to the main channel in each sub-basin is the area-weighted average value of the sub-basin's HRUs. Water from each sub-basin's main channel is then routed to the watershed outlet (Neitsch et al., 2011).

SWAT-MAC modifications were made to improve the projections of surface and subsurface flows in Quebec agri-environmental conditions. In previous modelling efforts, tile drain water yields tended to be underestimated under SWAT original algorithms (Deslandes et al., 2007; Michaud et al., 2007). Modifications included the ones proposed by Michaud et al. (2008) that replaced the tile drain flow equation with the one from SWAT 2000 (Neitsch et al., 2002). Another modification reordered the percolation processes, so that the simulation of lateral flow and seepage followed tile drainage in each soil layer, if tile drains are present in the HRU being simulated. SWAT-MAC (Poon, 2013) also added a macropore domain to the original SWAT (matrix) percolation algorithm. Briefly, the new algorithm partitions infiltration or seepage into each soil layer into the two domains. Water moving through the new macropore domain flows directly to tile drains if tile drains are present in the HRU considered. If tile drains are absent, water flow through the macropore domain into the vadose zone, the unsaturated zone between the bottom of the soil profile and the aquifer. The remainder of the infiltration or seepage enters the matrix domain, where water percolates by lateral flow, seepage, and tile drainage. The percolation algorithms are described in detail within Poon (2013) and summarized below.

In each soil layer, the amount of macropore flow is a fraction of the seepage that exceeds the matrix infiltration capacity according to the following:

$$q_{mac,ly} = [I_{ly} - IC_{mat,ly}] \times (f_{ly} \times \frac{SW_{ly}}{FC_{ly}}) \text{ if } SW_{ly} \leq FC_{ly} \quad [\text{Eq. 4.1a}]$$

$$q_{mac,ly} = [I_{ly} - IC_{mat,ly}] \times f_{ly} \quad \text{if } SW_{ly} > FC_{ly} \quad [\text{Eq. 4.1b}]$$

where $q_{mac,ly}$ is the water flowing through macropores in soil layer ly (mm day^{-1}), I_{ly} is the infiltration into layer ly from the surface or from seepage from the matrix in the above layer (mm day^{-1}), $IC_{mat,ly}$ is the infiltration capacity for layer ly (mm day^{-1}), related directly to the maximum seepage rate of the matrix domain of layer ly , f_{ly} is the macropore connectivity factor for layer ly (dimensionless value between 0 and 1), SW_{ly} is the soil water in layer ly (mm), and FC_{ly} is the field capacity of layer ly (mm).

The fraction of the excess seepage that flows through the macropores is controlled by two factors: the macropore connectivity factor (f_{ly}) and the moisture content in the soil layer. The f_{ly} is constant during a model simulation, but the modeller can adjust this parameter to account for the degree of connectivity between macropores and tile drains (if tile drains are present in the HRU being simulated) or the vadose zone (if tile drains are absent from the HRU being simulated, If all f_{ly} values are zero, no macropore flow is simulated and SWAT-MAC behaves according to SWAT's matrix flow algorithms. Macropore flow may be simulated regardless of the water content in a soil layer or profile. However, the fraction of excess infiltration that flows through macropores decreases as soil water in a layer decreases below field capacity (Eq. 4.1a), to account for greater lateral infiltration from macropores into the soil matrix (and less macropore flow reaching drains or the bottom of the soil profile) at lower water pressures.

Within SWAT-MAC, the algorithm improved SWAT's partitioning between surface runoff and subsurface flow. The capability of the model to separate macropore and matrix components of subsurface flow were also validated against flow pathways separation derived from a chemical-based hydrograph separation of the streamflow of an agricultural subwatershed of the Saint-Lawrence lowland presenting similar edaphic and land use patterns of the David river watershed (Michaud et al., 2019). A detailed description of the SWAT-MAC model's proof of concept, algorithms and validation are detailed within Poon (2013).

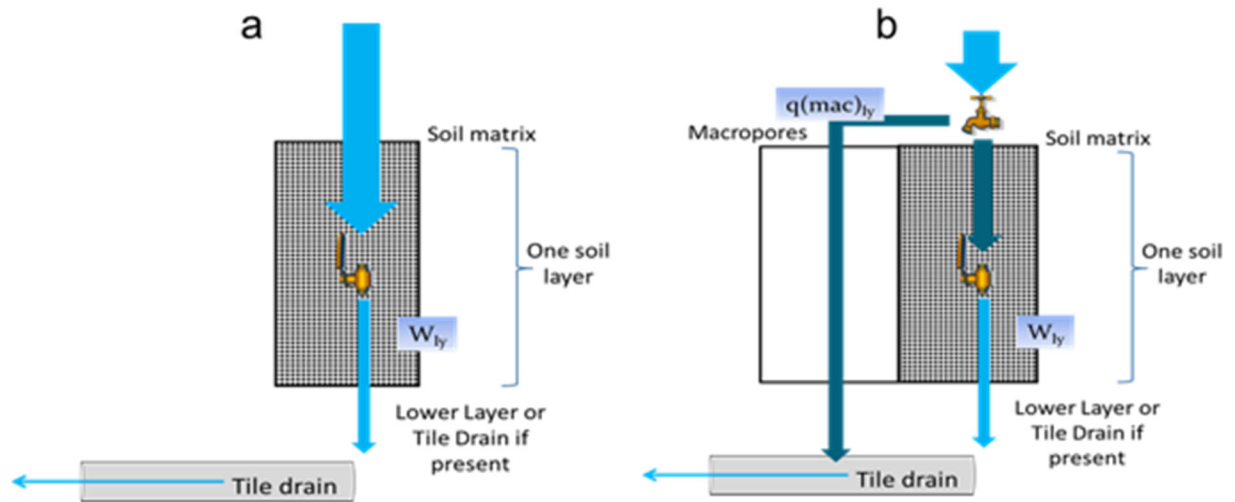


Figure 4-24. Conceptual representation of original SWAT matrix flow algorithms (a) and macropore domain flow algorithms within SWAT-MAC (b) (Adapted from Poon, 2013).

4.3.1.3 Watershed Setup in SWAT

ArcSWAT tool kit (Version 2012.10_4 released 1/23/2017), which combines SWAT model Fortran code with ArcGIS graphical interface, was used to set up the SWAT-MAC model. The input data sources, including the digital elevation model (DEM), land use map, soil map, streamflow, and meteorological data, are described in table 4.12. The soil properties of individual soil map units are described in Appendix 1. Based on the spatial analysis of the DEM and stream network, the entire basin was divided into 21 sub-basins. The HRUs were defined with a 10% threshold that eliminated land uses that each represented less than 1% of the watershed's area, resulting in a total of 1130 individual HRUs for the overall basin.

All cropped HRUs (71% of basin area) were assumed to have tile drains, with drain depth set at 900 mm. Assuming that crop rotation had marginal effects on the overall hydrology at the watershed scale, land use and management schedules were assumed to be the same every year during the simulation period (1980-2015). These schedules were based on the opinions of agrologists familiar with cropping practices in the study area (A. Michaud, personal communication), and they include tillage practices that differed by crop type and hydrologic soil group.

Table 4.14. Sources of data used for the parametrization of the SWAT-MAC model for the David river basin.

Data	Scale /resolution	Source
Stream network	1:20,000	Base de Données Topographiques du Québec
Digital elevation model(Lidar)	1.0 m	Inst. de R&D en Agroenvironnement (IRDA)
Land use: two sources	-	
1) agricultural crops	1:50,000	Financière Agricole du Québec, 2008
2) non-agricultural land	1:20,000	Min. des Ressources Naturelles et de la Faune, 2003
Soil map	1:63,360	Inst. de R&D en Agroenvironnement (IRDA)
Soil physical properties ^a	-	Tabi et al., 1991
Daily precipitation and temperature data	-	Environment Canada, 2018
Streamflow (hydrometric monitoring)	-	Dir. Expertise Hydrique, MDDELCC, Québec

^aSoil physical properties and organic carbon levels are reported in Appendix 1.0

4.3.1.4 Agri-climatic data for historic and future climate

The original calibration of the model was based on the meteorological historic observations (non-simulated) from three stations, including L'Assomption (45.81, -73.12), Saint-Hubert, 45.52, -73.41 and Nicolet 46.20, -72.62) from 1st January 1980 to 31st December 2015 (ECCC, 2018b). Further hydrologic simulations of climate change effects were based on climatic data time series data generated for the same three stations locations. Five climate scenarios were selected for this study for the reference period (1981-2010) and future climate (2041-2070) and post-processed by the OURANOS Climate scenarios and services group (Braun, 2017). The ten time series generated include daily precipitation (pcp), maximum and minimum temperature (tmp), solar radiation (slr), wind speed (wnd) and relative humidity (rh). The sources and designations of the climatic scenarios are reported in Table 4.15. For each climatic scenario, daily time series from three meteorological stations were used to support the bias correction procedure, namely L'Assomption, Saint-Hubert and Nicolet where complete sets of meteorological historical data were available for the reference period (1981-2010). These scenarios represent 72% of the simulated variability of the CMIP5 climate simulation ensemble (Taylor, et al. 2012). Sylvestre et al. (2017) described the variability inherent to the selection of climatic scenarios. Table 4.16 reports the resulting temporal gradients (future – historic climate) in cumulative summer rainfall, potential evapotranspiration, average temperature from April to October, number of days with temperatures above 30° C, length of growing season, wind speed, solar radiation and relative humidity.

For the selected climate change scenarios, the simulated temperatures increase significantly, with raises averaging 3°C for the April to October period. The projected increase in temperature is

however variable according to the scenarios, ranging from a rise of 2.0 ° C (MRI-CGCM3) whereas the warmer scenario (GFDL-CM3 with 43 days temperature superior of 30°C) projects a rise of 4.0 °C on average for the April to October period. The difference in growing season duration from historic to future climate (around 20 days) are equivalent for the scenarios GFDL-ESM2G and MIROC56, while MRI-CGCM3 project a lower increase (15-days), and scenario MIROC58, the largest extension of the growing season (41-days). Projeted rainfall in future climate for the different scenarios are contrasted, with cumulative rainfall increases from April to October ranging from 30 mm (MRI-CGCM3 scenario) to 83 mm (MIROC58 scenario).

Table 4.15. : Sources of the climatic scenarios used for the hydrologic modeling of David river.

Modelling Center	Model	RCP ¹	Institution	Members	Terms of Use	Code ²
NOAA GFDL	GFDL-CM3	4.5	Geophysical Fluid Dynamics Laboratory	1	unrestricted	GF3
	GFDL-ESM2G	8.5				GFG
MIROC	MIROC5	6.0	Atmosphere and Ocean Research Institute (The University of Tokyo)	1 - 3	non-commercial	MI56
	MIROC5	8.5	National Institute for Environmental Studies			MI58
			Japan Agency for Marine-Earth Science and Technology			
MRI	MRI-CGCM3	8.5	Meteorological Research Institute	1	non-commercial	MR3
¹ RCP: representative concentration pathway. In CMIP5, "rcp45" refers to a particular experiment in which a "representative concentration pathway" (RCP) has been specified which lead to an approximate radiative forcing of 4.5 W m ⁻² .						
¹ Code : Code used in this study						

Table 4.16. Observed and projected differences in selected climate indicators between historic and future climatic scenarios, averages for Saint-Hubert, L'Assomption and Nicolet meteorological stations.

	Average Temp.	Nb. Days	Length of growing	Cumul, PPT	Pot. Evap.	Wind Speed	Solar Radiation	Relative Humidity
Difference between Reference and Future scenarios	(April to October) (oC)	> 30oC	season (days)	(April to October) (mm)	(mm)	(m/s)	(MJ/m ²)	(%)
OBSERVED value	14.00	11	199	624	988	13.00	3781	73.00
GF3 Change	3.97	43	26	42	154	-0.60	165	2.67
GFG Change	2.10	16	21	58	68	0.57	8	1.00
MI56 Change	2.23	16	20	73	96	0.03	101	-0.33
MI58 Change	3.97	33	40	44	186	-0.37	218	-1.33
MR3 Change	1.97	9	16	34	52	7.30	141	1.00
Average change	2.87	23	24	50	114	1.39	127	0.60

dapted from Delmotte et al., 2017.

The potential evapotranspiration is directly correlated with the number of days of the growing season. Together with daily projections of temperatures and precipitations, the SWAT model simulations made use of projected wind speed, relative humidity and solar radiation for historic and future climate for the three selected meteorological stations to derive evapotranspiration estimates using Penman-Monteith formula. Globally, projected differences for future climate in solar radiation and relative humidity are marginal (Table 4.16). Wind speed temporal gradients are also marginal, except for the MR3 scenario, which seems to present some anomalies. The effect on evapotranspiration estimates, averaged over the five scenarios and three stations, remained marginal through the hydrologic modeling process.

4.3.1.5 Model calibration procedure

The model was run from 1st January 1980 to 31st December 2015 with some missing discharge data in 2006 and three years warm up period. The model was primarily calibrated to fit the daily discharges observed at the gauging station located near the basin outlet (45°57'13" N 72°51'34") and operated by the *Direction de expertise hydrique* (DEH, 2018) from the provincial department *Ministère du Développement durable, de l'Environnement et de la Lutte contre les Changements climatiques* (MDDELCC). Daily minimum, maximum and average stream discharge recorded for the David river station for the 1970-2014 period are illustrated in figure 4.25. Close attention was also given to the watershed hydric balance and flow pathways projected by the SWAT-MAC model. Continuous hydrograph separation data from the neighbouring 3e Petite-Rivière-Pot-au-Beurre (PRPB) hydrometric station were used to ensure a proper projection of surface runoff and subsurface flows. It was hypothesized that the hydrology of David basin and PRPB micro-watershed (20 km²) is characterized by similar pathways since these study regions share common spatial gradients in land use, soil types, hydrography and landscape. Also, the tile flow monitoring

data from the Yamaska field sites, representative of the clayey dominant soil type of the David basin provided additional background data to adjust the model performance with respect to tile water yields and time distribution.

The calibration procedure of the SWAT-MAC model for the David river basin was supported by the auto-calibration tool kit SWAT-CUP, a generic interface and stand-alone program developed for SWAT model calibration (Abbaspour *et al.*, 2015). The use of the Sequential Uncertainty Fitting Algorithm (SUFI-2) proved to be efficient in optimizing the uncertainty analysis, while handling a large number of parameters. The parameters selected for the calibration procedure are reported in Table 4.17. Their selection was based on the characteristics of the study area and previous research within the Montérégie region (Gombault *et al.*, 2015a; 2015b; Delandes *et al.*, 2007; Michaud *et al.*, 2007). Several cycles of iterations, typically including 1000 simulations, were necessary to obtain a satisfactory adjustment of the model, based on the fitted values of parameters reported in Table 6.

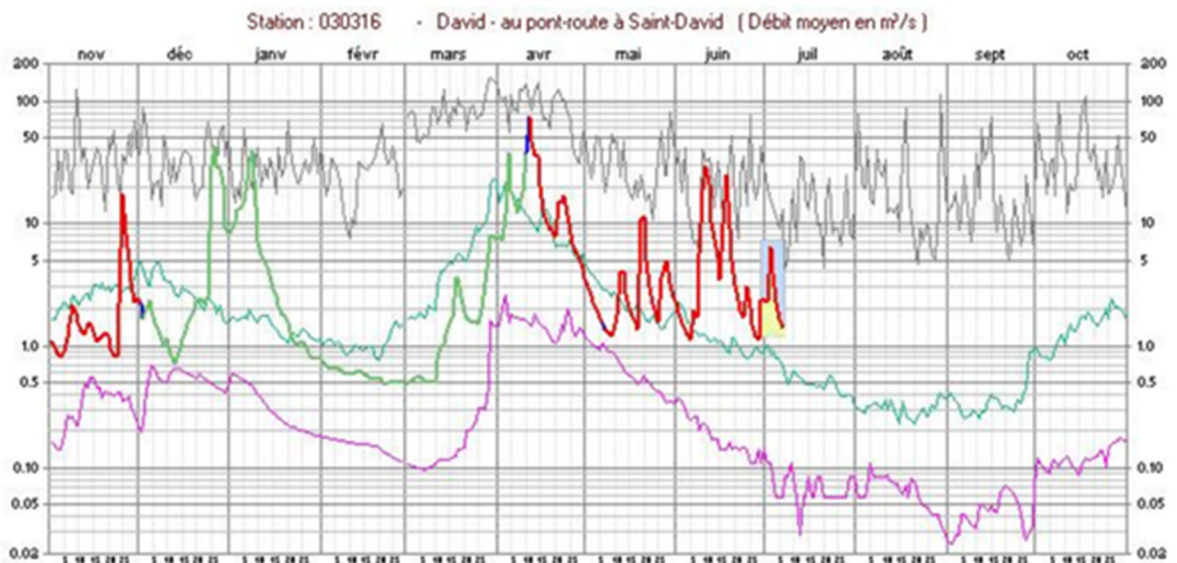


Figure 4-25. Daily minimum, maximum and average stream discharge (m^3sec^{-1}) of David river ($323 km^2$) for the 1970-2014 period.

Table 4.17. Selected parameters for the SWAT-CUP calibration procedure for the David basin.

SWAT files	Flow parameters	Lower bound	Upper bound	Fitted values
BSN	SFTMP: Snowfall temperature [oC]	-5	5	-2.48
	SMTMP: Snow melt base temperature [oC]	-5	5	1.25
	SMFMX: Melt factor for snow on June 21 [mm H2O/ oC-day]	-3	3	2.37
	SMFMN: Melt factor for snow on December 21 [mm H2O/ oC-day]	-3	3	0.008
	TIMP: Snow pack temperature lag factor	-3	3	0.64
	SNOCOVMX: Minimum snow water content that corresponds to 100% snow cover [mm]	0	120	49.59
	SNO50COV: Fraction of snow volume represented by SNOCOVMX that corresponds to 50% snow cover	0	1	0.05
	IPET: PET method: 0=priest-t, 1=pen-m, 2=har, 3=read into model			1
GW	GW_DELAY: Groundwater delay [days]			38.56
	ALPHA_BF: Baseflow alpha factor [days]	0	1	0.36
	GWQMN: Threshold depth of water in the shallow aquifer required for return flow to occur [mm]	0	100	27
	GW_REVAP : Groundwater "revap" coefficient	0	1	0.08
	REVAPMN: Threshold depth of water in the shallow aquifer for "revap" to occur [mm]	0	100	65.84
	RCHRG_DP : Deep aquifer percolation fraction	0	1	0.11
MGT	CN2: Initial SCS CN II value	-40	25	-40
	DDRAIN: depth to subsurface tile drain (mm)	0 No, 900 Free drainage		
	TDRAIN: time to drain soil to field capacity (hr)	0 No, 18 Free Drainage		
	GDRAIN: drain tile lag time (hr)	0 No, 12 Free Drainage		
HRU	ESCO : Soil evaporation compensation factor	0	1	0.12
	EPCO: Plant uptake compensation factor	0	1	0.84
	a DEP_IMP: Depth to impervious layer in soil profile [mm]	1000	4000	3922.5
SOL	fly is the macropore connectivity factor	0.1	0.35	0.3 Free, 0 No drainage

4.3.2 Results

The results of the hydrologic modeling simulations are successively reported for the historic period, using observed climatic and hydrometric data for the 1985 to 2015 period, and for the climate scenarios generated for actual (1981-2010) and future (2041-2070) periods.

4.3.2.1 Model performance under calibration period 1985-2015

A satisfactory projection accuracy for daily stream discharge was obtained with $R^2 = 0.5$, $NSE = 0.4$ and $PBIAS = 0.3 \text{ m}^3/\text{s}$ for the 30 year model simulations (Figure 4.26). Some discrepancies in peak flow rates are partially attributed to the limitation of the distant meteorological stations to fully reproduce the temporal and spatial patterns of high intensity rainfall over the basin. Another significant cause of discrepancies is presumably related to the SCS Curve number empirical method used within the SWAT-MAC model to estimate surface runoff calculate runoff which does not consider duration and intensity of precipitation.

The simulated annual and monthly water balance averaged over the historic period (1985-2015) is reported in Table 4.18. Globally, the water balance modelled over the study period is coherent with the hydrometric observations collected at the PRPB micro-watershed outlet and at the Yamaska field sites. The projected total subsurface water annual yield for at David river basin's outlet

(summation of tile, lateral and return flows) averages 289 mm per year, which accounts for 65% of the 446 mm annual total water yield. This ratio is similar to the 67% proportion of total water yield attributed to subsurface flow pathway following the hydrograph separation of flow data from the PRPB micro-watershed, as reported earlier for the 2014-2017 monitoring period (Table 4.3). For the same monitoring period, annualized tile water yields ranged between 190 and 313 mm at Yamaska field sites, as reported in Table 4.6, for an inter-site average of 251 mm per year. Concurrently, the tile flow yields projected by the SWAT-MAC for the David basin over the historic period averages 169 mm per year (Table 4.18). When area-weighted for the basin cropped area (71% of total basin area), the SWAT-MAC projected tile water yield averages 238 mm per year, which is close to the yearly 251 mm averaged over the 2014-2017 for the Yamaska field sites.

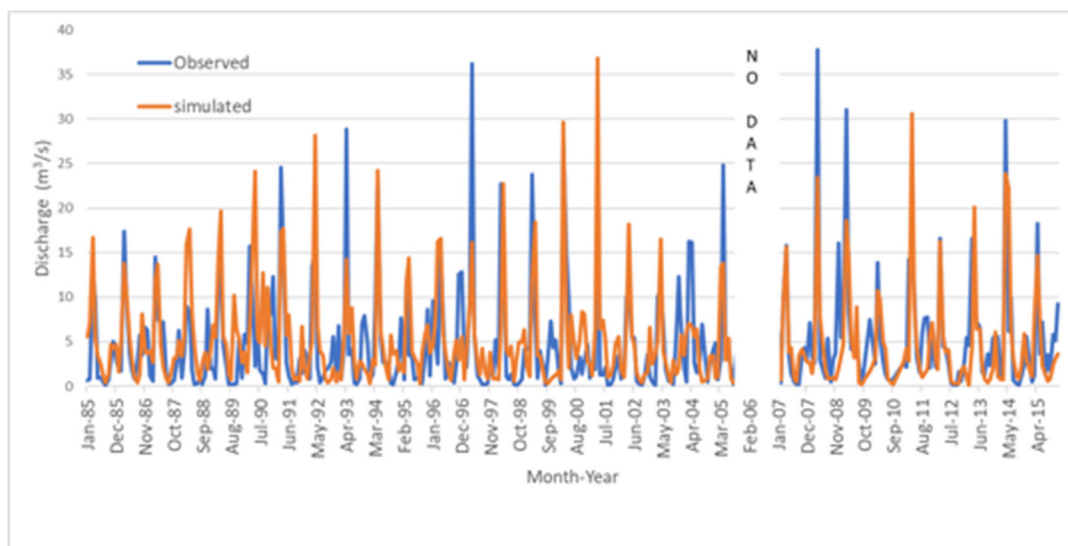


Figure 4-26. Average monthly observed and simulated discharges flow of David river basin for the 1985-2015 historic calibration period.

Moreover, the monthly distribution of tile flows projected by the SWAT-MAC model matches the tile monitoring data from the Yamaska sites previously reported in section 4.2. Projected tile flows totaled 151 mm for the March-April period for the cropped area of David river basin. Globally, 88% of the average SWAT-MAC projected tile flow tile water yield occurs during the non-growing season (October-April), while similar ratios (84-87 %) have been observed for the Yamaska filed sites, as previously reported within Table 4.6.

Globally, it is thus concluded that the calibration of the SWAT-MAC model enabled a satisfactory projection of the basin discharge temporal distribution, together with coherent hydrologic balances

and flow pathways that closely matched the observations concurrently monitored at the micro-watershed scale (PRPB) and field scale (Yamaska sites).

Table 4.18. Averaged annual hydrologic balance components for the David river basin for the 1985-215 historic period (a) and associated monthly standard deviations (b).

a. Monthly and annual averages													
Hydrologic Component (mm)	Janv	Feb	Mar	Apr	May	Jun	Aug	Jul	Sept	Oct	Nov	Dec	Annual
Precipitation	87	75	79	72	80	92	96	97	98	83	88	93	1039
Snow melt	1	6	48	117	10	0	0	0	0	0	1	0	182
Evapotranspiration	3	4	12	41	77	97	111	102	69	42	21	5	583
Water Percolation	4	4	14	36	19	8	3	3	3	5	7	8	113
Shallow Aquifer Recharge	6	4	6	17	21	15	9	6	4	4	4	6	101
Deep Aquifer Recharge	1	1	1	2	3	2	1	1	0	0	1	1	13
Surface Runoff	11	11	29	38	18	13	4	3	6	8	7	10	158
Lateral Flow	1	0	1	5	3	2	1	1	1	1	2	1	19
Groundwater Flow	6	4	5	16	21	15	10	6	4	4	4	6	101
Water Yield	19	19	69	133	51	34	17	11	15	24	27	27	446
Tile drainage	2	4	33	74	9	4	2	2	4	11	14	10	169

b. Monthly standard deviations													
Hydrologic Component (mm)	Janv	Feb	Mar	Apr	May	Jun	Jul	Aug	Sept	Oct	Nov	Dec	
Precipitation	30	32	31	26	29	33	41	50	45	36	28	24	
Snow melt	1	7	30	69	41	0	0	0	0	0	1	0	
Evapotranspiration	1	2	5	13	10	14	16	15	12	9	6	3	
Water Percolation	9	9	26	52	33	14	8	11	10	12	13	15	
Shallow Aquifer Recharge	10	7	11	25	30	22	15	10	8	9	9	11	
Deep Aquifer Recharge	1	1	1	3	4	3	2	1	1	1	1	1	
Surface Runoff	13	14	27	38	24	15	9	13	15	16	12	13	
Lateral Flow	1	2	5	13	8	4	3	3	3	4	4	3	
Groundwater Flow	10	7	10	24	31	23	15	10	8	9	9	10	
Water Yield	14	18	51	73	44	23	17	22	21	28	22	19	
Tile drainage	5	12	40	66	21	9	5	9	9	17	18	15	

4.3.2.2 Drainage scenarios effect under historic climate

The effects of controlled drainage scenarios on hydrologic balance and flow pathways were simulated by “virtually” closing the tile drainage systems of the overall David river basin cropped area (71 % of basin surface area). From a model parametrization perspective, this inactivation of the tile drainage systems was operated by setting the drainage parameters (DDRAIN, TDRAIN and

GDRAIN) to “0” value. The relative effect of the drainage inactivation was estimated by the difference of the model outputs between the *No drainage – Free drainage* scenario. From an operational perspective, the “*No drainage*” scenario imply that the tile collectors would be closed, year-round. We convene that this “extreme case scenario ” is not realistic, from a management perspective, considering the hydric excesses typically occurring in late winter and early spring, which calls for subsurface drainage. The point of interest here is to quantify the trade-off between tile water yield reduction and surface runoff increase in response to the operation (or not) of the tile drainage system, and to analyse these responses with respect to period of the year, as well as contrasting soil properties. Model performance for this regard are presented in two parts. Seasonal effects are first discussed by comparing water balances and flow pathways resulting from the *No drainage* and *Free drainage* scenarios for the overall basin. Secondly, modeling results for contrasting soil types are presented to support the discussion on the feasibility of controlled drainage within the study area with respect to soil properties.

Table 4.19. Averaged annual differences in hydrologic balance components resulting from contrasted drainage scenarios (No Drainage - Free drainage) for the David river basin for the 1985-2015 historic period.

Hydrologic Component (mm)	Free drainage		No drainage		Difference (No -Free)
	Mean	Std. Dev.	Mean	Std. Dev.	
Precipitation	1039	34	1039	34	0
Snow melt	182	13	170	12	-12
Evapotranspiration	583	9	663	10	81
Water Percolation	113	18	163	16	50
Shallow Aquifer Recharge	101	16	144	12	50
Deep Aquifer Recharge	13	2	19	1	6
Surface Runoff	158	17	201	19	43
Lateral Flow	19	4	14	3	-5
Groundwater Flow	101	14	144	11	44
Water Yield	446	29	359	20	-87
Tile drainage	169	19	0	0	-169

Table 4.19 report the average of the annual differences in hydrologic balance components resulting from contrasted drainage scenarios (No Drainage - Free drainage) for the David river basin for the 1985-2015 historic period. These results apply to the overall watershed, including the non-agricultural land uses (29% of basin surface area) that was not affected by the change in model parameterization. These averaged annual estimates offer a global perspective on how the model routes the water excesses in absence of the subsurface drainage systems. The hydrologic balance resulting from the *No drainage* scenario indicates that most of the 170 mm water yield that was initially transferred through the drainage systems is now reaching the stream through the shallow

aquifer (144 mm), together with an increase in surface runoff (43 mm over the basin total surface area). A marginal increase in the deep aquifer recharge (6 mm) is also projected by the model, resulting in a reduction of 87 mm in the stream annual discharge.

Figure 4.27 illustrates the monthly distribution of differences in hydrologic balance components resulting from the contrasting drainage scenarios (*No Drainage - Free drainage*) for the David river basin for the 1985-2015 historic period. The projected monthly distribution of surface runoff, in response to the *No drainage scenario*, is of particular interest from the perspective of estimating the feasibility of controlled drainage. At the basin scale, the model outputs project that the most significant increases in surface runoff resulting from tile drain inactivation occur in March and April, with respective increases of 7.8 and 20.5 mm. More water also infiltrates towards the shallow aquifer, especially in April, which causes a significant decrease in the monthly stream discharge (-45 mm).

In the subsequent months of May and June, the projected increase in stream discharge is in phase with the incoming return flow from the shallow aquifer. In short, the modeled outputs indicate that the *No drainage scenario* retains water within the soil profile and the shallow aquifer (vadose zone) during the critical snowmelt period, which translates into surface runoff and delayed stream discharge. The projected effect of the *No drainage* scenario on stream discharge is still noticeable in June, with a projected average of 7.1 mm of supplemental stream discharge, contributed by the return flow. From an agricultural production perspective, a slower release of excess water through return flow, instead of tile pathway, can be advantageous with respect to moisture stress abatement during the summer months. This potential benefit is suggested by the increases in evapotranspiration rates in June (+23 mm) and July (+12 mm), as well higher return flows in response to *No drainage* scenario, which reached on average 8.8 mm in June and 3.6 mm in July. Further detailed analysis of the model performance and effects regarding moisture stress would call for calibration of crop growth and yields based on field monitoring data.

The implications of drainage scenarios for crop production and water balances are better described through the analysis of the modeled outputs for specific soil types and land uses. The next presentation of results depicts water balance responses to the drainage scenarios for corn and soya crops cultivated on Sainte-Rosalie clay and Saint-Jude sandy loam. As presented in Table 4.20, these soil series have contrasting physico-chemical properties, which translated into different modeled hydrologic responses. Figure 4.28 illustrate the averaged differences in surface runoff resulting from the modeling of contrasted drainage scenarios (*No Drainage - Free drainage*) for the different Soil Type X Crop combinations for the 1985-2015 historic period. Elevated increases in annual surface runoff are projected for the Saint-Rosalie clay, under both crop scenarios (131mm

for corn; 122 mm for soya). For the Saint-Jude sandy loam, the increase in surface runoff is drastically lower, within the range of 24 to 12 mm for the corn and soya crops, respectively.

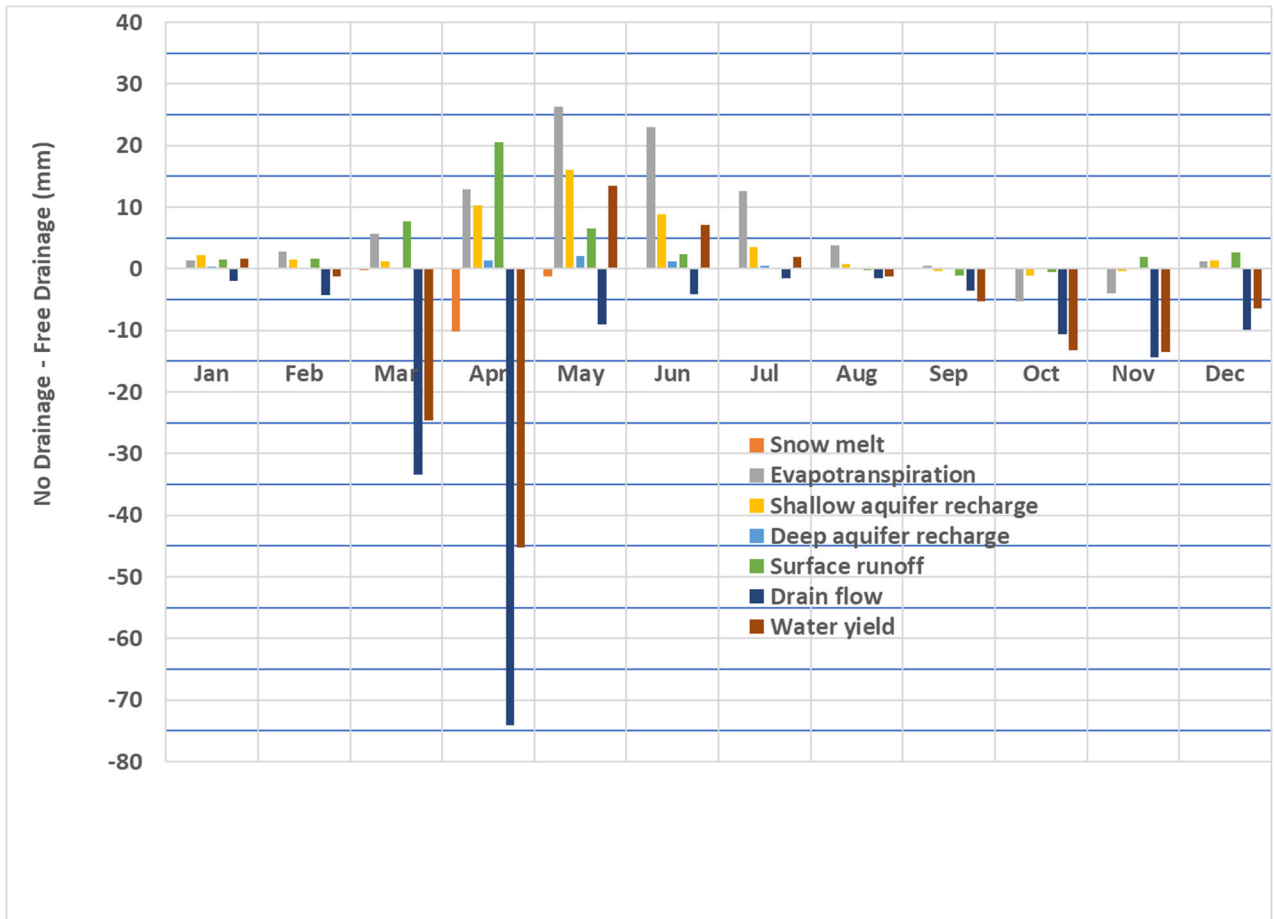


Figure 4-27. Average monthly differences in hydrologic balance components resulting from contrasted drainage scenarios (No Drainage - Free drainage) for the David river basin for the 1985-2015 historic period.

More abundant surface runoff emissions projected for the Sainte-Rosalie, in response to the *No drainage* scenario, is attributed to the fact that Sainte-Rosalie clay owes most of its tile flow to the macropores pathway, as projected by the SWAT-MAC macropore flow algorithms. The strong response of Saint-Rosalie clay is conceptually explained by the disconnection of its quick, macropore flow to the tiles. Oppositely, the physical properties of the sandy loam, namely its lighter soil texture, favour an effective transfer of excess water out of the soil profile to the vadose zone, and eventually to the stream by the return flow pathway. A practical implication of these projections,

is that the hydrologic response of a given field site to controlled drainage is soil properties dependant. Soils with important propensity for macropore flow connected to tiles network are likely to develop stronger surface runoff responses to controlled drainage.

Unsurprisingly, most of the annual surface runoff increases are projected during the month of April, which highlights the agri-environmental benefits provided by subsurface drainage systems. Thus, tile drainage systems must be operational during this critical snowmelt period. In May however, the projected contrast in surface runoff responses to drainage scenarios indicates that the feasibility of controlled drainage is soil type dependant. The marginal increases in surface runoff, below 5 mm, projected for the Saint-Jude soil series during the month of May, resulting from a complete shutdown of the tile collector, indicate a relatively high feasibility of controlled drainage scenarios for this soil type under current climate. In contrast, for the Saint-Rosalie clay, the projected monthly increase in surface runoff (ranging between 13 and 16 mm in May) is a concern. A practical implication of these projections is some subsurface drainage capacity must be maintained in May for heavier soil types to infiltrate excess precipitation. If total shutdown of collectors is not feasible, the magnitude of the projected surface runoff volume does not exclude the feasibility of controlling of the water table over the tile depth. Water retention benefits from stage control must however not compromise the infiltration of excess rainfall and promote surface runoff.

Table 4.20. Soil properties of Saint-Jude sandy loam and Sainte-Rosalie clay used as SWAT-MAC model inputs.

	Saint-Jude	Sainte-Rosalie
Soil Serie^a	(SJU) Podzol	(SSL) Gleysol
Hydrologic soil group	B	D
Texture	Sandy loam	Clay
Bulk density	1.67	1.36
AWC	0.06	0.17
Hydraulic Cond.	16.90	74.70
% Carbon	1.90	4.09
USLE K	0.190	0.190
^a Adapted from Tabi et al. (1991).		

4.3.3 Climate change effects under free drainage scenario

The annual averaged differences in water balance and flow pathways between future (2041-2070) and reference climate (1981-2010) are illustrated in Figure 4.29 as projected by the calibrated SWAT-MAC model using the five different climate scenarios of the CMIP5 ensemble. Globally, the

projected annual water balance reflects the temperature and precipitation patterns of the individual climate scenarios. All the climate scenarios projected increases in annual precipitation. The hydrologic simulation results also indicate reductions in snow fall and snow melt for all the climate scenarios, which vary considerably from the warmer MI58 scenario to almost no reduction for the GFG scenario. Higher precipitations caused increases in projected annual water yield at the watershed outlet for all climate scenarios, ranging from 35 mm for MI58 scenario to 93 mm for GFG scenario. However, the excess water yield projected by the different climate scenarios followed contrasted flow pathways. Moderate surface runoff increases (19 to 32mm on an annual basis) are projected by three out of five scenarios, namely GF3, GFG and MR3. The hydrologic response to MI56 and MI58 rather translated into elevated increases in tile flow pathway, from 156 to 156 mm on an annual basis, while tile water yields increased by 27 to 46 mm for the three other scenarios. These results indicate that the hydrologic model was sensitive to the temperature and precipitation gradient of individual climate scenarios (future – reference), which translated into contrasting flow pathways, especially during the late winter and early spring periods.

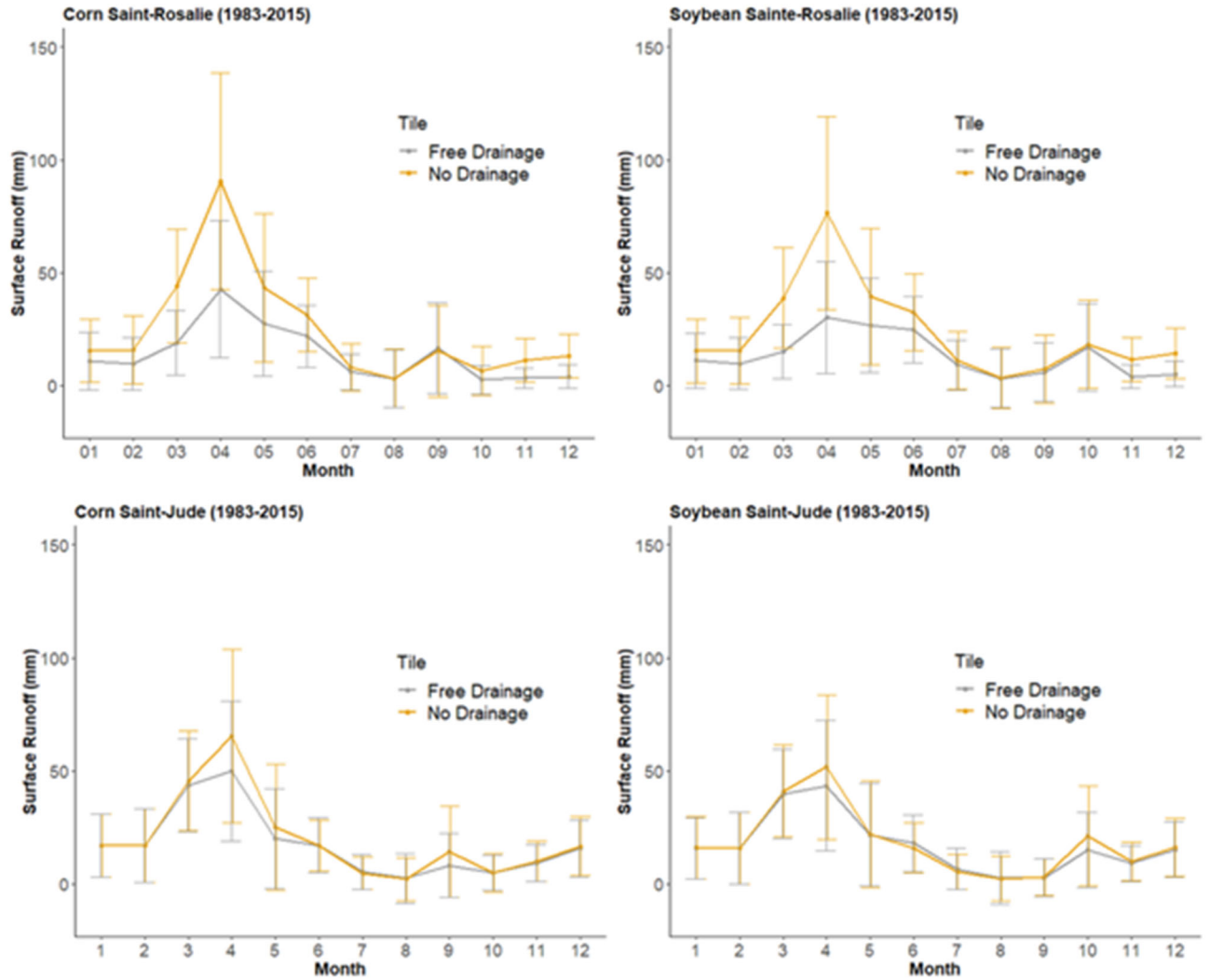


Figure 4-28. Monthly averages and standard deviation in surface runoff volumes resulting from the modeling of contrasted drainage scenarios (*No Drainage* - *Free drainage*) for corn and soybean crops cultivated on Saint-Rosalie clay and Saint-Jude sandy loam soil series for the 1985-2015 historic period.

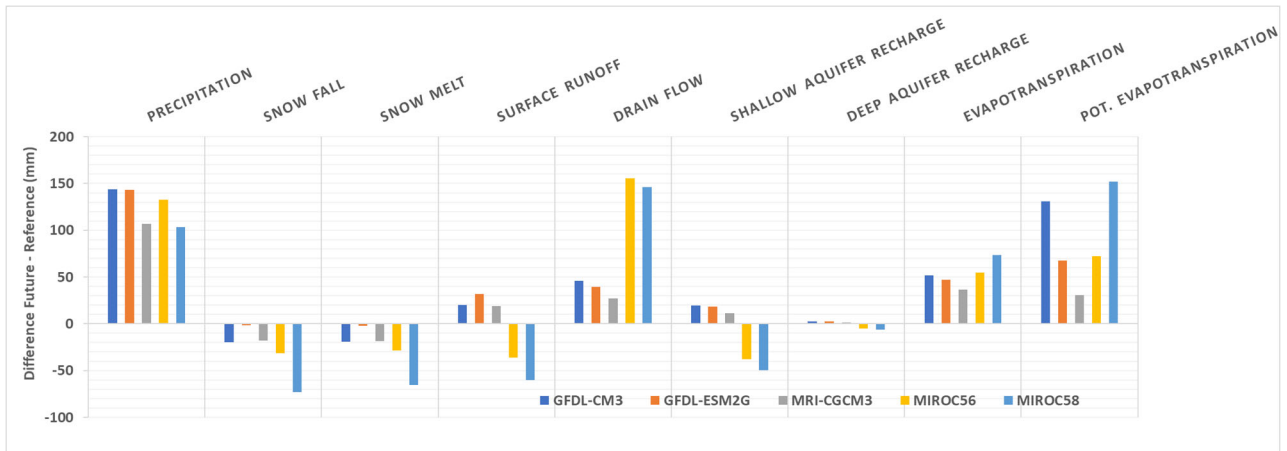


Figure 4-29. Annual averaged differences in water balance components between reference and future climate (Future 2041-2070 – Reference 1981-2010) projected by the five different climate scenarios of the CMIP5.

Table 4.21. Annual averaged differences in selected water balance components between reference and future climates (Future 2041-2070 – Reference 1981-2010) projected by the five different climate scenarios of the CMIP51.

Hydrologic Component (mm)	Climatic scenario				
	GF3	GFG	MR3	MI56	MI58
Precipitation	143.7	143.3	107.0	132.7	103.4
Snow fall	-19.5	-1.6	-18.0	-31.4	-73.4
Snow melt	-19.1	-1.9	-18.6	-28.8	-65.3
Sublimation	-2.0	-0.6	-2.8	-3.8	-6.8
Surface Runoff	19.9	31.9	19.1	-36.3	-60.1
Lateral Flow	3.6	3.3	2.6	-0.8	-1.4
Groundwater Flow	19.7	18.5	11.3	-37.7	-49.8
Deep Aquifer Recharge	2.6	2.4	1.5	-4.9	-6.5
Tile drainage	46.2	39.6	26.9	155.8	146.0

Relatively higher potential evapotranspiration rates are also projected for the GFE and MI58, resulting from the most elevated projected temporal gradient in temperature (3.8-3.9 °C); and solar radiation (165-218 MJ/m²), as previously presented in Table 4.16. Global increases in ET for the are projected by all scenarios, with totals differential ET ranging between 36 and 74 mm.

The annual and monthly simulation results for water balance and flow pathways averaged for the five climate scenarios are reported in Table 4.24 for the David river basin for the future climate (2041-2070). The monthly standard deviations are also presented to illustrate the effect of the climate scenario on the variability of projected water balance components. On a relative basis, surface runoff projection is the water balance component that is the most influenced by the climate

scenario. For an averaged monthly runoff depth of 33.5 mm in April, the standard deviation reach 8.9 mm.

Table 4.22. Averaged annual hydrologic balance components for the David river basin for the future climate (2041-2070) period (a) and associated monthly standard deviations.

a. Monthly and annual averages

Hydrologic Component (mm)	Janv	Feb	Mar	Apr	May	Jun	Jul	Aug	Sept	Oct	Nov	Dec	Total
Precipitation	106.4	84.5	82.6	99.2	92.5	103.3	92.1	92.9	97.6	115.5	117.0	106.0	1189.7
Snowmelt	1.2	10.0	69.2	51.8	0.0	0.0	0.0	0.0	0.0	0.0	0.7	0.3	133.2
Evapotranspiration	5.5	9.1	26.5	75.4	109.7	119.1	127.6	97.9	71.5	39.5	19.1	7.5	708.4
Water Percolation	7.9	7.5	22.3	28.3	11.5	3.7	1.7	1.3	1.7	4.6	8.8	11.0	110.2
Shallow Aquifer Recharge	6.8	5.7	9.1	16.2	15.2	9.3	5.3	2.9	1.9	2.3	3.8	6.3	84.8
Deep Aquifer Recharge	1.0	0.8	1.4	2.4	2.3	1.4	0.8	0.4	0.3	0.3	0.6	0.9	12.7
Surface Runoff	21.0	22.4	33.1	33.5	16.4	13.0	2.9	1.7	3.6	12.4	16.6	18.2	194.8
Lateral Flow	0.7	0.6	1.8	3.0	1.6	0.8	0.4	0.3	0.4	0.9	1.2	1.1	12.7
Groundwater Flow	7.9	6.5	9.9	18.2	17.9	11.1	6.4	3.5	2.2	2.5	4.2	7.0	97.4
Water Yield	35.9	39.1	93.7	94.9	39.7	26.7	10.4	6.0	9.0	27.4	41.9	42.7	467.5
Tile drainage	6.4	9.6	48.8	40.2	3.8	1.9	0.7	0.5	2.8	11.7	20.0	16.3	162.6

b. Monthly standard deviations

Hydrologic Component (mm)	Janv	Feb	Mar	Apr	May	Jun	Jul	Aug	Sept	Oct	Nov	Dec
Precipitation	7.7	8.7	10.1	9.2	7.5	6.2	7.9	17.3	6.3	15.5	12.7	11.3
Snowmelt	0.6	5.3	8.3	25.6	0.0	0.0	0.0	0.0	0.0	0.0	0.7	0.1
Evapotranspiration	0.9	1.2	6.6	12.2	4.7	4.1	4.5	10.1	3.7	2.7	2.1	0.7
Water Percolation	1.3	1.8	2.5	5.9	3.3	1.2	0.5	0.6	0.4	0.5	0.9	1.4
Shallow Aquifer Recharge	0.9	1.0	1.7	1.4	3.0	2.3	1.4	0.8	0.5	0.3	0.5	0.6
Deep Aquifer Recharge	0.1	0.1	0.2	0.2	0.4	0.3	0.2	0.1	0.1	0.0	0.1	0.1
Surface Runoff	3.7	4.4	5.0	8.9	3.3	2.1	1.7	1.1	0.9	1.8	3.2	2.8
Lateral Flow	0.1	0.2	0.3	0.5	0.3	0.2	0.1	0.1	0.0	0.1	0.1	0.1
Groundwater Flow	0.8	0.8	1.4	1.1	2.7	2.1	1.3	0.8	0.5	0.3	0.4	0.5
Water Yield	6.2	6.7	10.6	25.1	6.0	4.2	3.3	2.0	1.7	3.1	5.5	6.6
Tile drainage	2.7	5.1	6.0	15.6	1.1	0.6	0.5	0.3	0.6	1.5	2.4	3.8

The monthly distribution of differences (Future – Reference climate) in water balance components and flow pathways, averaged for the five climate scenarios combinations are illustrated in Figure 4.30. The projected averaged increase in winter precipitation caused significantly higher surface runoff depth, averaging 4.0, 4.2 and 15.4 mm in January, February and march, respectively. Marginal increases in surface runoff are also projected for the fall period (< 6 mm on a monthly basis), resulting from the relatively more abundant rainfall. The most significant effect of future climate on the water balance is projected for April. Snowmelt peak is henceforth occurring earlier, in March, which decreased tile water yield averaging 40 mm.

The future climate scenarios increases ET rate projections by 59 mm, while total water yield is reduced by a similar volume (66 mm). These projected gradients indicate that climate change will

increase the risks of water stress during the summer period and potentially reduce the availability of water resource when it is the most needed for agricultural productivity. The overall pattern of changes in water balance projected by this study has also been reported in other studies conducted on Quebec watersheds (Gombault et al., 2015; Mehdi et al., 2015; Boyer et al. 2010; Minville et al. 2008;). Higher precipitation and winter temperatures trigger earlier snowmelt runoff and onset of spring flooding, while warmer summers increase moisture deficits.

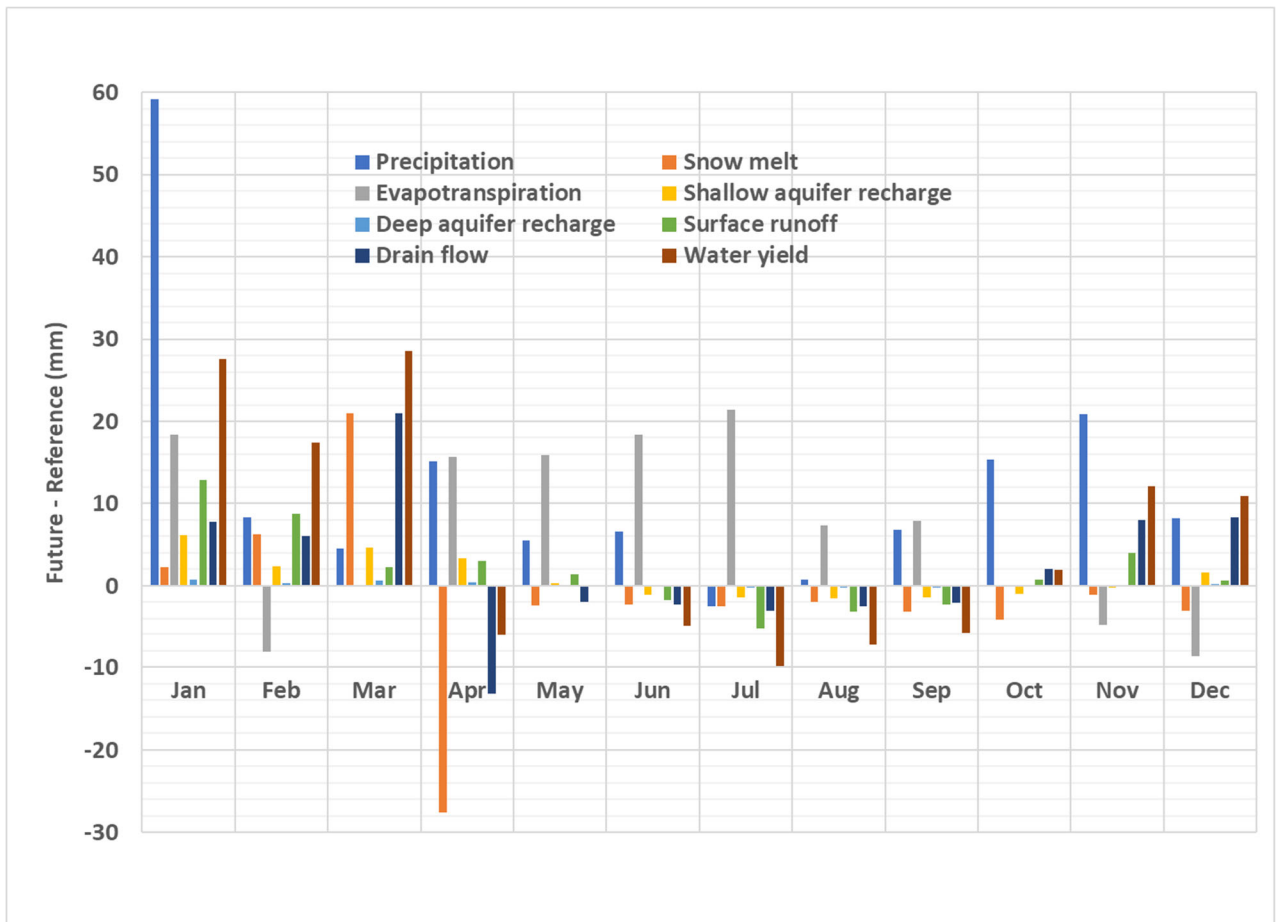


Figure 4-30. Monthly averaged differences in selected water balance components between reference and future climates (Future 2041-2070 – Reference 1981-2010) projected by the five different climate scenarios of the CMIP51.

Table 4.23. Annual averaged differences in selected water balance components between reference and future climate (Future 2041-2070 – Reference 1981-2010) projected by the five different climate scenarios of the CMIP51.

Hydrologic Component (mm)	Future		Reference		Difference (Fut.-Ref.)
	Mean	Std. Dev.	Mean	Std. Dev.	
Precipitation	1 189.7	10.0	1 060.1	3.3	129.6
Snow melt	133.2	3.4	161.1	1.1	-27.9
Evapotranspiration	708.4	4.5	649.1	1.1	59.3
Water Percolation	110.2	1.7	96.3	0.6	13.9
Shallow Aquifer Recharge	97.4	1.2	85.2	0.4	12.2
Deep Aquifer Recharge	12.7	0.1	11.1	0.0	1.6
Surface Runoff	194.8	3.2	173.2	1.4	21.6
Lateral Flow	12.7	0.2	28.8	3.3	-16.1
Groundwater Flow	97.4	1.1	65.8	3.1	31.7
Water Yield	467.5	6.7	401.9	2.4	65.6
Tile drainage	162.6	3.3	134.1	1.3	28.5

4.3.4 Drainage scenarios effect in future climate

From an agricultural production perspective, the earlier snowmelt projected in future climate is a potential asset. The projected increase in spring precipitations may however mitigate the benefits of an early start-up of field operations. The feasibility of controlled drainage thus remains a concern. For this last part of the hydrologic modeling exercise on the David river basin, the effects of the drainage scenarios (*Free vs No drainage*) are investigated under future climate. The main objective of this procedure is to foresee if future agri-climatic conditions will be favorable to the implementation of controlled drainage. To be clear, the principal research question addressed here is as follows: “Will future climatic conditions increase the feasibility of retaining water within the soil profile in spring and summer, without triggering the onset of surface runoff?”.

This question was addressed following the same procedure as with the historic data sets. Using the calibrated parameters of the SWAT-MAC model from the historic period, a *No drainage* scenario was applied to the overall cropped area of the David river watershed. Simulation results provided a portrait of hydrologic responses for contrasting soil types and crops, under variable projected future agri-climatic conditions (2041-2070). Table 4.24. reports the averaged annual hydrologic balance components for the David river basin for the future climate (2041-2070) period under No drainage scenario. Figure 4.31 highlights how this projected new water balance compares to the Free drainage scenario for the same future climatic period.

The effect on disconnecting the tile flow path on the total basin water yield is marginal in future's January and February months. During the spring peak flows, now happening in march, a 27 mm retention in water yield is projected, to accommodate for the 49 mm water depth that can no longer be evacuated by the tile drainage systems. The magnitude of the *No drainage* effect on water retention in March's future climate is similar to the one projected for the reference climate (-25 mm).

The most important differences of the effect of the drainage scenarios in future climate, as compared to the reference climate, are projected for the month of April. In future climate, the stream water yield is from now on marginally affected by the *No drainage* scenario (-4.5 mm on a monthly basis), since the spring flush already passed in March. In historic climate, over 45 mm of water yield in April was delayed in response to the *No drainage scenario*.

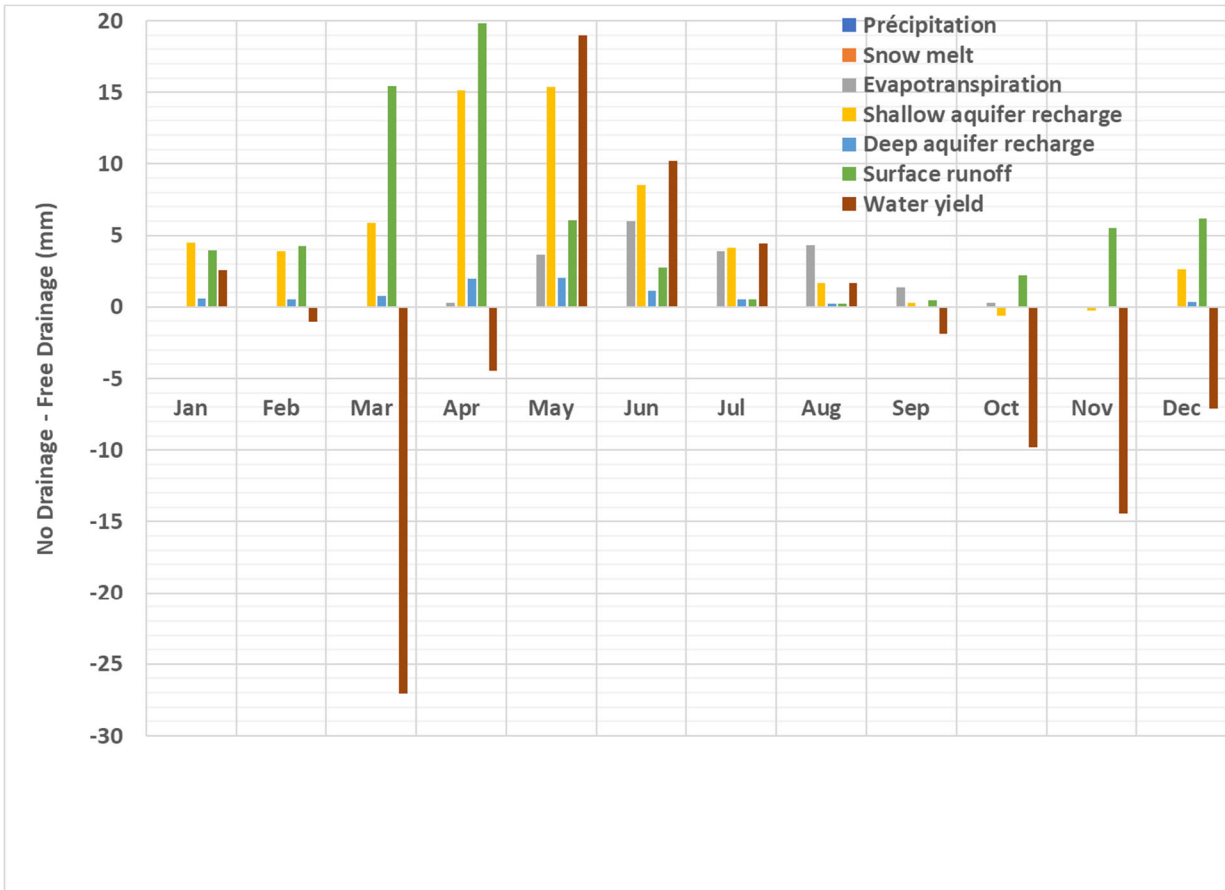


Figure 4-31. Monthly averaged differences in selected water balance components between *No drainage* and *Free drainage* scenario in future climates (Future 2041-2070 projected by the five different climate scenarios of the CMIP51.

Table 4.24. Averaged annual hydrologic balance components for the David river basin for the future climate (2041-2070) period under No drainage scenario (a) and associated monthly standard deviations (b).

a. Monthly and annual averages

Hydrologic Component (mm)	Janv	Feb	Mar	Apr	May	Jun	Aug	Jul	Sept	Oct	Nov	Dec	Total
Precipitation	106.4	84.5	82.6	99.2	92.5	103.3	92.1	92.9	97.6	115.5	117.0	106.0	1189.7
Snowmelt	1.2	10.0	69.2	51.8	0.0	0.0	0.0	0.0	0.0	0.0	0.7	0.3	133.1
Evapotranspiration	5.5	9.1	26.5	75.7	113.3	125.1	131.5	102.2	72.9	39.7	19.1	7.5	728.2
Water Percolation	14.0	11.2	36.9	56.8	20.6	5.1	1.5	0.6	0.6	3.0	10.6	18.6	179.4
Shallow Aquifer Recharge	12.4	10.4	16.3	33.8	32.9	19.2	10.3	5.1	2.5	2.0	4.1	9.8	158.6
Deep Aquifer Recharge	1.6	1.4	2.1	4.4	4.3	2.5	1.3	0.7	0.3	0.3	0.5	1.3	20.7
Surface Runoff	24.9	26.6	48.5	53.3	22.5	15.7	3.4	2.0	4.1	14.6	22.1	24.4	262.1
Lateral Flow	5.7	4.8	8.1	15.4	13.2	7.5	4.1	2.1	1.2	1.4	2.5	4.8	70.8
Groundwater Flow	7.9	6.7	9.9	21.6	22.9	13.7	7.4	3.7	1.9	1.7	3.0	6.3	106.7
Water Yield	38.5	38.1	66.6	90.4	58.6	37.0	14.9	7.7	7.1	17.6	27.5	35.6	439.5
Tile Drainage	0.0	0.0	0.0	0.0	0.0	0.0	0.0	0.0	0.0	0.0	0.0	0.0	0.0

b. Monthly standard deviations

Hydrologic Component (mm)	Janv	Feb	Mar	Apr	May	Jun	Jul	Aug	Sept	Oct	Nov	Dec
Precipitation	7.7	8.7	10.1	9.2	7.5	6.2	7.9	17.3	6.3	15.5	12.7	11.3
Snowmelt	0.6	5.3	8.3	25.6	0.0	0.0	0.0	0.0	0.0	0.0	0.7	0.1
Evapotranspiration	0.9	1.2	6.6	12.7	5.3	3.9	4.0	8.7	3.5	2.9	2.2	0.7
Water Percolation	2.0	3.4	6.6	12.3	6.1	1.8	0.6	0.3	0.3	0.6	1.1	2.4
Shallow Aquifer Recharge	1.6	1.7	3.8	3.1	6.0	4.3	2.4	1.3	0.7	0.6	0.7	0.8
Deep Aquifer Recharge	0.2	0.2	0.4	0.4	0.7	0.5	0.3	0.1	0.1	0.1	0.1	0.1
Surface Runoff	5.0	4.7	6.6	14.2	4.4	2.8	2.1	1.3	1.1	2.2	4.0	4.4
Lateral Flow	6.1	5.3	8.0	14.6	14.8	9.0	5.0	2.5	1.1	0.5	1.2	4.2
Groundwater Flow	6.2	5.3	6.8	16.4	19.0	11.6	6.2	3.0	1.3	0.6	1.4	4.3
Water Yield	4.9	5.1	8.4	16.2	8.5	6.1	4.1	2.3	1.4	2.3	4.2	4.8
Tile Drainage	0.0	0.0	0.0	0.0	0.0	0.0	0.0	0.0	0.0	0.0	0.0	0.0

Table 4.25. Annual averaged differences in selected water balance components between No Drainage – Free Drainage scenarios in future climate (2041-2070) projected by the five different climate scenarios of the CMIP51.

Hydrologic Component (mm)	Free drainage		No drainage		Difference (No -Free)
	Mean	Std. Dev.	Mean	Std. Dev.	
Precipitation	1 189.7	10.0	1 189.7	10.0	0.0
Snow melt	133.2	3.4	133.1	3.4	-0.1
Evapotranspiration	708.4	4.5	728.2	4.4	19.8
Water Percolation	110.2	1.7	179.4	3.1	69.3
Shallow Aquifer Recharge	97.4	1.2	158.6	2.2	61.2
Deep Aquifer Recharge	12.7	0.1	20.7	0.3	8.0
Surface Runoff	194.8	3.2	262.1	4.4	67.3
Lateral Flow	12.7	0.2	70.8	6.0	58.0
Groundwater Flow	97.4	1.1	106.7	6.8	9.2
Water Yield	467.5	6.7	439.5	5.7	-28.0
Tile drainage	162.6	3.3	0.0	0.0	-162.6

Notwithstanding the earlier spring snowmelt, the increase in projected surface runoff yield in April's future climate (20 mm on monthly basis) is similar to the reference climate's response to no drainage scenario. The amplitude of the *No drainage* effect on surface runoff is indebted to the projected increase in precipitation in April for the future climate scenarios. An implication of this relatively low impact of climate scenarios on projected surface runoff response to *No drainage* in April, is that that earlier implementation of controlled drainage in future climate may not be feasible.

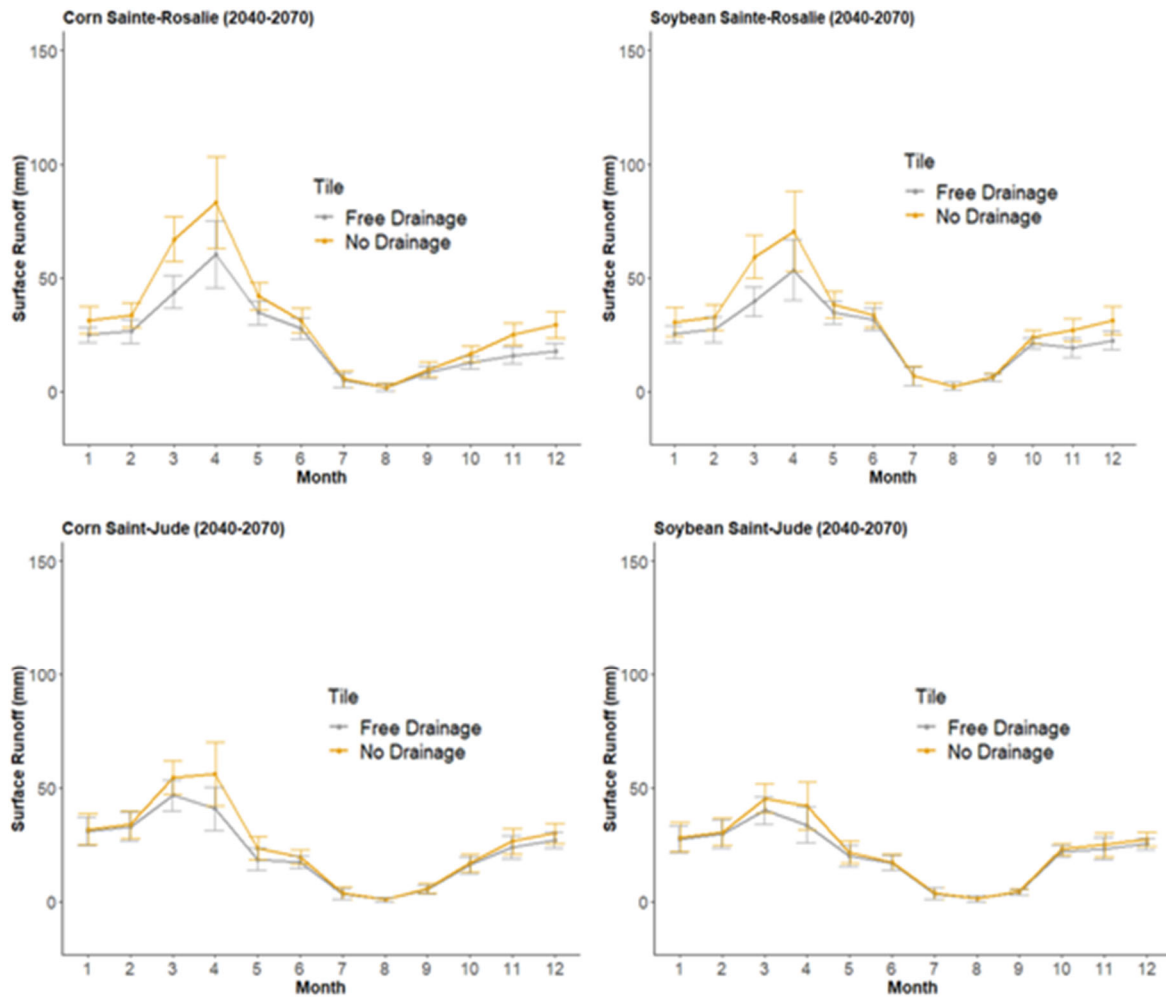


Figure 4-32. Monthly averages and standard deviation in surface runoff volumes resulting from the modeling of contrasted drainage scenarios (No Drainage - Free drainage) for corn and soybean crops cultivated on Saint-Rosalie clay and Saint-Jude sandy loam soil series for the 1985-2015 historic period.

The implications of future climate on the feasibility of controlled drainage for crop production are further detailed through the modeled outputs for corn and soybean land uses on contrasting soil types Sainte-Rosalie clay and Saint-Jude sandy loam. Figure 4.32 illustrates the surface runoff responses of the Sainte-Rosalie And Saint-Jude soil series to the drainage scenarios in future climate, following the same procedure previously applied to historic climate Comparisons with historic climate results (Figure 4.28) thus offer a direct appreciation on how future climate will influence the feasibility of controlled drainage.

Globally, the response of the contrasting soil types to drainage scenarios in future climate are similar to the ones in historic climate. In april, the increase in monthly surface runoff is still high for the Saint-Rosalie clay, but has a relatively lower amplitude than for historic climate. In may, the averaged increase in surface runoff is from now on marginal in future climate, which indicate a feasibility of tile collectors closure, without a significant risk for the clay soil. Contrasting surface runoff responses of Saint-Jude sandy loam confirms that controlled drainage feasibility remains soil type dependent in future climate. The risk of surface runoff emission is marginal in may for the sandy loam, as it was in historic climate, but april month remains at risk. In short, model projections indicate that controlled drainage is relatively more feasible in future climate, but remains risky option for early (april) implementation. If the temperature increase will trigger an earlier snowmelt in future climate, higher precipitation will also restrain the agri-environmental feasibility of controlled drainage by triggering the onset of surface runoff.

5 GENERAL CONCLUSIONS

This project examined the impacts of controlled drainage on agronomic factors and environmental quality, now and in future, using a combination of field data and modelling exercises. Studies were undertaken at multiple scales (field, small (micro) watershed and larger watershed), and this was done in both Quebec and Ontario. The outcomes of the studies were largely in agreement. In both studies, the future climate scenarios provided by OURANOS project winters with more freeze-thaw cycles, a higher frequency of rainfall and earlier snowmelts. More precipitation as rainfall in winter and early spring results in increased surface runoff rates. The simulations also project a longer growing season with warmer temperatures and greater evapotranspiration rates in future. A shift towards more sporadic, high intensity/magnitude rainfall in summer implies a more 'flashy' hydrologic cycle (termed an 'intensification' of the hydrologic cycle), where periods of drought will be interrupted by more heavy rainfall. This will lead to the potential for considerable moisture stress,

where crops may struggle to have enough water to succeed, but may also experience periods of flooding. This intensification of the hydrologic cycle will also lead to more runoff, which may result in degraded water quality. In this project, we explored whether or not controlled drainage (CD) could play a role in mitigating these issues.

Agronomic Potential of Controlled Drainage:

The Ontario studies primarily focussed on water quality. Thus, most of the findings on agronomic impacts of CD resulted from the Quebec work. The Quebec team found limited feasibility of CD due to the early drawdown of the water table following snowmelt. Water tables have already receded by the time of planting and closure of the CD structures, such that marginal benefits are given by the closure of the tiles. The monitored water table stages indicate that some retention was effective during one growing season (2017) out of three at the controlled drainage site. In fact, surface drainage, more than subsurface drainage control, was the driver of water table stage and tile flows. More water infiltrated and contributed to tile flow, for a longer period, at the free drainage site. High density (2km/km²) and deep municipal drains (over three m), systematic subsurface drainage systems (80% of cropped area) and narrow, elongated field configurations are interpreted as factors contributing to a rapid drawdown the water table in early spring, despite the closure of tile collectors.

Yield benefits on the CD site were monitored over the three growing seasons, which cannot be attributed to a controlled drainage effect. In fact, relatively lower crop yields within the free drainage site are attributed to the deficient surface drainage conditions and related, unfavorable soil physical conditions. In short, the wetter soil, despite free drainage, had lower yields. A practical implication of these observations is that surface and internal drainage are determinant drivers of the agronomic feasibility and benefits of controlled drainage.

Although not considered substantially in the Ontario studies, a limited feasibility of CD was observed in the Ontario data and also anecdotally in the field (Essex field site, M. Macrae and ERCA, unpublished data). To achieve agronomic benefit, we suggest either (a) early water stage control immediately following snowmelt (although this may impact field trafficability), combined with control of surface waters to maintain water levels in adjacent streams, which calls for concerted actions at the micro-watershed scale to enhance/permit effective water tables in the field. This will become more pertinent in future due to increased moisture stress. However, it is noted that agronomic benefits such as this may be at the expense of water quality. **Environmental Potential of Controlled Drainage:**

As has been observed in previous watershed and edge-of-field studies, the timing of the nutrient flux is concentrated during the March/April snowmelt period but may also occur during autumn

recharge and occasional mild winter spells (more frequent at the Ontario sites than the Quebec sites). With regards to the loss of P in tile drainage, the various sites yielded different results. There was evidence of preferential transport through macropores into tile drains at the flat clay sites (Yamaska sites in Quebec), where tile flow rate and flow-dependent P concentrations in tile water were the dominant drivers of sediment and P exports, which reached up to 688 kg/ha-yr in TSS and 0.87 kg/ha-yr in total phosphorus. Considering annual loadings were within the 1.0 kg P/ha range documented for the micro-watershed, P export from the drainage tiles likely accounts for most of the P transferred from the field to the stream within the study region. From a land and river stewardship perspective, the effective reduction of P loadings to the stream thus calls for mitigations measures on subsurface P transfers, together with surface runoff abatement.

The Ontario field site (Londesborough) did not demonstrate significant potential for P loss in tile drains in a clay loam. Sediment loading, P loss and the speciation between DRP and PP was dependent on flow conditions, where greater concentrations of all were observed under high flow conditions, and the DRP:PP ratio was lower under such conditions. This is indicative of the dominance of subsurface particulate transport processes, presumably triggered by macropores connectivity to tiles.

Given the significant preferential flow at the Yamaska sites, the Quebec team found that there was potential for CD to reduce P fluxes by limiting the rapid macropore flow that carries the most significant P loads, as long as surface runoff was not exacerbated. The hydrologic modeling results indicate that this feasibility is soil type dependent. In contrast, given the significant differences in P concentrations between surface runoff and tile drainage at the Londesborough sites, the Ontario team found that CD would increase P loads from the Londesborough site by increasing overland flow from the site.

Our results suggest that maintaining a water table stage above drains during critical periods has potential to reduce macropore connectivity and reduce the fluxes of water, sediment and nutrients, although this is at clay sites that are more prone to macropore flow. However, in CD management, we must avoid having the CD accompanied by an increase in surface runoff, as this is a significant trade-off that may be associated with CD. Our results demonstrate that the increased surface runoff caused by CD may considerably increase P loss. A possible solution to this is the use of "Precision drainage management", where drains are controlled in a site-specific way that maintains the water table (and associated nutrient fluxes) as long as possible to limit subsurface nutrient exports, and provide moisture stress abatement benefits, but, drains are opened if surface runoff may potentially occur.

Impacts of Climate Change on Runoff and Nutrient Fluxes and the Potential for Drainage Control to Regulate Impacts of These Changes:

As noted above, the challenge associated with climate change will be a temperature and precipitation gradient, with higher precipitation earlier in spring, and with warmer temperatures in spring and summer that may lead to higher moisture stress. Given the wetter winter and flashier summer hydrologic cycles that are projected, there is increased potential for nutrient loss due to increased peak flow conditions.

With regards to the feasibility/efficiency of CD, the greater spring precipitation that is expected under future climates limits the feasibility of the use of CD, as water table control must accommodate the management of a higher water subsurface yield without exacerbating surface runoff. It is likely that the use of CD in spring will be accompanied by increased surface runoff. Although it may be possible to only employ CD in the summer months, when less surface runoff is anticipated, this period is not the primary period for nutrient loss and thus, CD will ultimately have little effect on mitigating nutrient losses during this time.

Perspectives:

This joint project has used a combination of observational and modelling approaches to examine the impacts of climate change on nutrient transport and the potential for controlled drainage to mitigate nutrient losses both now and in future. The studies have shown that the anticipated intensification of the hydrologic cycle will lead to more moisture stress in future, but CD is unlikely to mitigate this unless it can be employed earlier in the season than it currently is. However, the use of CD during the early spring, or throughout the non-growing season is problematic as it exacerbates water quality issues due to the increases in surface runoff that it causes. This is the case now and will continue to be the case in future. However, these findings are based on how CD is currently used (manual closures). If the technology of CD can be advanced to allow “precision management” of tile drains (where tiles are opened or closed based on critical water table stages that vary seasonally), there may be more potential for the use of CD as it may offset moisture stress without enhancing surface runoff.

REFERENCES CITED

- Abbaspour, K. C. (2015). *SWAT - CUP: SWAT Calibration and Uncertainty Programs-A User Manual*. Eawag: Swiss Federal Institute of Aquatic Science and Technology.
- Abbaspour, K. C., Rouholahnejad, E., Vaghefi, S., Srinivasan, R., Yang, H., & Kløve, B. (2015). A continental-scale hydrology and water quality model for Europe: Calibration and uncertainty

- of a high-resolution large-scale SWAT model. *Journal of Hydrology*, 524, 733–752. <http://doi.org/10.1016/j.jhydrol.2015.03.027>
- Abbaspour, K. C., Yang, J., Maximov, I., Siber, R., Bogner, K., Mieleitner, J., ... Srinivasan, R. (2007). Modelling hydrology and water quality in the pre-alpine/alpine Thur watershed using SWAT. *Journal of Hydrology*, 333(2–4), 413–430. <http://doi.org/10.1016/j.jhydrol.2006.09.014>
- Agriculture and Agri-Food Canada. (2016). *Annual Crop Inventory 2014*. [Data file]. Retrieved from <https://open.canada.ca/data/en/dataset/ae61f47e-8bcb-47c1-b438-8081601fa8fe>
- Agriculture and Agri-Food Canada, (2013). WEB program, In line. / Eastman, M., et al. 2010. *Agricultural Water Management* 97:596-604.
- Ahmadi, M., Records, R., & Arabi, M. (2014). Impact of climate change on diffuse pollutant fluxes at the watershed scale. *Hydrological Processes*, 28(4), 1962–1972. <http://doi.org/10.1002/hyp.9723>
- Ale, S., Bowling, L. C., Youssef, M. A., & Brouder, S. M. (2012). Evaluation of Simulated Strategies for Reducing Nitrate–Nitrogen Losses through Subsurface Drainage Systems. *Journal of Environmental Quality*, 41(1), 217. <http://doi.org/10.2134/jeq2010.0466>
- Alexander, C. (1988). *ADAPT—A model to simulate pesticide movement into drain tiles* (Master's thesis). Retrieved from https://etd.ohiolink.edu/!etd.send_file?accession=osu1145373108&disposition=inline
- Andreini, M. S., & Steenhuis, T.S. (1990). Preferential paths of flow under conventional and conservation tillage. *Geoderma*, 46, 85-102. [http://doi.org/10.1016/0016-7061\(90\)90009-X](http://doi.org/10.1016/0016-7061(90)90009-X)
- Arbuckle, K. E., & Downing, J. A. (2001). The influence land use on lake N : P in a predominantly of watershed agricultural landscape. *Limnology and Oceanography*, 46(4), 970–975.
- Ardón, M., Montanari, S., Morse, J. L., Doyle, M. W., & Bernhardt, E. S. (2010). Phosphorus export from a restored wetland ecosystem in response to natural and experimental hydrologic fluctuations. *Journal of Geophysical Research: Biogeosciences*, 115, 1–12. <http://doi.org/10.1029/2009JG001169>
- Arenas Amado, A., Schilling, K. E., Jones, C. S., Thomas, N., & Weber, L. J. (2017). Estimation of tile drainage contribution to streamflow and nutrient loads at the watershed scale based on

continuously monitored data. *Environmental Monitoring and Assessment*, 189(9).
<http://doi.org/10.1007/s10661-017-6139-4>

Arnold, J. G., Kiniry, J. R., Srinivasan, R., Williams, J. R., Haney, E. B., & Neitsch, S. L. (2012a). *Soil and Water Assessment Tool: Input/Output Documentation, version 2012*.

Arnold, J. G., Moriasi, D. N., Gassman, P. W., Abbaspour, K. C., White, M. J., Srinivasan, R., ... Jha, M. K. (2012b). SWAT: Model Use, Calibration, and Validation. *American Society of Agricultural and Biological Engineers*, 55(4), 1491–1508.

Arnold, J. G., Youssef, M. A., Yen, H., Sheshukov, A. Y., Sadeghi, A. M., Moriasi, D. N., ... Gowda, P. H. (2015). Hydrological Processes and Model Representation: Impact of Soft Data on Calibration. *American Society of Agricultural and Biological Engineers*, 58(6), 1637–1660.
<http://doi.org/10.13031/trans.58.10726>

Ball Coelho, B., Murray, R., Lapen, D., Topp, E., & Bruin, A. (2012). Phosphorus and sediment loading to surface waters from liquid swine manure application under different drainage and tillage practices. *Agricultural Water Management*, 104, 51–61.
<http://doi.org/10.1016/j.agwat.2011.10.020>

Barnard, R., Leadley, P. W., & Hungate, B. A. (2005). Global change, nitrification, and denitrification: A review. *Global Biogeochemical Cycles*, 19(GB1007), 1–13.
<http://doi.org/10.1029/2004GB002282>

Bauwe, A., Kahle, P., & Lennartz, B. (2016). Hydrologic evaluation of the curve number and Green and Ampt infiltration methods by applying Hooghoudt and Kirkham tile drain equations using SWAT. *Journal of Hydrology*, 537, 311–321. <http://doi.org/10.1016/j.jhydrol.2016.03.054>

Beauchemin, S., Simard, R. R., & Cluis, D. (1998). Forms and Concentration of Phosphorus in Drainage Water of Twenty-Seven Tile-Drained Soils. *Journal of Environment Quality*, 27(3), 721. <http://doi.org/10.2134/jeq1998.00472425002700030033x>

Bengtson, R. L., Carter, C. E., Fouss, J.L., Southwick, L.M., & Willis, G.H. (1995). Agricultural drainage and water quality in the Mississippi delta. *Journal of Irrigation and Drainage Engineering*, 121(4), 292–295. [http://doi.org/10.1061/\(ASCE\)0733-9437\(1995\)121:4\(292\)](http://doi.org/10.1061/(ASCE)0733-9437(1995)121:4(292))

Beven, K. (2001). *Rainfall-runoff modelling: The primer. Benchmark papers in hydrology*. Chichester, U.K.: John Wiley and Sons.

- Beven, K. (2006). A manifesto for the equifinality thesis. *Journal of Hydrology*, 320(1–2), 18–36.
<http://doi.org/10.1016/j.jhydrol.2005.07.007>
- Beven, K., & Binley, A. M. (1992). The future of distributed models: model calibration and uncertainty estimation. *Hydrological Processes*, 6, 279–298.
- Bingham, M., Sinha, S. K., & Lupi, F. (2015). *Economic benefits of reducing harmful algal blooms in Lake Erie*. Retrieved from <http://ijc.org/files/tinymce/uploaded/Publications/Economic-Benefits-Due-to-Reduction-in-HABs-October-2015.pdf>
- Bohne, B., Storchenegger, I. J., & Widmoser, P. (2012). An easy to use calculation method for weir operations in controlled drainage systems. *Agricultural Water Management*, 109, 46–53.
<http://doi.org/10.1016/j.agwat.2012.02.005>
- Bolster, C. H., & Sistani, K. R. (2009). Sorption of phosphorus from swine, dairy, and poultry manures. *Communications in Soil Science and Plant Analysis*, 40(7–8), 1106–1123.
<http://doi.org/10.1080/00103620902753822>
- Bolton, E. F., Aylesworth, J. W., & Hore, F. R. (1970). Nutrient losses through tilled rains under three cropping systems and two fertility levels on a Brookston clay soil. *Canadian Journal of Soil Science*, 50, 275–279. <http://doi.org/10.4141/cjss70-038>
- [Bosch, N. S., Evans, M. A., Scavia, D., & Allan, J. D. \(2014\). Interacting effects of climate change and agricultural BMPs on nutrient runoff entering Lake Erie. *Journal of Great Lakes Research*, 40\(3\), 581–589. <http://doi.org/10.1016/j.jglr.2014.04.011>](http://doi.org/10.1016/j.jglr.2014.04.011)
- Boyer, C., D. Chaumont, I. Chartier, and A.G. Roy. 2010. Impact of climate change on the hydrology of St. Lawrence tributaries. *Journal of Hydrology* 384(1-2): 65-83.
- Braun, M. 2017. Personal communication. OURANOS. Climate scenarios and services group.
- Boström, B. (1984). Potential Mobility of Phosphorus in Different Types of Lake Sediment. *Internationale Revue Der Gesamten Hydrobiologie Und Hydrographie*, 69(4), 457–474.
<http://doi.org/10.1002/iroh.19840690402>
- Carpenter, S. R., Caraco, N. F., Correll, D. L., Howarth, R. W., Sharpley, A. N., & Smith, V. H. (1998). Nonpoint pollution of surface waters with phosphorus and nitrogen. *Ecological Applications*, 8(3), 559–568.

- Carter, T. R., Parry, M. L., Harasawa, H., & Nishioka, S. (1994). *IPCC technical guidelines for assessing climate change impacts and adaptations*. London, United Kingdom: University College and Center for Global Environmental Research.
- Casajus, N., Périé, C., Logan, T., Lambert, M.-C., De Bois, S., & Berteaux, D. (2016). An Objective Approach to Select Climate Scenarios when Projecting Species Distribution under Climate Change. *PLOS ONE*, *11*(3), 1–17. <http://doi.org/10.1371/journal.pone.0152495>
- Chan-Hilton, A. B., & Culver, T. B. (2000). Constraint Handling for Genetic Algorithms in Optimal Remediation Design. *Journal of Water Resources Planning and Management*, *126*(3), 128–137. <http://doi.org/http://dx.doi.org/10.1061>
- Chapi, K., Rudra, R. P., Ahmed, S. I., Khan, A. A., Gharabaghi, B., Dickinson, W. T., & Goel, P. K. (2015). Spatial-Temporal Dynamics of Runoff Generation Areas in a Small Agricultural Watershed in Southern Ontario. *Water Resource and Protection*, *7*(January), 14–40. <http://doi.org/10.4236/jwarp.2015.71002>
- Chen, J., Brissette, F. P., & Lucas-Picher, P. (2015). Assessing the limits of bias-correcting climate model outputs for climate change impact studies. *Journal of Geophysical Research: Atmospheres*, *120*(3), 1123–1136. <http://doi.org/10.1002/2014JD022635>
- Coelho, B., Murray, R., Lapen, D., Topp, E., & Bruin, A. (2012). Phosphorus and sediment loading to surface waters from liquid swine manure application under different drainage and tillage practices. *Agricultural Water Management*, *104*, 51–61. <http://doi.org/10.1016/j.agwat.2011.10.020>
- Columbo, S. J., McKenney, D. W., Lawrence, K. M., & Gray, P. a. (2007). *Climate Change Projections for Ontario : Policymakers and Planners*.
- Correll, D. L. (1998). The Role of Phosphorus in the Eutrophication of Receiving Waters: A Review. *Journal of Environmental Quality*, *27*, 261-266. doi:10.2134/jeq1998.00472425002700020004x
- Cousino, L. K., Becker, R. H., & Zmijewski, K. A. (2015). Modeling the Effects of Climate Change on Water, Sediment, and Nutrient Yields from the Maumee River Watershed. *Journal of Hydrology: Regional Studies*, *4*, 762–775. <http://doi.org/10.1016/j.ejrh.2015.12.039>
- Crabbé, P., Lapen, D. R., Clark, H., Sunohara, M., & Liu, Y. (2012). Economic benefits of controlled tile drainage: Watershed Evaluation of Beneficial Management Practices, South Nation River

basin, Ontario. *Water Quality Research Journal of Canada*, 47(1), 30–41.
<http://doi.org/10.2166/wqrjc.2012.007>

Crossman, J., Futter, M. N., Oni, S. K., Whitehead, P. G., Jin, L., Butterfield, D., ... Dillon, P. J. (2013). Impacts of climate change on hydrology and water quality: Future proofing management strategies in the Lake Simcoe watershed, Canada. *Journal of Great Lakes Research*, 39, 19–32. <http://doi.org/10.1016/j.jglr.2012.11.003>

Daggupati, P., Pai, N., Ale, S., Zeckoski, R. W., Jeong, J., Parajuli, P. B., ... Youssef, M. A. (2015). A Recommended Calibration and Validation Strategy for Hydrologic and Water Quality Models. *Transactions of the ASABE*, 58(6), 1705–1719.
<http://doi.org/10.13031/trans.58.10712>

Daloğlu, I., Cho, K. H., & Scavia, D. (2012). Evaluating causes of trends in long-term dissolved reactive phosphorus loads to Lake Erie. *Environmental Science and Technology*, 46(19), 10660–10666. <http://doi.org/10.1021/es302315d>

Daly, K., Jeffrey, D., & Tunney, H. (2001). The effect of soil type on phosphorus sorption capacity and desorption dynamics in Irish grassland soils. *Soil Use and Management*, 17, 12-20.
<http://doi.org/10.1111/j.1475-2743.2001.tb00003.x>

Delmotte, S., Jegou and R. Morissette. 2017. Analyse des scénarios climatiques fournis par Ouranos dans le cadre du projet RADEAU. Communication personnelle.

Demaria, E. M. C., Roundy, J. K., Wi, S., & Palmer, R. N. (2016). The effects of climate change on seasonal snowpack and the hydrology of the Northeastern and Upper Midwest United States. *American Meteorological Society*, 29, 6527–6541. <http://doi.org/10.1175/JCLI-D-15-0632.1>

Deslandes, J., I. Beaudin, A. Michaud, F. Bonn, and C.A. Madramootoo. 2007. Influence of Landscape and Cropping System on Phosphorus Mobility within the Pike River Watershed of Southwestern Quebec: Model Parameterization and Validation. *Canadian Water Resources Journal* 32:24-42.

Diaz, R. J. (2001). Overview of Hypoxia around the World. *Journal of Environment Quality*, 30(2), 275. <http://doi.org/10.2134/jeq2001.302275x>

Dils, R. M., & Heathwaite, A. L. (1999). The controversial role of tile drainage in phosphorus export from agricultural land. *Water Science and Technology*, 39(12), 55–61.
[http://doi.org/10.1016/S0273-1223\(99\)00318-2](http://doi.org/10.1016/S0273-1223(99)00318-2)

http://climate.weather.gc.ca/climate_normals/results_1981_2010_e.html?searchType=stnProv&lstProvince=&txtCentralLatMin=0&txtCentralLatSec=0&txtCentralLongMin=0&txtCentralLongSec=0&stnID=4545&dispBack=0

Environment and Climate Change Canada. (2018b). *Historical Data*. [Data file]. Retrieved from http://climate.weather.gc.ca/historical_data/search_historic_data_e.html

Environmental Protection Agency (2015). *Recommended Phosphorus Loading Targets for Lake Erie: Annex 4 Objectives and Targets Task Team Final Report to the Nutrients Annex Subcommittee*. Retrieved from <https://www.epa.gov/sites/production/files/2015-06/documents/report-recommended-phosphorus-loading-targets-lake-erie-201505.pdf>

Fang, Q.X., et al. 2012. *Agricultural Water Management*. 103:150-161.

Fertilizer Canada (2016). *4R Nutrient Stewardship in Ontario*. Retrieved from <https://fertilizercanada.ca/wp-content/uploads/2017/01/Ontario-2016-Report.pdf>

Fleming, R., Macalpine, M., & Tiffin, C. (1998). Nitrate levels in soil, tile drainage water and shallow groundwater under a variety of farm management systems. *Canadian Society for Engineering in Agricultural Food, and Biological Systems*, 98–101, 1–10.

Fowler, H. J., Blenkinsop, S., & Tebaldi, C. (2007). Linking climate change modelling to impacts studies: recent advances in downscaling techniques for hydrological modelling. *International Journal of Climatology*, 27, 1547–1578. <http://doi.org/10.1002/joc.1556>

Fox, R. L., & Kamprath, E. J. (1970). Phosphate Sorption Isotherms for Evaluating the Phosphate Requirements of Soils. *Soil Science Society of America Journal*, 34, 902-907. <http://doi.org/10.2136/sssaj1970.03615995003400060025x>

Fraser, H., & Fleming, R. (2001). *Environmental Benefits of Tile Drainage - Literature Review*. Ridgetown, Ontario.

Gaines, T. P., & Gaines, S. T. (2008) Soil texture effect on nitrate leaching in soil percolates. *Communications in Soil Science and Plant Analysis*, 25(13-14), 2561-2570, <http://doi.org/10.1080/00103629409369207>

Gao, L., & Li, D. (2014). A review of hydrological/water-quality models. *Frontiers of Agricultural Science and Engineering*, 1(4), 267–276. <http://doi.org/10.15302/J-FASE-2014041>

- Gaynor, J. D., & Findlay, W. I. (1995). Soil and Phosphorus Loss from Conservation and Conventional Tillage in Corn Production. *Journal of Environmental Quality*, 24, 734-741. <http://doi.org/10.2134/jeq1995.00472425002400040026x>
- Gentry, L. E., David, M. B., Below, F. E., Royer, T. V., & McIsaac, G. F. (2009). Nitrogen Mass Balance of a Tile-drained Agricultural Watershed in East-Central Illinois. *Journal of Environmental Quality*, 38, 1841-1847. <http://doi.org/10.2134/jeq2008.0406>
- Gentry, L. E., David, M. B., Royer, T. V., Mitchell, C. A., & Starks, K. M. (2007). Phosphorus Transport Pathways to Streams in Tile-Drained Agricultural Watersheds. *Journal of Environment Quality*, 36(2), 408. <http://doi.org/10.2134/jeq2006.0098>
- Giroux, M., et al. (2008). *Agrosolutions* 19(1) :Pp 4-14.
- Geohring, L. D., McHugh, O. V., Walter, M. T., Steenhuis, T. S., Akhtar, M. S., & Walter, M. F. (2001). Phosphorus transport into subsurface drains by macropores after manure applications: Implications for best manure management practices. *Soil Science*, 166(12), 896–909. <http://doi.org/10.1097/00010694-200112000-00004>
- George, T. S., Giles, C. D., Menezes-Blackburn, D., Condrón, L. M., Gama-Rodrigues, A. C., Jaisi, D., ... Haygarth, P. M. (2017). Organic phosphorus in the terrestrial environment: a perspective on the state of the art and future priorities. *Plant Soil*, 1–18. <http://doi.org/10.1007/s11104-017-3391-x>
- Giorgi, F. (2010). Uncertainties in climate change projections, from the global to the regional scale. *EPJ Web of Conferences*, 9, 115–129.
- Golmohammadi, G., Prasher, S., Madani, A., Rudra, R., & Youssef, M. A. (2016a). SWATDRAIN, a new model to simulate the hydrology of agricultural Lands, model development and evaluation. *Biosystems Engineering*, 141, 31–47. <http://doi.org/10.1016/j.biosystemseng.2015.11.003>
- Golmohammadi, G., Rudra, R., Prasher, S., Madani, A., Goel, P., & Mohammadi, K. (2016b). Modeling the effects of controlled drainage at a watershed scale using SWATDRAIN. *Arabian Journal of Geosciences*, 9(11). <http://doi.org/10.1007/s12517-016-2608-2>
- Golmohammadi, G., Rudra, R., Prasher, S., Madani, A., Mohammadi, K., Goel, P., & Daggupatti, P. (2017). Water Budget in a Tile Drained Watershed under Future Climate Change Using SWATDRAIN Model. *Climate*, 5(39), 1–12. <http://doi.org/10.3390/cli5020039>

- Gombault, C., M.F.Sottile, F. Ngwa, C.A. Madramootoo, A.R. Michaud, I.Beaudin, M. Chikhaoui. 2015a. Modelling climate change impacts on the hydrology of an agricultural watershed in southern Québec. *Canadian Water Resources Journal / Revue canadienne des ressources hydriques*, 1–16.
- Gombault, C., Madramootoo, C. A., Michaud, A., Beaudin, I., Sottile, M. F., Chikhaoui, M., & Ngwa, F. 2015b. Impacts of climate change on nutrient losses from the Pike River watershed of southern Québec. *Canadian Journal of Soil Science*, 95, 337–358. <http://doi.org/10.4141/CJSS-2014-012>
- Goss, M. J., Barry, D. A. J., & Rudolph, D. L. (1998). Contamination in Ontario farmstead domestic wells and its association with agriculture: 1. Results from drinking water wells. *Journal of Contaminant Hydrology*, 32(3–4), 267–293. [http://doi.org/10.1016/S0169-7722\(98\)00054-0](http://doi.org/10.1016/S0169-7722(98)00054-0)
- Greenberg, E.A., L.S. Clesceri et A.D. Eaton. 1992a. Total Suspended Solids Dried at 103-105oC. Standard method for examination of waste and waster water, 18th edition, pp 2-56.
- Greenberg, E.A., L.S. Clesceri et A.D. Eaton. 1992b. Persulfate Digestion Method. Standard method for examination of waste and waster water, 18th edition, pp 4-112.
- Greenberg, A.E., S. Lenore et S. Clesceri. 1992c. No: 4500-NH3 H. Automated Phenate Method, p. 4-84; No: 4500-NO3- F. Automated Cadmium Reduction Method, p. 4-84, In E. A.D., ed. Standard Methods For Examination of Waste and Waste Water, 18th Edition ed. Corporation Tarrytown, N.Y. 10591.
- Grillakis, M. G., Koutroulis, A. G., & Tsanis, I. K. (2011). Climate change impact on the hydrology of Spencer Creek watershed in Southern Ontario, Canada. *Journal of Hydrology*, 409(1–2), 1–19. <http://doi.org/10.1016/j.jhydrol.2011.06.018>
- Guo, T., Gitau, M., Merwade, V., Arnold, J., Srinivasan, R., Hirschi, M., & Engel, B. (2018). Comparison of performance of tile drainage routines in SWAT 2009 and 2012 in an extensively tile-drained watershed in the Midwest. *Hydrology and Earth System Sciences*, 22(1), 89–110. <http://doi.org/10.5194/hess-22-89-2018>
- Gupta, V. H., Sorooshian, S., & Yapo, P. O. (1999). Status of automatic calibration for hydrologic models: Comparison with multilevel expert calibration. *Journal of Hydrologic Engineering*, 4(2), 135–143.

- Hart, M. R., Quin, B. F., & Nguyen, M. L. (2004). Phosphorus Runoff from Agricultural Land and Direct Fertilizer Effects. *Journal of Environment Quality*, 33(6), 1954–1951. <http://doi.org/10.2134/jeq2004.1954>
- Haygarth, P. M., Hepworth, L., & Jarvis, S. C. (1998). Forms of phosphorus transfer in hydrological pathways from soil under grazed grassland. *European Journal of Soil Science*, 49(1), 65–72. <http://doi.org/10.1046/j.1365-2389.1998.00131.x>
- Heisler, J., Glibert, P., Burkholder, J., Anderson, D., Cochlan, W., Dennison, W., ... Suddleson, M. (2008). Eutrophication and harmful algal blooms: A scientific consensus. *Harmful Algae*, 8(1), 3–13. <http://doi.org/10.1016/j.hal.2008.08.006>
- Henry, H. a L. (2008). Climate change and soil freezing dynamics: Historical trends and projected changes. *Climatic Change*, 87(3–4), 421–434. <http://doi.org/10.1007/s10584-007-9322-8>
- Honti, M., Scheidegger, A., & Stamm, C. (2014). The importance of hydrological uncertainty assessment methods in climate change impact studies. *Hydrology and Earth System Sciences*, 18, 3301–3317. <http://doi.org/10.5194/hess-18-3301-2014>
- Hooghoudt, S.B. (1940). Contributions to the knowledge of some physical constants of the soil. *Report Agric. Res*, 46, 515–707.
- Ikenberry, C. D., Soupir, M. L., Helmers, M. J., Crumpton, W. G., Arnold, J. G., & Gassman, P. W. (2017). Simulation of Daily Flow Pathways, Tile-Drain Nitrate Concentrations, and Soil-Nitrogen Dynamics Using SWAT. *Journal of the American Water Resources Association*, 53(6), 1251–1266. <http://doi.org/10.1111/1752-1688.12569>
- Intergovernmental Panel on Climate Change. (2015). *Climate Change 2014: Synthesis Report*. Geneva, Switzerland.
- International Joint Commission (IJC) (2012). *Great Lakes Water Quality Agreement*. Retrieved from <http://ijc.org/files/tinymce/uploaded/GLWQA%202012.pdf>
- Irwin, R. W. (1977). Economics of Farm Drainage in Ontario. *Canadian Water Resources Journal*, 2(2), 62–73. <http://doi.org/10.4296/cwrj0202062>
- Isard, S. A., & Schaetzl, R. J. (1998). Effects of Winter Weather Conditions on Soil Freezing in Southern Michigan. *Physical Geography*, 19(1), 71–94.

- Jarvie, H. P., Sharpley, A. N., Withers, P. J. A., Scott, J. T., Haggard, B. E., & Neal, C. (2013). Phosphorus Mitigation to Control River Eutrophication: Murky Waters, Inconvenient Truths, and “Postnormal” Science. *Journal of Environment Quality*, 42(2), 295. <http://doi.org/10.2134/jeq2012.0085>
- Jiao, P., Xu, D., Wang, S., Wang, Y., Liu, K., & Tang, G. (2012). Nitrogen loss by surface runoff from different cropping systems. *Soil Research*, 50(1), 58–66. <http://doi.org/10.1071/SR11152>
- Jyrkama, M. I., & Sykes, J. F. (2007). The impact of climate change on spatially varying groundwater recharge in the Grand River watershed (Ontario). *Journal of Hydrology*, 338(3–4), 237–250. <http://doi.org/10.1016/j.jhydrol.2007.02.036>
- Kaluli, J., et al. *Journal of Irrigation and Drainage Engineering*, 125(2), 52-58.
- Karmakar, R., Das, I., Dutta, D., & Raksh, A. (2016). Potential effects of climate change on soil properties: A review. *Science International*, 4, 51-73.
- King, K. W., Williams, M. R., Macrae, M. L., Fausey, N. R., Frankenberger, J., Smith, D. R., ... Brown, L. C. (2015). Phosphorus Transport in Agricultural Subsurface Drainage: A Review. *Journal of Environment Quality*, 44(2), 467–485. <http://doi.org/10.2134/jeq2014.04.0163>
- King, L. M., Irwin, S., Sarwar, R., McLoed, I. A., & Simonovic, P. (2012). The effects of climate change on extreme precipitation events in the Upper Thames River Basin: A comparison of downscaling approaches. *Canadian Water Resources Journal*, 37(3), 253–274.
- Kirkham, D. (1957). Theory of land drainage. In *Drainage of Agricultural Lands, Agronomy Monograph 7* (pp. 79-285). Madison, WI: American Society of Agronomy.
- Kleinman, P. J. A., Sharpley, A. N., Saporito, L. S., Buda, A. R., & Bryant, R. B. (2009). Application of manure to no-till soils: phosphorus losses by sub-surface and surface pathways. *Nutrient Cycling in Agroecosystems*, 84(3), 215–227. <http://doi.org/10.1007/s10705-008-9238-3>
- Kung, K.-J. S., Steenhuis, T. S., Kladvik, E. J., Gish, T. J., Bubenzer, G., & Helling, C. S. (2000). Impact of Preferential Flow on the Transport of Adsorbing and Non-Adsorbing Tracers. *Soil Science Society of America Journal*, 64(4), 1290. <http://doi.org/10.2136/sssaj2000.6441290x>
- Labeau, M. B., Mayer, A., Griffis, V., Watkins, D., Robertson, D., & Gyawali, R. (2015). The importance of considering shifts in seasonal changes in discharges when predicting future

phosphorus loads in streams. *Biogeochemistry*, 126(1–2), 153–172.
<http://doi.org/10.1007/s10533-015-0149-5>

Labeau, M. B., Robertson, D. M., Mayer, A. S., Pijanowski, B. C., & Saad, D. A. (2014). Effects of future urban and biofuel crop expansions on the riverine export of phosphorus to the Laurentian Great Lakes. *Ecological Modelling*, 277, 27–37.
<http://doi.org/10.1016/j.ecolmodel.2014.01.016>

Lalonde, V., Madramootoo, C. A., Trenholm, L., & Broughton, R. S. (1996). Effects of controlled drainage on nitrate concentrations in subsurface drain discharge. *Agricultural Water Management*, 29(2), 187–199. [http://doi.org/10.1016/0378-3774\(95\)01193-5](http://doi.org/10.1016/0378-3774(95)01193-5)

Lam, W. V., Macrae, M. L., English, M. C., O'Halloran, I. P., Plach, J. M., & Wang, Y. (2016). Seasonal and event-based drivers of runoff and phosphorus export through agricultural tile drains under sandy loam soil in a cool temperate region. *Hydrological Processes*, 30(15), 2644–2656. <http://doi.org/10.1002/hyp.10871>

Lavaire, T., Gentry, L. E., David, M. B., & Cooke, R. A. (2017). Fate of water and nitrate using drainage water management on tile systems in east-central Illinois. *Agricultural Water Management*, 191, 218–228. <http://doi.org/10.1016/j.agwat.2017.06.004>

Leytem, A. B., Mikkelsen, R. L., & Gilliam, J. W. (2002). Sorption of Organic Phosphorus Compounds in Atlantic Coastal Plain Soils. *Soil Science*, 167(10), 652–658.

Li, H., Sivapalan, M., Tian, F., & Liu, D. (2010). Water and nutrient balances in a large tile-drained agricultural catchment: A distributed modeling study. *Hydrology and Earth System Sciences*, 14(11), 2259–2275. <http://doi.org/10.5194/hess-14-2259-2010>

Li, X., Wang, B., Yang, T., Zhu, D., Nie, Z., & Xu, J. (2017). Identification of soil P fractions that are associated with P loss from surface runoff under various cropping systems and fertilizer rates on sloped farmland. *PLoS ONE*, 12(6), 1–16. <http://doi.org/10.1371/journal.pone.0179275>

Li, Z., Huang, G., Huang, W., Lin, Q., & Liao, R. (2017). Future changes of temperature and heat waves in Ontario, Canada. *Theoretical and Applied Climatology*, 1–10.
<http://doi.org/10.1007/s00704-017-2123-8>

Lilienfein, J., Qualls, R. G., Uselman, S. M., & Bridgham, S. D. (2004). Adsorption of Dissolved Organic and Inorganic Phosphorus in Soils of a Weathering Chronosequence. *Soil Science Society of America Journal*, 68(2), 620–628. <http://doi.org/10.2136/sssaj2004.6200>

- Liu, Y., Yang, W., Leon, L., Wong, I., Mccrimmon, C., Dove, A., & Fong, P. (2016). Hydrologic modeling and evaluation of Best Management Practice scenarios for the Grand River watershed in Southern Ontario. *Journal of Great Lakes Research*, 42(6), 1289–1301. <http://doi.org/10.1016/j.jglr.2016.02.008>
- Ludsin, S. A., Kershner, M. W., Blocksom, K. A., Knight, R. L., & Stein, A. (2013). Life After Death in Lake Erie: Nutrient Controls Drive Fish Species Richness, Rehabilitation. *Ecological Applications*, 11(3), 731–746. [http://doi.org/10.1890/1051-0761\(2001\)011](http://doi.org/10.1890/1051-0761(2001)011)
- Luo, L., Lin, H., & Li, S. (2010). Quantification of 3-D soil macropore networks in different soil types and land uses using computed tomography. *Journal of Hydrology*, 393(1–2), 53–64. <http://doi.org/10.1016/j.jhydrol.2010.03.031>
- Macrae, M.L. (2003). PhD Thesis, Wilfrid Laurier University.
- Macrae, M. L., English, M. C., Schiff, S. L., & Stone, M. (2007a). Intra-annual variability in the contribution of tile drains to basin discharge and phosphorus export in a first-order agricultural catchment. *Agricultural Water Management*, 92(3), 171–182. <http://doi.org/10.1016/j.agwat.2007.05.015>
- Macrae, M. L., English, M. C., Schiff, S. L., & Stone, M. (2007b). Capturing temporal variability for estimates of annual hydrochemical export from a first-order agricultural catchment in southern Ontario, Canada. *Hydrological Processes*, 1663(December 2006), 1651–1663. <http://doi.org/10.1002/hyp>
- Macrae, M. L. ; English, M. C. ; Schiff, S. L. ; Stone, M.. *Journal of Hydrology* (2010), 389, 101-110.
- Malagó, A., Bouraoui, F., Vigiak, O., Grizzetti, B., & Pastori, M. (2017). Modelling water and nutrient fluxes in the Danube River Basin with SWAT. *Science of the Total Environment*, 603–604, 196–218. <http://doi.org/10.1016/j.scitotenv.2017.05.242>
- Marcinkowski, P., Piniewski, M., Kardel, I., Szcześniak, M., Benestad, R., Srinivasan, R., ... Okruszko, T. (2017). Effect of climate change on hydrology, sediment and nutrient losses in two lowland catchments in Poland. *Water*, 9(156), 1–23. <http://doi.org/10.3390/w9030156>
- Marianne, A., Mortsch, L., & Scheraga, J. (2003). *Climate Change and Water Quality in the Great Lakes Region*.

- Maraun, D. (2016). Bias Correcting Climate Change Simulations - a Critical Review. *Current Climate Change Reports*, 2(4), 211–220. <http://doi.org/10.1007/s40641-016-0050-x>
- Matott, L. S. (2017). *OSTRICH: an Optimization Software Tool, Documentation and User's Guide, Version 17.12.19*. Buffalo, NY: University at Buffalo Center for Computational Research. Retrieved from www.eng.buffalo.edu/~lsmatott/Ostrich/OstrichMain.html.
- McDermid, J., Fera, S., & Hogg, A. (2015). *Climate Change projections for Ontario: An updated synthesis for policymakers and planners*.
- McDonnell, J., Sivapalan, M., Vaché, K., Dunn, S., Grant, G., Haggerty, R., ... Weiler, M. (2007). Moving beyond heterogeneity and process complexity: A new vision for watershed hydrology. *Water Resources Research*, 43(7), 1–6. <http://doi.org/10.1029/2006WR005467>
- McDowell, R. W., Monaghan, L. C., Smith, L. C., Koopmans, G. F., & Stewart, I. (2005). Enhanced losses of phosphorus in mole-tile drainage water following short-term applications of dairy effluent to pasture. *Water Pollution: New Research*, 55–76.
- McDowell, R. W., Sharpley, A. N., Condrón, L. M., Haygarth, P. M., & Brookes, P. C. (2001). Processes controlling soil phosphorus release to runoff and implications for agricultural management. *Nutrient Cycling in Agroecosystems*, 59(3), 269–284. <http://doi.org/10.1023/A:1014419206761>
- McKenney, D., Hutchinson, M., Papadopol, P., Lawrence, K., Pedlar, J., Campbell, K., & Owen, T. (2011). Customized Spatial Climate Models for North America. *Bulletin of the American Meteorological Society*, 1611–1622. <http://doi.org/10.1175/2011BAMS3132.1>
- McKenney, D., Pedlar, J., Hutchinson, M., Papadopol, P., Lawrence, K., Campbell, K., & Price, D. (2013). Spatial climate models for Canada's forestry community. *The Forestry Chronicle*, 89(5), 659–663.
- Me, W., Abell, J. M., & Hamilton, D. P. (2015). Effects of hydrologic conditions on SWAT model performance and parameter sensitivity for a small, mixed land use catchment in New Zealand. *Hydrology and Earth System Sciences*, 19(10), 4127–4147. <http://doi.org/10.5194/hess-19-4127-2015>
- Mehdi, B., Lehner, B., Gombault, C., Michaud, A., Beaudin, I., Sottile, M. F., & Blondlot, A. (2015). Simulated impacts of climate change and agricultural land use change on surface water

quality with and without adaptation management strategies. *Agriculture, Ecosystems and Environment*, 213, 47–60. <http://doi.org/10.1016/j.agee.2015.07.019>

Mehdi, B., Ludwig, R., & Lehner, B. (2016). Simulated future changes of extreme nutrient loads in a mesoscale agricultural watershed in Bavaria. *Journal of Land Management Food and Environment*, 67(2), 77–90. <http://doi.org/10.1515/boku-2016-0008>

Meinshausen, M., Smith, S. J., Calvin, K., Daniel, J. S., Kainuma, M. L. T., Lamarque, J., ... van Vuuren, D. P. P. (2011). The RCP greenhouse gas concentrations and their extensions from 1765 to 2300. *Climatic Change*, 109(1), 213–241. <http://doi.org/10.1007/s10584-011-0156-z>

Mengis M, et al. (1999). *Ground Water* 37: 448-457.

Mejia, M. and Madramootoo, C. (1998). *J. Irrig. Drain Eng.*, 124(2), 116–122.

Merriman, K., Russell, A., Rachol, C., Daggupati, P., Srinivasan, R., Hayhurst, B., & Stuntebeck, T. (2018). Calibration of a Field-Scale Soil and Water Assessment Tool (SWAT) Model with Field Placement of Best Management Practices in Alger Creek, Michigan. *Sustainability*, 10, 851. <http://doi.org/10.3390/su10030851>

Michalak, A. M., Anderson, E. J., Beletsky, D., Boland, S., Bosch, N. S., Bridgeman, T. B., & Zagorski, M. A. (2013). Record-setting algal bloom in Lake Erie caused by agricultural and meteorological trends consistent with expected future conditions. *Proceedings of the National Academy of Sciences*, 110(16), 6448–6452. <http://doi.org/10.1073/pnas.1216006110>

Michaud, A.R., Lauzier, R., et M.R. Laverdière. 2005. Mobilité du phosphore et intervention agroenvironnementale en bassin versant agricole: Etude de cas du bassin versant du ruisseau au Castor, tributaire de la rivière aux Brochets, Québec. *Agrosol* 16(1), pp. 57-59.

Michaud, A.R., I. Beaudin, J. Deslandes, F. Bonn, and C.A. Madramootoo. (2007). SWAT-predicted influence of different landscape and cropping system alterations on phosphorus mobility within the Pike River watershed of south-western Québec. *Canadian Journal of Soil Science* 87:329-344.

Michaud, A., Seydoux, A. S., Beaudin, I., & Gombault, C. (2008). *Beneficial Management Practices and Water Quality: Hydrological Modelling of Two Basins in the Montérégie Region, Quebec* (Report No. 4-65). Gatineau, QC: Environment Canada.

- Michaud, A.R. , J. Deslandes, J. Desjardins et M. Grenier. (2009a). Réseau d'actions concertées en bassins versants agricoles. Rapport final de projet. Institut de recherche et de développement en agroenvironnement (IRDA), MAPAQ, Club du bassin LaGuerre, Dura-Club, Club de fertilisation de la Beauce, Fonds d'action québécois pour le développement durable, Conseil pour le développement de l'agriculture du Québec et Programme d'aide technique de Couverture végétale du Canada. Québec, Québec, 155 p. <https://www.irda.qc.ca/fr/publications/reseau-d-actions-concertees-en-bassins-versants-agricoles/>
- Michaud, A.R, J. Desjardins, M. Grenier et R. Lauzier. 2009b. Suivi de la qualité de l'eau des bassins versants expérimentaux Ewing et Aux Castor – Dans le cadre du projet Lisière verte. Rapport final de projet. Institut de recherche et de développement en agroenvironnement (IRDA), Coopérative de solidarité du bassin versant de la rivière aux brochets, AAC (PASCAA) et MAPAQ, Québec, Québec, 27 p. <https://www.irda.qc.ca/fr/publications/suivi-de-la-qualite-de-l-eau-des-bassins-versants-experimentaux-ewing-et-aux-castors-dans-le-cadre-du-projet-lisiere-verte/>
- Michaud, A.R, S.-C. Poirier, J. Desjardins, Grenier, M., et I. Saint-Laurent. (2009c). Évaluation des exportations de surface et souterraines de phosphore en sol drainé. Rapport final de projet. Institut de recherche et de développement en agroenvironnement (IRDA) et MAPAQ, Québec, Québec, 39 p. <https://www.irda.qc.ca/fr/publications/evaluation-des-exportations-de-surface-et-souterraines-de-phosphore-en-sol-draine/>
- Michaud, A.R., M. Giroux, I. Beaudin, J. Desjardins, G. Gagné, M. Duchemin, J. Deslandes, C. Landry, P. Beudet et J. Lagacé. (2009b). ODEP; un Outil de diagnostic des exportations de phosphore. Institut de recherche et de développement en agroenvironnement inc. (IRDA) et le Centre de référence en agriculture et agroalimentaire du Québec (CRAAQ), Québec, Canada. 107 p. http://www.irda.qc.ca/ftbFiles/Nouvelles/ODEP_Manuel_utilisateur2009.pdf
- Michaud, A.R., J. Desjardins, N. Coté, I. Beaudin, A. Drouin, S. Seydoux et I. Saint-Laurent. 2012a. Rapport de l'Observatoire de la qualité de l'eau de surface en bassins versants agricoles. Rapport sommaire pour la période de référence 2009-2011. Institut de recherche et de développement en agroenvironnement inc. (IRDA), Ministère de l'Agriculture, des Pêcheries et de l'Alimentation du Québec (MAPAQ). Québec, Canada. 87 pages et annexes.
- Michaud, A.R., A. Drouin, A. Mailhot, G. Talbot, D. Huard, S. Biner, R. Lagacé, N-R. Rocha et G. Gagné. 2012b. Mise à jour des normes et procédures de conception d'ouvrages hydrauliques en milieu rural dans un contexte de changements. Consortium de recherche OURANOS.

Institut de recherche et de développement en agroenvironnement inc. (IRDA), Québec, Canada. 181 p. <https://www.irda.qc.ca/fr/publications/mise-a-jour-des-normes-et-procedures-de-conception-des-ouvrages-hydro-agricoles-dans-un-contexte-de-changements-climatiques/>

Michaud, A.R., S-C Poirier et J.K Whalen. 2019. Tile Drainage as a Hydrologic Pathway for Phosphorus Export from an Agricultural Subwatershed. *Journal of Environmental Quality*. 48: 1: 64-72 doi:10.2134/jeq2018.03.0104

Ministry of Agriculture, Food and Rural Affairs. (2015). *Tile drainage area*. [Data file]. Retrieved from <https://www.javacoeapp.lrc.gov.on.ca/geonetwork/srv/en/main.home>

Ministry of Agriculture and Rural Affairs. (2017). *Agronomy Guide for Field Crops - Publication 811*. Toronto, Canada. Retrieved from <http://www.omafra.gov.on.ca/english/crops/pub811/pub811.pdf>

Ministry of Agriculture, Food and Rural Affairs, & Canadian Soil Information Service. (2015). *Ontario Soil Survey Complex*. [Data file]. Retrieved from <https://www.javacoeapp.lrc.gov.on.ca/geonetwork/srv/en/main.home>

Ministry of the Environment and Climate Change. (2012). *Water quality of 15 streams in agricultural watersheds of Southwestern Ontario 2004-2009*.

Ministry of Finance. (2017). *Ontario Population Projections Update, 2016-2041*. Ontario: Author. Retrieved from <https://www.fin.gov.on.ca/en/economy/demographics/projections/projections2016-2041.pdf>

Ministry of Natural Resources and Forestry. (2015). *The Southwestern Ontario Orthophotography Project, 2010 digital elevation model*. [Data file]. Retrieved from <https://www.ontario.ca/data/2010-digital-elevation-model>

Minville, M., F. Brissette, and R. Leconte. (2008). Uncertainty of the impact of climate change on the hydrology of a nordic watershed. *Journal of Hydrology* 358(1-2): 70-83.

Moazed, H., Hoseini, Y., Naseri, A. A., & Abbasi, F. (2010). Determining phosphorus adsorption isotherm in soil and its relation to soil characteristics. *Journal of Food, Agriculture & Environment*, 8(2), 1153–1157. <http://doi.org/10.3923/ijss.2010.131.139>

- Molder, B., Cockburn, J., Berg, A., Lindsay, J., & Woodrow, K. (2015). Sediment-assisted nutrient transfer from a small, no-till, tile drained watershed in Southwestern Ontario, Canada. *Agricultural Water Management*, 152, 31–40. <http://doi.org/10.1016/j.agwat.2014.12.010>
- Moriasi, D., Arnold, J., & Green, C. (2007a). Incorporation of Hooghoudt and Kirkham tile drain equations into SWAT2005. *Proc. 4th Intl. SWAT Conf*, 139–147. Retrieved from <http://scholar.google.com/scholar?hl=en&btnG=Search&q=intitle:INCORPORATION+of+Hooghoudt+and+Kirkham+Tile+Drain+Equations+into+SWAT2005#0>
- Moriasi, D., Arnold, J., Van Liew, M. W., Binger, R. L., Harmel, R. D., & Veith, T. L. (2007b). Model evaluation guidelines for systematic quantification of accuracy in watershed simulations. *American Society of Agricultural and Biological Engineers*, 50(3), 885–900. <http://doi.org/10.13031/2013.23153>
- Moriasi, D., Arnold, J., Vasquez-Amabile, G. G., Angel, B. A., & Rossi, C. G. (2009). Incorporation of a New Shallow Water Table Depth Algorithm into SWAT2005. *American Society of Agricultural and Biological Engineers*, 52(3), 771–784. <http://doi.org/10.13031/2013.27398>
- Moriasi, D., Gowda, P. H., Arnold, J., Mulla, D. J., Ale, S., Steiner, J. L., & Tomer, M. D. (2013). Evaluation of the Hooghoudt and Kirkham Tile Drain Equations in the Soil and Water Assessment Tool to Simulate Tile Flow and Nitrate-Nitrogen. *Journal of Environmental Quality* (Vol. 42).
- Moriasi, D., Rossi, C., Arnold, J., & Tomer, M. (2012). Evaluating hydrology of the Soil and Water Assessment Tool (SWAT) with new tile drain equations. *Journal of Soil and Water Conservation*, 67, 513–524. <https://doi.org/10.2489/jswc.67.6.513>
- Mpelasoka, F. S., & Chiew, F. H. S. (2009). Influence of Rainfall Scenario Construction Methods on Runoff Projections. *Journal of Hydrometeorology*, 10, 1168–1183. <http://doi.org/10.1175/2009JHM1045.1>
- Muma, M., Rousseau, A. N., & Gumiere, S. J. (2016). Assessment of the impact of subsurface agricultural drainage on soilwater storage and flows of a small watershed. *Water*, 8(326). <http://doi.org/10.3390/w8080326>
- Murphy, J., et J.R. Riley. (1962). A modified single solution method for the determination of phosphates in surface waters. *Anal. Acta* 27:31-36.

- Nash, J. E., & Sutcliffe, J. V. (1970). River flow forecasting through conceptual models part 1- A discussion of principles. *Journal of Hydrology*, 10, 282–290.
- Neilsen, G. H., Culley, J. L., & Cameron, D. R. (1978). *Nitrogen Loadings From Agricultural Activities in the Great Lakes Basin Integration Report on Nitrogen, Agricultural Watershed Studies, Task C, Canadian Section, Activity 1*. Ottawa, Ontario.
- Neitsch, S.L., J.G. Arnold, J.R. Kiniry, J.R. Williams, and King, K.W. (2002). Soil and water assessment tool: theoretical documentation, version 2000, Temple, TX.
- Neitsch, S. L., Arnold, J. G., Kiniry, J. R., & Williams, J. R. (2011). *Soil & Water Assessment Tool Theoretical Documentation, version 2009*. College Station, Texas.
- Ouranos. (2018). *Climate simulation and analysis*. Retrieved from <http://www.ouranos.ca/en/scientific-program/climate-science/climate-simulations/default.php>
- Panno, S. V., Kelly, W. R., Hackley, K. C., Hwang, H. H., & Martinsek, A. T. (2008). Sources and fate of nitrate in the Illinois River Basin, Illinois. *Journal of Hydrology*, 359(1–2), 174–188. <http://doi.org/10.1016/j.jhydrol.2008.06.027>
- Parkin, G. W., Fallow, D. J., & Brown, D. M. (1999). Estimated Seasonal and Annual Water Surplus in Ontario. *Canadian Water Resources Journal*, 24(4), 277–292. <http://doi.org/10.4296/cwrj2404277>
- Pärm, J., Pinay, G., & Mander, Ü. (2012). Indicators of nutrients transport from agricultural catchments under temperate climate: A review. *Ecological Indicators*, 22, 4–15. <http://doi.org/10.1016/j.ecolind.2011.10.002>
- Pease, L. A., King, K. W., Williams, M. R., LaBarge, G. A., Duncan, E. W., & Fausey, N. R. (2018). Phosphorus export from artificially drained fields across the Eastern Corn Belt. *Journal of Great Lakes Research*, 44(1), 43–53. <http://doi.org/10.1016/j.jglr.2017.11.009>
- Peron, H., Hueckel, T., Laloui, L., & Hu, L. B. (2009). Fundamentals of desiccation cracking of fine-grained soils: experimental characterization and mechanisms identification. *Canadian Geotechnical Journal*, 46(10), 1177–1201. <http://doi.org/10.1139/T09-054>

- Petry, J., Soulsby, C., Malcolm, I. A., & Youngson, A. F. (2002). Hydrological controls on nutrient concentrations and fluxes in agricultural catchments. *Science of the Total Environment*, 294(1–3), 95–110. [http://doi.org/10.1016/S0048-9697\(02\)00058-X](http://doi.org/10.1016/S0048-9697(02)00058-X)
- Plach, J. M., Macrae, M. L., Ali, G. A., Brunke, R. R., English, M. C., Ferguson, G., ... Van Esbroeck, C. J. (2018). Supply and Transport Limitations on Phosphorus Losses from Agricultural Fields in the Lower Great Lakes Region, Canada. *Journal of Environment Quality*, 47(1), 96–105. <http://doi.org/10.2134/jeq2017.06.0234>
- Plach, J. M., Macrae, M. L., Williams, M., Lee, B., & King, K. (in press). Dominant glacial landforms in the Lake Erie watershed exhibit differences in soil phosphorus chemistry and potential risk for phosphorus loss. *Journal of Great Lakes Research*.
- Poirier, S.C., J.K. Whalen et A. R. Michaud. 2012. Bioavailable Phosphorus in Fine-Sized Sediments Transported from Agricultural Fields. *Soil Sci. Soc. Am. J.* 76:258–267.
- Poon, D. (2013). *Re-Conceptualizing the SWAT to Better Predict Subsurface Water Flow through Macroporous Soils* (Master's thesis). Retrieved from http://digitool.library.mcgill.ca/webclient/StreamGate?folder_id=0&dvs=1523834861472~686
- Prodanovi, P., & Simonovi, S. P. (2006). *Inverse Drought Risk Modelling of the Upper Thames River Basin. CFCAS Project: Assessment of Risk and Vulnerability to Changing Climatic Conditions* (Report No. 052). London, Ontario.
- Puustinen, M., Tattari, S., Koskiahho, J., & Linjama, J. (2007). Influence of seasonal and annual hydrological variations on erosion and phosphorus transport from arable areas in Finland. *Soil and Tillage Research*, 93(1), 44–55. <http://doi.org/10.1016/j.still.2006.03.011>
- Qi, H., & Qi, Z. (2017). Simulating phosphorus loss to subsurface tile drainage flow: a review. *Environmental Reviews*, 25, 150–162. <http://doi.org/10.1139/er-2016-0024>
- Qi, J., Li, S., Li, Q., Xing, Z., Bourque, C. P. A., & Meng, F. R. (2016). A new soil-temperature module for SWAT application in regions with seasonal snow cover. *Journal of Hydrology*, 538, 863–877. <http://doi.org/10.1016/j.jhydrol.2016.05.003>
- Rabotyagov, S. S., Kling, C. L., Gassman, P. W., Rabalais, N. N., & Turner, R. E. (2014). The Economics of Dead Zones: Causes, Impacts, Policy Challenges, and a Model of the Gulf of Mexico Hypoxic Zone. *Review of Environmental Economics and Policy*, 8(1), 58–79.

- Rahman, M., Bolisetti, T., & Balachandar, R. (2012). Hydrologic modelling to assess the climate change impacts in a Southern Ontario watershed. *Canadian Journal of Civil Engineering*, 39(1), 91–103. <http://doi.org/10.1139/I11-112>
- Rajib, M. A., & Merwade, V. (2016). Improving soil moisture accounting and streamflow prediction in SWAT by incorporating a modified time-dependent Curve Number method. *Hydrological Processes*, 30(4), 603–624. <http://doi.org/10.1002/hyp.10639>
- Randall, G. W., Huggins, D. R., Russelle, M. P., Fuchs, D. J., Nelson, W. W., & Anderson, J. L. (1997). Nitrate Losses through Subsurface Tile Drainage in Conservation Reserve Program, Alfalfa, and Row Crop Systems. *Journal of Environment Quality*, 26(5), 1240–1247. <http://doi.org/10.2134/jeq1997.00472425002600050007x>
- Rasouli, S., Whalen, J. K., & Madramootoo, C. A. (2014). Review : Reducing residual soil nitrogen losses from agroecosystems for surface water protection in Quebec and Ontario, Canada: Best management practices, policies and perspectives. *Canadian Journal of Soil Science*, 94, 109–127. <http://doi.org/10.4141/CJSS2013-015>
- Reid, D. K., Ball, B., & Zhang, T. Q. (2012). Accounting for the Risks of Phosphorus Losses through Tile Drains in a Phosphorus Index. *Journal of Environmental Quality*, 41, 1720-1729. <http://doi.org/10.2134/jeq2012.0238>
- Reid, S., Smit, B., Caldwell, W., & Belliveau, S. (2007). Vulnerability and adaptation to climate risks in Ontario agriculture. *Mitigation and Adaptation Strategies for Global Change*, 12(4), 609–637. <http://doi.org/10.1007/s11027-006-9051-8>
- Riley, K.D., Helmers, M.J., Lawlor, P.A., & Singh, R. (2009). Water balance investigation of drainage water management in non-weighing lysimeters. *American Society of Agricultural and Biological Engineers*, 25, 507–513. <http://doi.org/10.13031/2013.27470>
- Robertson, D. M., Saad, D. A., Christiansen, D. E., & Lorenz, D. J. (2016). Simulated impacts of climate change on phosphorus loading to Lake Michigan. *Journal of Great Lakes Research*, 42(3), 536–548. <http://doi.org/10.1016/j.jglr.2016.03.009>
- Robinson, M. (1990). *Impact of improved land drainage on river flows*. Institute of Hydrology (Vol. 113). Wallingford, UK.
- Robinson, M., & Rycroft, D. W. (1999). The impact of drainage on streamflow. *Agronomy Monographs*, 38, 767–800.

- Ross, J. A., Herbert, M. E., Sowa, S. P., Frankenberger, J. R., King, K. W., Christopher, S. F., ... Yen, H. (2016). A synthesis and comparative evaluation of factors influencing the effectiveness of drainage water management. *Agricultural Water Management*, 178, 366–376. <http://doi.org/10.1016/j.agwat.2016.10.011>
- Rouholahnejad, E., Abbaspour, K. C., Srinivasan, R., Bacu, V., & Lehmann, A. (2014). Water resources of the Black Sea Basin at high spatial and temporal resolution. *Water Resources Research*, 50(7), 586–5885. <http://doi.org/10.1002/2013WR014132.Received>
- Royer, T. V., David, M. B., & Gentry, L. E. (2006). Timing of Riverine Export of Nitrate and Phosphorus from Agricultural Watersheds in Illinois: Implications for Reducing Nutrient Loading to the Mississippi River. *Environmental Science & Technology*, 40(13), 4126–4131. doi:10.1021/es052573n
- Rozemeijer, J. C., Van Der Velde, Y., Van Geer, F. C., Bierkens, M. F. P., & Broers, H. P. (2010). Direct measurements of the tile drain and groundwater flow route contributions to surface water contamination: From field-scale concentration patterns in groundwater to catchment-scale surface water quality. *Environmental Pollution*, 158(12), 3571–3579. <http://doi.org/10.1016/j.envpol.2010.08.014>
- Rudra, R. P., Dickinson, W. T., Ahmed, S. I., Patel, P., Zhou, J., Gharabaghi, B., & Khan, A. A. (2015). Changes in rainfall extremes in Ontario. *International Journal of Environmental Research*, 9(4), 1117–1126.
- Sanchez Valero, C., C.A. Madramootoo and N. Stämpfli.2007. Water table management impacts on phosphorus loads in tile drainage. *Agricultural Water Management*. 89: 1–2, Pp.71-80.
- Santhi, C., Arnold, J. G., Williams, J. R., Dugas, W. A., Srinivasan, R., & Hauk, L. M. (2001). Validation of the SWAT model on a large river basin with point and nonpoint sources. *Journal of the American Water Resources Association*, 37(5), 1169–1188.
- Saxton, K. E., & Rawls, W. J. (2006). Soil Water Characteristic Estimates by Texture and Organic Matter for Hydrologic Solutions. *Soil Science Society of America Journal*, 70, 1569–1578. <http://doi.org/10.2136/sssaj2005.0117>
- Scavia, D., David Allan, J., Arend, K. K., Bartell, S., Beletsky, D., Bosch, N. S., ... Zhou, Y. (2014). Assessing and addressing the re-eutrophication of Lake Erie: Central basin hypoxia. *Journal of Great Lakes Research*, 40(2), 226–246. <http://doi.org/10.1016/j.jglr.2014.02.004>

- Schwab, G., Fausey, N. R., Desmond, E. D., & Holman, J. R. (1985). *Tile and Surface Drainage of Clay Soils* (Vol. Research B). Wooster, Ohio, US.
- Sharpley, A.N., W.W. Troeger et S.J. Smith. 1991. The measurement of bioavailable phosphorus in agricultural runoff. *J. Env. Qual.* 20:235-238.
- Sharpley, A. N., Gburek, W. J., Folmar, G., & Pionke, H. B. (1999). Sources of phosphorus exported from an agricultural watershed in Pennsylvania. *Agricultural Water Management*, 41(2), 77–89. [http://doi.org/10.1016/S0378-3774\(99\)00018-9](http://doi.org/10.1016/S0378-3774(99)00018-9)
- Sharpley, A. N., Jarvie, H. P., Buda, A., May, L., Spears, B., & Kleinman, P. (2014). Phosphorus Legacy: Overcoming the Effects of Past Management Practices to Mitigate Future Water Quality Impairment. *Journal of Environmental Quality*, 42(5), 1308–1308. <http://doi.org/10.1017/CBO9781107415324.004>
- Sharpley, A. N., Kleinman, P. J. A., Flaten, D. N., & Buda, A. R. (2011). Critical source area management of agricultural phosphorus: experiences, challenges and opportunities. *Water Science & Technology*, 64(4), 945. <http://doi.org/10.2166/wst.2011.712>
- Sharpley, A. N., McDowell, R. W., & Kleinman, P. J. A. (2001). Phosphorus loss from land to water: integrating agricultural and environmental management. *Plant and Soil*, 237(2), 287–307. <http://doi.org/Doi 10.1023/A:1013335814593>
- Sharpley, A. N., Smith, S. J., & Naney, J. W. (1987). Environmental impact of agricultural nitrogen and phosphorus use. *Journal of Agricultural and Food Chemistry*, 35(5), 812–817.
- Shrestha, N. K., & Wang, J. (2018). Predicting sediment yield and transport dynamics of a cold climate region watershed in changing climate. *Science of the Total Environment*, 625, 1030–1045. <http://doi.org/10.1016/j.scitotenv.2017.12.347>
- Sinha, T., & Cherkauer, K. A. (2010). Impacts of future climate change on soil frost in the midwestern United States. *Journal of Geophysical Research*, 115(D08105). <http://doi.org/10.1029/2009JD012188>
- Skaggs, R. W. (1978). *A water management model for shallow water table soils*. Raleigh, NC, USA.
- Skaggs, R. W., Brevé, M. A., & Gilliam, J.W. (1994). Hydrologic and water quality impacts of agricultural drainage. *Critical Reviews in Environmental Science and Technology*, 24, 1–32. <https://doi.org/10.1080/10643389409388459>

- Skaggs, R. W., Fausey, N. R., & Evans, R. O. (2012). Drainage water management. *Journal of Soil and Water Conservation*, 67(6), 167A–172A. <http://doi.org/10.2489/jswc.67.6.167A>
- Skaggs, R.W., Youssef, M., Gilliam, J. W., & Evans, R. (2010). Effect of Controlled Drainage on Water and Nitrogen Balances in Drained Lands. *Transactions of the ASABE*, 53, 1843-1850. <https://doi.org/10.13031/2013.35810>
- Soil Conservation Service. (1972). *National Engineering Handbook*. Washington, DC: USDA Soil Conservation Service.
- Simard, R. R., Beauchemin, S., & Haygarth, P. M. (2000). Potential for Preferential Pathways of Phosphorus Transport. *Journal of Environment Quality*, 29(1), 97-105. <http://doi.org/10.2134/jeq2000.00472425002900010012x>
- Singh, B., Bardgett, R. D., Smith, P., & Reay, D. S. (2010). Microorganisms and climate change: terrestrial feedbacks and mitigation options. *Nature Reviews Microbiology*, 8(11), 779–790. <http://doi.org/10.1038/nrmicro2439>
- Singh, B., El Maayar, M., André, P., Bryant, C. R., & Thouez, J. P. (1998). Impacts of a GHG-induced climate change on crop yields: Effects of acceleration in maturation, moisture stress and optimal temperature. *Climatic Change*, 38(1), 51–86. <http://doi.org/10.1023/A:1005392517715>
- Sloan, B. P., Mantilla, R., Fonley, M., & Basu, N. B. (2017). Hydrologic impacts of subsurface drainage from the field to watershed scale. *Hydrological Processes*, 31(17), 3017–3028. <http://doi.org/10.1002/hyp.11218>
- Smith, K. A., Jackson, D. R., & Pepper, T. J. (2001). Nutrient losses by surface run-off following the application of organic manures to arable land. 2. Nitrogen. *Environmental Pollution*, 112, 53–60. [http://doi.org/10.1016/S0269-7491\(00\)00098-1](http://doi.org/10.1016/S0269-7491(00)00098-1)
- Spivakov, B. Y., Maryutina, T. A., & Muntau, H. (1999). Phosphorus Speciation in Water and Sediments. *Pure and Applied Chemistry*, 71(11), 2161–2176. <http://doi.org/10.1351/pac199971112161>
- Starks, P. J., & Moriasi, D. N. (2009). Spatial resolution effect of precipitation data on SWAT calibration and performance: implications for CEAP. *Transactions of the ASABE*, 52(4), 1171–1180. <http://doi.org/ISSN 0001-2351 1171>

- Steenvoorden, J., Claessen, F., Willems J. (2002). *Agricultural Effects on Ground and Surface Waters: Research at the Edge of Science and Society*. Wallingford, UK: Intl. Assn. of Hydrological Sciences.
- Sunohara, M. D., Gottschall, N., Craiovan, E., Wilkes, G., Topp, E., Frey, S. K., & Lapen, D. R. (2016). Controlling tile drainage during the growing season in Eastern Canada to reduce nitrogen, phosphorus, and bacteria loading to surface water. *Agricultural Water Management*, 178(3), 159–170. <http://doi.org/10.1016/j.agwat.2016.08.030>
- Sunohara, M.D., Gottschall, N., Wilkes, G., Craiovan E., Topp E., Que Z., Seidou O., Frey S. K., & Lapen, D. R. (2015). Long-Term Observations of Nitrogen and Phosphorus Export in Paired-Agricultural Watersheds under Controlled and Conventional Tile Drainage. *Journal of Environmental Quality*, 44(5), 1589-1604. <http://doi.org/10.2134/jeq2015.01.0008>
- Sunohara, M., Youssef, M. A., Topp, E., & Lapen, D. R. (2010). Measured Effect of Agricultural Drainage Water Management on Hydrology, Water Quality, and Crop Yield. In *ASABE - 9th International Drainage Symposium 2010, Held Jointly with CIGR and CSBE/SCGAB*. <http://doi.org/10.13031/2013.32147>
- Stämpfli, N. and C.A. Madramootoo. 2006. Dissolved Phosphorus Losses in Tile Drainage under Subirrigation. *Water Qual. Res. J. Canada*, 2006 • Volume 41, No. 1, 63–71.
- Tan, C. S., & Zhang, T. Q. (2011). Surface runoff and sub-surface drainage phosphorus losses under regular free drainage and controlled drainage with sub-irrigation systems in southern Ontario. *Canadian Journal of Soil Science*, 91, 349–359. <http://doi.org/10.4141/CJSS09086>
- Taylor, K.E., Stouffer, R.J., Meehl, G.A. (2012). An Overview of CMIP5 and the experiment design. *Bulletin of the American Meteorological Society*, 93, 485-498. <http://dx.doi.org/10.1175/BAMS-D-11-00094.1>
- Tolson, B. A., & Shoemaker, C. A. (2007). Dynamically dimensioned search algorithm for computationally efficient watershed model calibration. *Water Resources Research*, 43(1), 1–16. <http://doi.org/10.1029/2005WR004723>
- Tsakiris, G., & Alexakis, D. (2012). Water quality models : An overview. *European Water*, 37, 33–46.

- Ulén, B., Aronsson, H., Bechmann, M., Krogstad, T., Øygarden, L., & Stenberg, M. (2010). Soil tillage methods to control phosphorus loss and potential side-effects: A Scandinavian review. *Soil Use and Management*, 26(2), 94–107. <http://doi.org/10.1111/j.1475-2743.2010.00266.x>
- Upper Thames River Conservation Authority. (2012). *Medway Creek: Watershed Report Card*. London, Ontario.
- Uusi-Kämppe, J., Braskerud, B., Jansson, H., Syversen, N., & Uusitalo, R. (2000). Buffer Zones and Constructed Wetlands as Filters for Agricultural Phosphorus. *Journal of Environmental Quality*, 29, 151-158. <http://doi.org/10.2134/jeq2000.00472425002900010019x>
- Uusitalo, R., Turtola, E., Kauppila, T., & Lilja, T. (2001). Particulate Phosphorus and Sediment in Surface Runoff and Drainflow from Clayey Soils. *Journal of Environment Quality*, 30(2), 589–595. <http://doi.org/10.2134/jeq2001.302589x>
- Vadas, P. A., Bolster, C. H., & Good, L. W. (2013). Critical evaluation of models used to study agricultural phosphorus and water quality. *Soil Use and Management*, 29(Suppl. 1), 36–44. <http://doi.org/10.1111/j.1475-2743.2012.00431.x>
- Van Dijk, J., Stroetenga, M., Bos, L., Van Bodegom, P. M., Verhoeff, H. A., & Arerts, R. (2011). Reduction of Organic Matter Decomposition and Soil Nutrient Dynamics on former Restoring natural seepage conditions agricultural grasslands does not lead to reduction of organic matter decomposition and soil. *Biogeochemistry*, 71, 317–337.
- Van Esbroeck, C. J., Macrae, M. L., Brunke, R., & McKague, K. (2016). Annual and seasonal phosphorus export in surface runoff and tile drainage from agricultural fields with cold temperate climates. *Journal of Great Lakes Research*, 42(6), 1271–1280. <http://doi.org/10.1016/j.jglr.2015.12.014>
- Van Esbroeck, C. J., Macrae, M. L., Brunke, R., & McKague, K. (2017). Surface and subsurface phosphorus export from agricultural fields during peak flow events over the nongrowing season in regions with cool, temperate climates. *Journal of Soil and Water Conservation*, 72(1), 65–76. <http://doi.org/10.2489/jswc.72.1.65>
- Van Meter, K. J., Basu, N. B., Veenstra, J. J., & Burras, C. L. (2016). The nitrogen legacy: Emerging evidence of nitrogen accumulation in anthropogenic landscapes. *Environmental Research Letters*, 11, 35014. <http://doi.org/10.1088/1748-9326/11/3/035014>

- Van Meter, K. J., Van Cappellen, P., & Basu, N. B. (2018). Legacy nitrogen may prevent achievement of water quality goals in the Gulf of Mexico. *Science*. Retrieved from <http://science.sciencemag.org/content/early/2018/03/21/science.aar4462.abstract>
- Veith, T. L., & Ghebremichael, L. T. (2009). How To: Applying and Interpreting the SWAT Auto-calibration Tools. In *2009 International SWAT Conference: Conference Proceedings* (pp. 43–50). College Station, Texas: Texas Water Resources Institute.
- Veraart, A.J., de Klein, J. J.M., & Scheffer, M. (2011). Warming Can Boost Denitrification Disproportionately Due to Altered Oxygen Dynamics. *PLOS ONE*, 6(3). <https://doi.org/10.1371/journal.pone.0018508>
- Verma, S., Bhattarai, R., Bosch, N. S., Cooke, R. C., Kalita, P. K., & Markus, M. (2015). Climate Change Impacts on Flow, Sediment and Nutrient Export in a Great Lakes Watershed Using SWAT. *Clean - Soil, Air, Water*, 43(11), 1464–1474. <http://doi.org/10.1002/clen.201400724>
- Vidon, P., & Cuadra, P. E. (2010). Impact of precipitation characteristics on soil hydrology in tile-drained landscapes. *Hydrological Processes*, 24(March), 1821–1833. <http://doi.org/10.1002/hyp.7627>
- Vidon, P., & Cuadra, P. E. (2011). Phosphorus dynamics in tile-drain flow during storms in the US Midwest. *Agricultural Water Management*, 98(4), 532–540. <http://doi.org/10.1016/j.agwat.2010.09.010>
- Vidon, P., Hubbard, L. E., & Soyeux, E. (2009). Seasonal solute dynamics across land uses during storms in glaciated landscape of the US Midwest. *Journal of Hydrology*, 376(1–2), 34–47. <http://doi.org/10.1016/j.jhydrol.2009.07.013>
- Walker, W. W. (1996). *Simplified Procedures for Eutrophication Assessment and Prediction: User Manual*. U.S. Army Corps of Engineers.
- Wallace, C. W., Flanagan, D. C., & Engel, B. A. (2017). Quantifying the Effects of Future Climate Conditions on Runoff, Sediment, and Chemical Losses at Different Watershed Sizes. *Transactions of the ASABE*, 60(3), 915-929. <http://doi.org/10.13031/trans.12094>
- Wang, H., Gao, J., Li, X., Zhang, S., & Wang, H. (2015a). Nitrate Accumulation and Leaching in Surface and Ground Water Based on Simulated Rainfall Experiments. *Plos One*, 10(8), 1–18. <http://doi.org/10.1371/journal.pone.0136274>

- Wang, L., Flanagan, D. C., Wang, Z., & Cherkauer, K. A. (2018). Climate Change Impacts on Nutrient Losses of Two Watershed in the Great Lakes Region. *Water*, 10(4), 442. <http://doi.org/10.3390/w10040442>
- Wang, X., Huang, G., & Liu, J. (2014). Projected increases in intensity and frequency of rainfall extremes through a regional climate modeling approach. *Journal of Geophysical Research: Atmospheres*, 119(23), 271–286. <http://doi.org/10.1002/2014JD022564>.Received
- Wang, X., Huang, G., Liu, J., Li, Z., & Zhao, S. (2015b). Ensemble Projections of Regional Climatic Changes over Ontario, Canada. *American Meteorological Society*, 28, 7327–7346. <http://doi.org/10.1175/JCLI-D-15-0185.1>
- Wang, X., & Melesse, A. M. (2005). Evaluation of the SWAT Model's Snowmelt Hydrology in a Northwestern Minnesota Watershed. *Transactions of the American Society of Agricultural Engineers*, 48(4), 1359–1376. <http://doi.org/10.13031/2013.19194>
- Wesström, I., Joel, A., & Messing, I. (2014). Controlled drainage and subirrigation – A water management option to reduce non-point source pollution from agricultural land. *Agriculture, Ecosystems & Environment*, 198, 74–82. <http://doi.org/10.1016/j.agee.2014.03.017>
- Wesström, I., & Messing, I. (2007). Effects of controlled drainage on N and P losses and N dynamics in a loamy sand with spring crops. *Agricultural Water Management*, 87(3), 229–240. <http://doi.org/10.1016/j.agwat.2006.07.005>
- Wilkes, G., Brassard, J., Edge, T. A., Gannon, V., Gottschall, N., Jokinen, C. C., ... Lapen, D. R. (2014). Long-term monitoring of waterborne pathogens and microbial source tracking markers in paired agricultural watersheds under controlled and conventional tile drainage management. *Applied and Environmental Microbiology*, 80(12), 3708–3720. <http://doi.org/10.1128/AEM.00254-14>
- Williams, M. R., King, K. W., & Fausey, N. R. (2015). Drainage water management effects on tile discharge and water quality. *Agricultural Water Management*, 148, 43–51. <http://doi.org/10.1016/j.agwat.2014.09.017>
- Williams, M.R., King, K.W., & Penn, C.J. (2018). Integrating Temporal Inequality into Conservation Planning to Improve Practice Design and Efficacy. *Journal of the American Water Resources Association*, 1–16. <https://doi.org/10.1111/1752-1688.12662>

- Wiskow, E., & Van Der Ploeg, R. R. (2003). Calculation of drain spacings for optimal rainstorm flood control. *Journal of Hydrology*, 272, 163–174. [http://doi.org/10.1016/S0022-1694\(02\)00262-7](http://doi.org/10.1016/S0022-1694(02)00262-7)
- Woznicki, S. A., & Nejadhashemi, A. P. (2012). Sensitivity analysis of best management practices under climate change scenarios. *Journal of the American Water Resources Association*, 48(1), 90–112. <http://doi.org/10.1111/j.1752-1688.2011.00598.x>
- Xiao, Y., Tang, J., Wang, M., Zhai, L., & Zhang, X. (2017). Impacts of soil properties on phosphorus adsorption and fractions in purple soils. *Journal of Mountain Science*, 14(12), 2420–2431. <http://doi.org/10.1007/s11629-017-4545-2>
- Xiuqing, Z., & Flerchinger, G. N. (2001). Infiltration into freezing and thawing soils under differing field treatments. *Journal of Irrigation and Drainage Engineering*, 127(3), 176–182.
- Yaghi, N., & Hartikainen, H. (2013). Enhancement of phosphorus sorption onto light expanded clay aggregates by means of aluminum and iron oxide coatings. *Chemosphere*, 93(9), 1879–1886. <http://doi.org/10.1016/j.chemosphere.2013.06.059>
- Ye, L., & Grimm, N. B. (2013). Modelling potential impacts of climate change on water and nitrate export from a mid-sized, semiarid watershed in the US Southwest. *Climatic Change*, 120, 419–431. <http://doi.org/10.1007/s10584-013-0827-z>
- Youssef, M. A., Abdelbaki, A. M., Negm, L. M., Skaggs, R. W., Thorp, K. R., & Jaynes, D. B. (2018). DRAINMOD-simulated performance of controlled drainage across the U.S. Midwest. *Agricultural Water Management*, 197, 54–66. <http://doi.org/10.1016/j.agwat.2017.11.012>
- Zabaleta, A., Meaurio, M., Ruiz, E., & Antigüedad, I. (2014). Simulation Climate Change Impact on Runoff and Sediment Yield in a Small Watershed in the Basque Country, Northern Spain. *Journal of Environment Quality*, 43, 235–245. <http://doi.org/10.2134/jeq2012.0209>
- Zhang, D., Chen, X., Yao, H., & Lin, B. (2015). Improved calibration scheme of SWAT by separating wet and dry seasons. *Ecological Modelling*, 301, 54–61. <http://doi.org/10.1016/j.ecolmodel.2015.01.018>
- Zhang, T. Q., Tan, C. S., Zheng, Z. M., Welacky, T., & Wang, Y. T. (2017). Drainage water management combined with cover crop enhances reduction of soil phosphorus loss. *Science of the Total Environment*, 586, 362–371. <http://doi.org/10.1016/j.scitotenv.2017.02.025>
- Walker, W. 1998. Flux version 5.0. Environmental laboratory USAE.

Zhou, X., Madramootoo, C.A., MacKenzie, A.F., Kaluli, J.W., and Smith, D.L. (2000). Corn Yield and Fertilizer N Recovery in Water-Table-Controlled Corn-Rye-Grass Systems. *European Journal Agronomy*, 2000, 12: 83-92.

APPENDIX 1. Physico-chemical properties of the soil series from the David river basin

(Input to SWAT-MAC modeling procedure).

Soil name ^a (Hydrologic soil group ^b)	Texture ^e .	Depth (mm)	Bulk density (g cm-3)	AWC ^c (mm H ₂ O/mm soil)	Ksat ^d . (mm h-1)	Organic carbon (%) ^e	Clay (%)	Sand (%)	Rock (%)
Layer 1									
ALL (C)	LLiA	0-500	1.27	0.17	65	6	35	10	0
AST (B)	LS	0-300	1.83	0.08	6.2	1.97	2	84	0
BDF (B)	L	0-300	1.4	0.12	29.2	2.98	18	52	0
CUV (B)	LS	0-300	1.54	0.09	0	1.63	12	72	0
DGU (C)	S	0-150	1.68	0.07	119.17	3.47	6	90	0
DGX (B)	L_LS	0-200	1.53	0.11	19.1	4.35	8	58	0
GTH (C)	LA	0-152	1.3	0.14	9.89	2.71	31	35	0
HVL (D)	ALi	0-300	1.45	0.15	35	2.39	16	38	0
RMB (B)	L	0-300	1.58	0.1	10.5	2.88	9	70	0
RRR (B)	LS	0-300	1.46	0.12	26.69	2.67	19	43	0
SAL (B)	LS	0-300	1.62	0.08	11.4	2.3	8	81	0
SBL (A)	S	0-300	1.62	0.09	17	1.85	8	80	0
SDM (B)	LS	0-140	1.2	0.11	90.34	3.47	8	71	0
SEO (B)	LS	0-300	1.53	0.09	16.2	2.57	13	72	0
SIT (B)	L_LS	0-300	1.35	0.13	11.4	3.52	18	47	0
SJU (B)	LS	0-300	1.67	0.06	16.9	1.9	6	86	0
SOL (A)	S	0-200	1.39	0.05	124.81	1.64	3.6	88.6	0
SRC (B)	L_LS	0-150	1.54	0.09	53.89	2.34	11.9	70.9	0
SSL (D)	A	0-300	1.36	0.17	74.7	4.09	51	5	0
SSM (D)	S	0-200	1.7	0.08	16.2	3.06	4.3	85.8	0
SSO (A)	S	0-300	1.6	0.14	14.6	4.08	6	83	0
SOL (A)	S	0-200	1.39	0.05	124.81	1.64	3.6	88.6	0

SRC (B)	L_LS	0-150	1.54	0.09	53.89	2.34	11.9	70.9	0
SSL (D)	A	0-300	1.36	0.17	74.7	4.09	51	5	0
SSM (D)	S	0-200	1.7	0.08	16.2	3.06	4.3	85.8	0
SSO (A)	S	0-300	1.6	0.14	14.6	4.08	6	83	0
SUB (D)	A	0-300	1.21	0.14	478.9	3.48	65	3	0
SYV (B)	LS	0-152	1.65	0.18	196.68	6.88	5.2	61.6	0
TNH (D)	L	0-410	1.1	0.35	206.91	14.1	24.8	38.8	0
TOF (D)	Tourbe	0-300	1.55	0.13	217.32	10	12	53	0

Soil name^a (Hydrologic soil group^b)	Texture^e	Depth (mm)	Bulk density (g cm-3)	AWC^c (mm H2O/m soil)	Ksat^d (mm h-1)	Organic carbon (%)^e	Clay (%)	Sand (%)	Rock (%)
Layer 2 (continued from previous page)									
ALL (C)	LLiA	500-2000	1.27	0.17	65	6	35	10	0
AST (B)	LS	300-2000	1.42	0.08	10.6	0.22	2	87	0
BDF (B)	L	300-400	1.18	0.12	9.8	1.15	16	52	0
CUV (B)	LS	300-400	1.6	0.11	0	0.45	32	46	0
DGU (C)	S	150-350	1.68	0.07	65.5	3.47	6	90	0
DGX (B)	L_LS	200-500	1.51	0.12	11.7	1.06	12	55	0
GTH (C)	LA	152-381	1.31	0.14	2.8	0.6	35	31	0
HVL (D)	ALi	300-400	1.55	0.14	24.4	0.98	23	37	0
RMB (B)	L	300-2000	1.59	0.1	6.2	0.42	9	73	0
RRR (B)	LS	300-400	1.55	0.13	11.3	2.43	18	44	0
SAL (B)	LS	300-2000	1.62	0.08	24.8	1.09	8	83	0

SBL (A)	S	300-2000	1.68	0.08	28.5	1.49	6	89	0
SDM (B)	LS	140-170	1.55	0.19	50	0.51	4	69	0
SEO (B)	LS	300-2000	1.61	0.09	41.1	0.91	8	77	0
SIT (B)	L_LS	300-400	1.68	0.13	8.8	0.34	17	46	0
SJU (B)	LS	300-2000	1.7	0.08	32.9	0.97	5	89	0
SOL (A)	S	200-300	1.7	0.08	76.8	0.46	2.8	88.6	0
SRC (B)	L_LS	150-380	1.6	0.08	8.5	0.33	18.4	65.4	0
SSL (D)	A	300-400	1.39	0.1	25.2	1.33	64	2	80
SSM (D)	S	200-360	1.71	0.07	26.5	0.59	4	89.6	0
SSO (A)	S	300-2000	1.65	0.07	72.2	1.15	5	90	60
SOL (A)	S	200-300	1.7	0.08	76.8	0.46	2.8	88.6	0
SRC (B)	L_LS	150-380	1.6	0.08	8.5	0.33	18.4	65.4	0
SSL (D)	A	300-400	1.39	0.1	25.2	1.33	64	2	80
SSM (D)	S	200-360	1.71	0.07	26.5	0.59	4	89.6	0
SSO (A)	S	300-2000	1.65	0.07	72.2	1.15	5	90	60
SUB (D)	A	300-400	1.18	0.15	193	1.51	72	2	0
SYV (B)	LS	152-304.8	1.34	0.07	61.5	2.29	5.6	82.2	0
TNH (D)	L	410-2000	1.21	0.13	68.5	0.66	56.8	14.8	0
TOF (D)	tourbe	300-2000	1.55	0.13	68.9	2.78	8	64	0

a. Abbreviations for soil names and soil orders are described by Lamontagne and Nolin (1997):

b. Hydrologic Soil Group A indicates high infiltration rates and low runoff, D indicates very slow infiltration rates and high runoff, and B and C are intermediate.

c. AWC, Available water capacity

d. K_{sat} , Saturated hydraulic conductivity (of the soil matrix), determined using the %clay, %sand, and %organic carbon as inputs in the pedotransfer function of Saxton and Rawls (2006).

e. For organic carbon and rock, the percentages refer to % total weight; for sand and clay, the percentages refer to % fine earth fraction.

E: Refer to following texture code:

Texture codes

A – Clay
L – Loam
LA -- Clay loam
LLiA -- Silty clay loam
LS -- Sandy loam
LSA -- Silty clay loam
L_LS --Fine sandy loam
LSF --Fine sandy loam
S – Sand